LOW PRESSURE LIQUID PHASE SINTERED DIAMOND COMPOSITES

Prepared by

Mandisa Queeneth Mkhize

765198

Supervisor

Professor Iakovos Sigalas

Submitted in fulfilment of the requirements for the degree of Master of Science in Engineering, School of Chemical and Metallurgical Engineering, Faculty of Engineering and the Built Environment, University of the Witwatersrand, Johannesburg, South Africa.

July 2018

PLAGIARISM DECLARATION

I, Mandisa Queeneth Mkhize, declare that this thesis is my own work. It was submitted to the degree of Master of Science in Engineering to the University of the Witwatersrand, Johannesburg. It has not been submitted before for any degree or examination to any other University.

Mandisa Mkhize

This _____ day of _____, 20___.

ACKNOWLEDGEMENTS

Firstly, I would like to thank God and all the events in my life that have led to this very moment. I am deeply grateful for the opportunities and privileges I have enjoyed because of Your Grace.

Thank you to Professor Iakovos Sigalas for inviting me to pursue this degree under his supervision. Your ability to recognise the potential and capability in me to accomplish this work has inspired to me to always believe in myself; and be courageous enough to pursue excellence. Your support, patience and knowledge, all pushed me beyond what I believed was my greatest potential.

I would like to express my deep-felt gratitude to Dr. Mathias Herrmann for your direction, knowledge and articulate recommendations that helped me to understand the work better; and do better as a student.

Thank you to the Centre of Excellence in Strong Materials (DST-NRF CoE-SM), NRF and Element Six (Pty) Ltd for the financial assistance that allowed me the opportunity to pursue and complete this dissertation.

Thank you to Wits University, Element Six (Pty) Ltd and Mintek academic and technical staff, for the assistance and resources to accomplish this degree.

To all my research colleagues; thank you for your knowledge, your concern for my wellbeing and the advice on ways to improve my research work.

Mother, thank you for your prayers, tireless support, compassion, wisdom and kind affirming words whenever the journey seemed daunting and overwhelming. To my friends and family; thank you for your constant words of encouragement, your abilities to uplift my spirit and help me tackle my work more effectively. Thank you for walking this journey with me.

My little siblings; I hope I can be an example of the fruitful experiences you enjoy when you work hard; show resilience and commitment to your goals; because these qualities coupled with right the opportunities will open doors for you and you will enjoy invaluable privileges. Banzi, I hope this is testament to you that I am a fighter; and I will fight for and by you; always.

ABSTRACT

Polycrystalline diamond (PCD) materials form part of tool components used in automobile, aerospace and mining applications. These components are commonly prepared using high pressure high temperature (HPHT) techniques. The importance of PCD is due to properties such as very high hardness, toughness and wear resistance at extreme conditions in a reproducible manner. However, few studies have examined the feasibility of using liquid phase sintering aids, such as the Y_2O_3-Al_2O_3-SiO_2 oxide binder system to sinter PCD at low pressures using the Spark Plasma Sintering (SPS) method. In this study we aimed to produce a dense, strong, liquid phase-sintered diamond composite without undergoing the diamond phase's solution re-precipitation stage, under a low pressure of 30 – 70 MPa. Diamond composites using monomodal and bimodal diamond feedstock powders were fabricated using yttrium alumino-silicate additives, with compositions of 40wt%Y_2O_3-25wt%Al_2O_3-35wt%SiO_2 (yttria-rich) and 30.78wt%Y_2O_3-13.65wt%Al_2O_3-55.58wt%SiO_2 (silica-rich) labelled as LPI and LPII, respectively. Diamond powder and the yttria alumina silica powders were mixed using the planetary ball milling technique and the ad-mixed components were heated and pressed using the SPS furnace. This showed that the silica-rich liquid phase sintering aid produced low density composites due to amorphous grain boundary and the move of the softening point to high temperatures. However, the yttria–rich additive produced bimodal diamond composites of high relative density of ~97% and hardness of ~13GPa due to faster densification rates. All the samples were measured for density using the Archimedes' method. Characterization was performed using powder X-Ray diffraction (XRD), Scanning Electron Microscopy (SEM), Energy Dispersion Spectroscopy (EDS) and Vickers hardness measurement. Examination of fracture surfaces resulted in linking microstructural features such as intergranular cracks, crack branching and intergranular phases to the behavior of these additives under the sintering conditions used in this work. This study revealed that high densities were attainable using the yttria-rich binder under low pressures using an SPS furnace. The effect of the heating/cooling rates via the SPS were also observed to affect the microstructural behavior of the composites and consequently their properties.

TABLE OF CONTENTS

LIST OF TABLES

LIST OF FIGURES

GLOSSARY

PCD – Polycrystalline diamond

XRD –X-ray Diffraction

SEM – Scanning Electronic Microscopy

SPS – Spark Plasma Sintering

CTE – Coefficient Thermal Expansion

PDC – Polycrystalline diamond compact

LPS – Liquid Phase Sintering

SCD – Single Crystal Diamond

HPHT – High Pressure, High Temperature

K_{1C} – fracture toughness

K – thermal conductivity

K_d – thermal conductivity of dispersed phase (diamond)

K_m – thermal conductivity of matrix phase

a – radius of dispersed phase

h_c – bonding conductance

V_d – volume of the dispersed phase

θ_Y – Young's contact angle; degree of wetting between the solid-vapour-liquid system

γ_{ab} - interfacial energies between the solid (s), liquid (l) and vapour (v) phases

W_{sl} - work of adhesion between the solid and liquid is defined by the Young - Dupre's equation

HIP - Hot Isostatic Pressure

hBN – hexagonal Boron Nitride

Chapter 1

INTRODUCTION

Background study

The mining industry has an insatiable need for yet better materials suitable for drilling under ever tougher conditions, more efficiently and at lower cost. Thus, the need for thermally-stable diamond materials that offer flexible shapes and sizes of drill bits to enhance drilling is always present and supported by these highly competitive manufacturing and mining industries. The technologies of particular relevance to this work include oil and gas drilling, machining of ceramic and hard non-ferrous materials etc. (Miess & Rai, 1996). Researchers have encountered challenges regarding sintering diamond composites using low pressures whilst avoiding the graphitisation process. These materials are preferred due to the range of their superior properties that include hardness, good thermal conductivity and wear resistance (Miess & Rai, 1996). In addition, low pressure sintering is a cost-effective process. Therefore, this study highlights alternative methods of producing strong and thermally stable materials using low-pressure, cost-effective methods. Conventionally, diamond composite production is associated with HPHT (high pressure/high temperature) conditions that expose diamond to the danger of graphitisation. In order to successfully sinter diamond composites without graphitisation, extremely high pressures – a costly method - are required. Modern HPHT technologies afford various industries the flexibility to make various large quantities of reproducible ultrahard diamond composite materials with high fracture toughness (Field, 1992). Researchers have paid attention to the fabrication of PCD under high pressures. Dennis (Dennis M.D., 1992) and Yahiaoui (Yahiaoui, Gerbaud, Paris, Denape, & Dourfaye, 2013) fabricated polycrystalline diamond compact (PDC) using WC-Co substrates at 5.5GPa. However, Qian *et al.* (Qian, Voronin, Zerda, He, & Zhao, 2002) and Zhao *et al.* (Zhao et al., 2004) developed an alternative method of sintering based on the ball milling of diamond and silicon carbide mixtures. Little has been documented about production of diamond composites at low pressures. Diamond composites have been traditionally associated with transition element-based sintering aides such as cobalt, nickel etc. and infiltration methods whereby the molten sintering aid enters a powder compact preform. This study attempts to achieve equally strong materials under much lower pressures using chemically/thermally stable sintering aides, specifically the yttrium aluminasilicates (Y_2O_3, Al_2O_3 and SiO_2). To date, little is known about low pressure diamond composites made by using such a system as sintering aid in combination with SPS as the sintering technology.

The main purpose of this work is to investigate and identify the best sintering parameters and the mixture compositions of the matrix that will be used to make diamond composites with high relative densities.

More specifically, the study aims to achieve the following research-specific objectives:

- Sinter high density composites using the particle rearrangement method;
- Determine whether SiO_2-rich or Y_2O_3-rich liquid phase additives produce dense diamond composites;
- Investigate the optimal sintering conditions in order to produce high density composites.

The results produced from this study should provide a greater understanding of the effects of low pressure on the strength of the diamond composites.

1.1. Polycrystalline diamonds

PCD-based materials are extensively used as key components of drill bits used in oil and gas drilling; and in cutting tools used for the machining of ceramics and hard non-ferrous materials. This range of applications is made possible by the superior hardness, good thermal conductivity and wear resistance of this class of materials (Miess D., 1996). Because of the very strong covalent bonds of the carbon atoms in diamond, the activation energies for the diffusion processes in this material are very high; as a result, solid state sintering of diamond requires extremely high temperatures, with a concomitant requirement for very high (and therefore uneconomical) pressures, in order to suppress graphitisation. In fact, solid-state sintering has been reported to happen under HPHT conditions (1500 ^oC-2500^oC, 6-8.5GPa) (Stromberg & Stephens, 1970). Such conditions are commercially expensive. Alternatively, liquid phase sintering is utilized for the manufacture of PCD (Katzman & Libby, 1971). Liquid phase sintering (LPS) aids typically used for this purpose are 3d transition elements such as Co, Fe or Ni, or more recently, carbonate salts such as those of Ba and Ca. Of the metallic liquid phase sintering aids, Co is the most commonly used because of its high carbon solubility at high temperatures. Typically PCD has a microhardness of 45GPa (Kidalov & Shakhov, 2009). The Co liquid phase sintering aid partially remains in the PCD body at the end of the sintering process. This metal then acts as a graphitizing catalyst at temperatures exceeding 700^oC (Ko, Tsurumi, Fukunaga, & Yano, 2001). This problem has motivated a different approach to liquid phase diamond sintering, one that involves metallic oxides such as Al_2O_3, Y_2O_3 and TiO_2 which would catalyse diamond graphitisation at much higher temperatures. The LPS options mentioned above require the use of ultra-high pressures during sintering in order to avoid diamond graphitisation during this process. In this work the possibility of Liquid Phase Sintering (LPS) of diamond at low pressures is explored. The Y_2O_3-Al_2O_3-SiO_2 system is used as a liquid phase sintering aid for the production of structural ceramics such as Si_3N_4, SiC and

SiAlON (Arita I., Wilkinson D.S., Purdy G.R., 1992). This system forms a liquid at high temperatures, with SiO_2 bringing the sintering temperature below ~1600ºC. This is important in the case of LPS of diamond as it can help avoid graphitisation. Upon cooling, certain phases crystallise at the grain boundaries and these phases directly affect the mechanical and thermal properties of the composite. In addition, the mismatch of the thermal expansion coefficients of diamond and the solidified LPS aid phases contribute to improved toughness due to the residual stresses between the second phase and diamond (Kim D-H., 1990). The mismatch significantly contributes to crack deflection and encourages an intergranular fracture mode leading to improved toughness. Ultra–hard diamond-SiC composites have been widely produced due to their unique mechanical properties, using either HPHT techniques (Montross & Sithebe, 2008), or reactive infiltration (Mlungwane, Sigalas, Herrmann, & Rodríguez, 2009). However, when coarse diamond is used to make the preform, the diamond-Si reaction is not complete and some metallic silicon remains unreacted. The presence of metallic Si limits the application temperatures below 1400ºC, because of the low melting point of this metal. Using fine diamond to make the preforms eliminates this problem. Sintering diamond-oxide ceramics composites would help raise the operating temperature of such composites. It is the intention of this work to explore the possibility of using oxide-based LPS aids to sinter diamond composites at low pressures i.e. 50 – 70 MPa. In-order to avoid the possibility of diamond graphitisation, it is proposed to use Spark Plasma Sintering (SPS) as the sintering technique. SPS ensures densification through the rapid application of temperature and pressure in a very short time, thus avoiding as much as possible the onset of graphitisation of the diamond particles (Sciti D., 2000).

1.2. Hypothesis

Diamond composites made from monomodal or bimodal diamond starting powders and an appropriate liquid phase sintering aid can be successfully sintered at low pressures (30MPa – 70MPa) and reach a high relative density of ~97%. A liquid phase sintering aid comprising Y_2O_3, Al_2O_3 and SiO_2 will facilitate sintering, using the SPS method for rapid sintering and enhanced densification.

1.3. Aims and objectives of this research

The aim of this work is to identify the best sintering parameters and composition of the binder/s that will be used to make diamond composites with high relative densities. Liquid Phase Sintering will be performed under sintering conditions ranging between 1200ºC-1600ºC, 30MPa–70MPa using an SPS furnace. The diamond mixtures were formulated using the following two liquid phase sintering aids: Liquid phase additive I (LPI: 40wt%Y_2O_3-25wt%Al_2O_3-35wt%SiO_2) and liquid phase additive II (LPII: 30.78wt%Y_2O_3-13.65wt%Al_2O_3-55.58wt%SiO_2). The diamond composites made were of two types: those containing monomodal diamond powder as feedstock and those containing bimodal powder for the same purpose. The monomodal diamond composites contained 25, 35and 60vol% of diamond and were sintered only using the LPI sintering aid. The bimodal diamond mixture of 60vol% (30wt%4µm+70wt%20µm) diamond was liquid phase sintered using both the LPSI and LPSII aids.

Densification rates, relative densities, phase composition, microstructures and mechanical properties such as hardness were evaluated.

Chapter 2

LITERATURE REVIEW

2.1. Diamond

Diamond is the hardest commercial material known to man. It has a maximum Vickers hardness of 100 GPa (Field, 1979). With its unique combination of chemical, thermal, optical, mechanical and electrical properties, diamond has received attention from various industries attempting to study, exploit and incorporate these materials in high-tech applications. Diamonds are extensively used in the jewellery production industry due to their high dispersion of light (Y. Chen & Zhang, 2009). The above superlative properties are manipulated in a wide range of industries such as mining, manufacturing, automobile, aerospace and civil construction. Diamonds are used in manufacturing drill bits, wire drawings dies, saw blades, drill crowns, cutting tools, heat sinks for electronic devices, turbine engines and abrasive slurries (Prinsloo, Spektorov, & Linde, 2011). However, diamonds have relatively low fracture toughness due to relatively easy cleavage along weak crystallographic planes (Lammer, 1988). Using PCD instead of single crystal diamond significantly alleviates the problem of cleavage by virtue of the enhanced fracture toughness resulting from a polycrystalline structure. The production of PCD affords various industries the flexibility to synthesize various diamond-based polycrystalline materials in high volumes and reproducibly. These have very high hardness and high fracture toughness. The sintering pathways used to produce PCD adopt production methods that can be easily adapted to the particular application (Field, 1992). Lammer proved, through the measurement of a series of mechanical properties such as transverse rupture and impact strength, that PCD behaves in a similar fashion to engineered ceramic materials but has higher fracture toughness (Lammer, 1988). In addition, particles made up of PCD were observed to sinter faster than single-crystal ones. This was attributed to the larger number of connected grain boundaries contributing to mass transport (Slamovich & Lange, 1990). Slamovish et al. also showed that polycrystalline particles obtained significantly higher end-point densities than their single-crystal counterparts and microstructural observations revealed that while single-crystal particle necks reached a stable size, necks between the polycrystalline particles continued to grow (Slamovich & Lange, 1990).

Table 1: Comparison of the properties of strong materials with PCD (US6494918 B1, 2000)

Material	Hardness (Knoop)	Thermal conductivity (W/m.K)	Coefficient of Thermal Expansion (X 10^{-6})
PCD	9000	100	1.50-4.8
cBN	4500	800	1.0-4.0
SiC	2500	84	4.7-5.3

Aluminium oxide	2000	35	7.8.-8.8
Tungsten carbide (10wt%Co)	2200	112	4-6
Zirconium oxide	10.7 - 12GPa **	3	10.5 - 11
Cobalt chrome	43 RC	11	16.9
Ti6Al6V	38 HRC	6.6-17.5	11/9
Silicon Nitride	14.2 GPa **	15-20	2-3.7

** Vickers hardness values

Metals presented in Table 1 exhibited high coefficients of thermal expansion (CTE) compared to ceramics that exhibited high hardness values. These properties confirm the superiority of PCD over other known strong hard materials.

2.2. Polycrystalline diamond (PCD)

PCD is formed by sintering individual, micron-sized diamond crystals under conditions of high temperature and pressure. The LPS approach causes diamond to diamond bonding. The sintering conditions of HPHT induce plastic deformation in the diamond crystals**,** thus ensuring extended densification of the compact prior to the infiltration of the molten sintering aid used. This technique of sintering avoids preferred orientation within the compact**,** making tool material equally hard in all directions, a feature lacking in single crystal diamonds (SCDs). The isotropic toughness of PCD allows for standardization and reproducibility (Field, 1992).

2.2.1. Manufacturing of diamond composite materials

Polycrystalline diamond composites developed under high pressures

Typically, PCD is sintered directly onto tungsten carbide-cobalt substrates to form what is commercially called a Polycrystalline Diamond Compact (PDC). This typically happens at temperatures above 1400ºC, and pressures of at least 5.5GPa. In the case of oil drilling bits manufacture the substrate part of the resulting PDC is brazed to the oil drilling drill bit (Dennis M.D., 1992). The grains of the PCD table range in size from submicron to about 100µm. The thickness of the table is of the order of 2mm. In order to further endow the PCD table with extra stiffness, the top of the WC-Co substrate frequently has ridges which are filled with PCD, which is sintered during the high pressure/high temperature (HPHT) process. The PCD table then has a thickness greater than the depth of the grooves and the diamond polycrystalline layer occupies the grooves in order to interlock with the substrate (Dennis, 1992). The ridges are designed to provide radial reinforcement against formation and propagation of

cracks that commonly occur around them. During the sintering process, a diamond powder preform is placed on top of a WC-Co substrate. The Co content in the substrate is of the order of 12wt%, but varies depending on the desired result. Once the sintering temperature exceeds the melting point of cobalt, this metal infiltrates the diamond preform, where it acts as a liquid phase sintering aid, rapidly causing the diamond particles to bond to each other through the formation of extensive necks. This results in greater strengthening of the sintered material through this diamond intergrowth process. Thus, the diamond grains bonded together form a layer which is bonded to the substrate in a planar or ridged (depending on design) interface. However, the cooling of the compact at the end of the sintering cycle generates residual stresses along the diamond/substrate interface due to the mismatch of the coefficient of thermal expansion (Yahiaoui et al., 2013). This alternating arrangement of ridges of diamond and cemented carbide minimises the magnitude of the thermally induced stresses at the interface (Dennis, 1992).

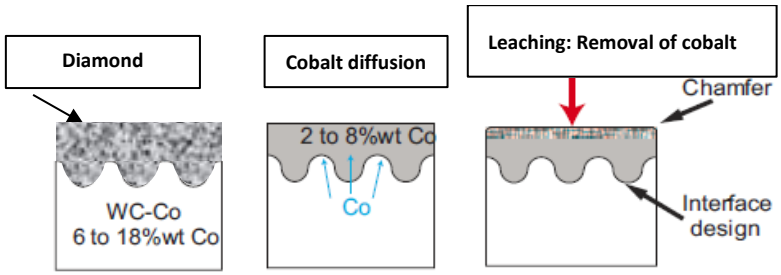

Figure 1: Diagram illustrating step-wise process of PDC manufacturing (Yahiaoui et al., 2013)

These resulting PDCs are called cutters; they are brazed on to drill bits. These are then used to drill for oil and gas. They can drill twice as fast and for twice as long as roller cone bits**,** even in hard formations (Wise, Raymond, Cooley, & Bertagnolli, 2002). They are used for soft-abrasive**,** as well as hard rock formations**,** because of a superior wear resistance (Yahiaoui et al., 2013). Due to the high-pressure process used to make them, these materials have limitations in size and shape. Therefore, different production methods not involving ultrahigh pressures were explored. The main composites made in this way included diamond aluminium, diamond copper, diamond SiC-TiC, diamond SiC, diamond Si_3N_4 and diamond WC-Co composites. A brief description of the method of sintering, sintering conditions and properties of these composites is given below.

2.2.2. Diamond composites produced at low pressures

Diamond is a metastable allotrope of carbon, in which the atoms are arranged in the Zinc-blende structure. Diamond is metastable at atmospheric pressure, with graphite being the thermodynamically stable phase of carbon at ambient conditions (Berman & Simon, 1955). Figure 2 shows that diamond converts to graphite at decreasing pressures or/and increasing temperatures (pressures below ~4.8GPa).

Diamond can be converted to graphite either through exposure to high temperatures, or through the action of a catalyst at somewhat lower temperatures. The activation energy for this conversion is ~1160kJ/mol (Davies & Evans, 1972) and therefore the probability of spontaneous graphitisation is extremely low (Gordeev, Zhukov, Danchukova, & Ekstrom, 2001). Successful attempts to sinter dense diamond composites at low pressures using a wide variety of binders proved that the metastability of diamond at low pressures can be exploited. Fabrication of diamond composites at low pressures is achieved via chemical reactions that occur between the matrix constituents alone and/or with diamond at set sintering conditions. Further, sintering of diamond composites with bonding matrices can enhance the fracture toughness, without significantly diminishing wear resistance and hardness. The additives used have a pronounced influence on the strength of the resulting composites.

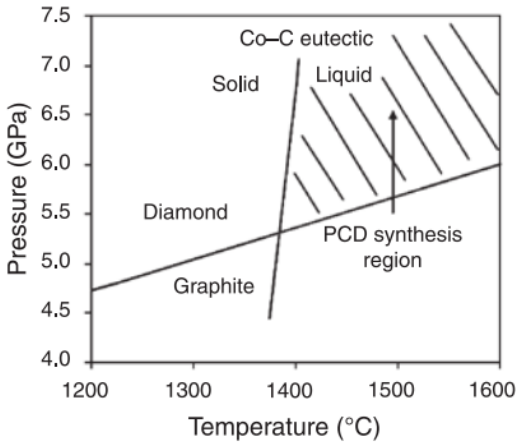

Figure 2: A schematic of the Berman-Simon equilibrium between graphite and diamond (Berman & Simon, 1955)

Because of its metastability, diamond requires high pressures to prevent its transformation into the stable graphitic modification as temperature is raised for whatever reason. A possible approach for the development of high density diamond-containing materials, without the application of high pressure, can involve the use of a system-sintering aid that generates a sufficient amount of liquid at the sintering temperature (Herrmann et al., 2012), that temperature being below that of diamond graphitisation. It is essential to investigate and match the volume fraction of the liquid phase aides with the set sintering conditions. This will ensure that the sintering aides produce sufficient liquid to improve sintering and densification. In addition, utilizing fast sintering processes such as SPS is effective in preventing graphitisation of diamond at the metastable conditions such as high temperatures and low pressures (Moriguchi, Tsuduki, Ikegaya, Miyamoto, & Morisada, 2007). Examples of diamond composites sintered with various liquid phase additives at low pressures are discussed below.

2.2.2.1. Diamond aluminium composites

Diamond aluminium composites were sintered at low pressures of 30MPa at 520°C, 550°C, 580°C and 600°C with a heating rate of 50°C/min using an SPS furnace. Aluminium was selected as the matrix material due to its high thermal conductivity and ease of processing. 50vol% of 70µm diamond powder was used with 200+ mesh of aluminium. The behaviour of the diamond-Al matrix composites under different sintering conditions was governed by the volume fraction of the liquid phase additive generated at each temperature. At 520°C, there were signs of insufficient sintering as indicated by the pores in the microstructures. The highest relative density of 97% and thermal conductivity of 325 W/(m.K) were reached at 550°C (Chu, Jia, Liang, & Chen, 2010). Microstructural observations of the sintered diamond composites displayed ductile dimples and tear ridges demonstrating the presence of a strong interfacial bonding between diamond and Al in diamond composites sintered at 550°C. By increasing the sintering temperature to 580°C and 600°C, the diamond composites sintered displayed weak interfacial bonding due to the promoted plastic flow and evaporation-condensation of the matrix, and the Al atoms at the interface tended to diffuse into pores among the diamond particles, which initially releases the compressive stress and weakens the mechanical bonding between the matrix and diamond (Liang et al., 2012).

2.2.2.2. Diamond-SiC-TiC composites

Diamond-SiC-TiC composites were produced using SPS at various sintering temperatures with constant uniaxial pressure of 50MPa. Diamond (~40µm) was combined with Si (<10µm), Ti (<10µm), the latter used to consume the graphite that was formed during the sintering process generating SiC and TiC chemically bonded to the diamond particles.

Table 2: Relative densities of composites sintered at sintered at 1300°C and 1400°C with different mass fractions of Si, Ti and diamond indicated (Zhou et al., 2015)

Sample name	Mass fraction (%)			Bending strength		R.D. (%)	
	Si	Ti	Diamond	1300°C	1400°C	1300°C	1400°C
S1	40	20	40	293	536	90.3	93.5
S2	30	30	40	383	637	93.7	94.1
S3	20	40	40	230	496	89.2	90.7
S4	25	25	50	197	342	80.3	82.6

Initial sintering tests were performed at 1300°C and 1400°C in order to study and evaluate the sintering behaviour of each mixture composition and the maximum relative densities reached, as shown in Table

2. The S2 sample provided equal parts of Ti (30wtl%) and Si (30wt%); the latter generated liquid phase that facilitated diamond-to-SiC bonding as well as particle rearrangement resulting in the highest relative density. Sintering temperature range was between 1200°C-1800°C under 50MPa. Zhou et al. conducted Gibbs free energy calculations. The graphite formed was consumed by the Ti/Si. However, at 1300°C and 1400°C, SiC, TiC and Ti_3SiC_2 formed with increasing temperature, Ti_3SiC_2 disappeared, indicating an enhanced reactive ability of Ti, Si and diamond. Maximum 3-point bending strength achieved by S2 was up to 829MPa and with 99% of relative density. However, the sample population was very low (Zhou et al., 2015).

2.2.2.3. Diamond copper composites

Diamond copper composites are increasingly considered as the next generation of thermal management materials for electronic heat sink applications. These composites were produced with high thermal conductivity and low CTE**,** suitable for maximizing heat dissipation**,** minimizing thermal stress and adjusting the composition of the composite which can influence its CTE to match the matrix (Tao, Zhu, Tian, Yang, & Yang, 2014). Copper does not naturally wet diamond; this leads to weak interfacial bonding between the two components. However, Tao et al. produced diamond copper composites using the SPS at 700°C - 950°C at 50MPa pressure for a 5min holding time. The starting materials were diamond (40µm) and copper (400µm) with diamond volume fractions varying between 50vol%, 60vol% and 70vol%. Relative density and thermal conductivity increased with a decreasing diamond volume fraction from 70vo%, 60vol% and 50vol%, with corresponding relative densities of 74.5%, 86.2% and 91.8%, respectively at 750°C. The occurrence of cracks surrounding diamond particles decreased with decreasing diamond volume fraction, with the most substantial cracks found samples with 70vol% diamond content. The 700°C sintering cycle resulted in poor wettability between copper and diamond. Further tests were conducted at higher temperatures (700°C, 750°C, 850°C and 950°C) for the 50vol% diamond due to its high relative density attainment. Thermal conductivity increased from 71.8W/(m.K) at 750°C to 190.5W/(m.K) at 950°C, and relative density reached a maximum of 94% at 950°C. Both the relative density and thermal conductivity increased with increasing sintering temperatures**,** due to improved interface adherence and lower copper viscosity. Kang et al. reported that the copper- Cr_7C_3 coated diamond composites exhibited a thermal conductivity of 562W/(m.K), with a thermal expansion coefficient of 7.8×10^{-6} K^{-1} when these powders were heat treated at 1150°C under 20MPa applied pressure to infiltrate the molten copper into the diamond preform for 5min (Q. Kang et al., 2013).

2.2.2.4. Diamond SiC composites

Bulk superhard materials, such as diamond-SiC composites, were prepared by sintering. These composites are of great interest due to their thermal stability, compared to traditional Co- and Ni-bonded diamond composites (Zhao et al., 2004). Qian et al. and Zhao et al. proposed an alternative method of sintering that was based on simultaneous ball milling of diamond and silicon carbide mixtures (Zhao et al., 2004) and (Qian et al., 2002). This process forms amorphous Si precursors followed by rapid reactive sintering at 6 GPa/1400°C and 8 GPa/2000°C. Zhao et al. showed how this method allows for better control of reactive sintering of a nanocrystalline SiC matrix. Zhao et al. designed nanostructured diamond-SiC composites that were reported to possess enhanced fracture toughness, while maintaining superabrasive and superhard properties (Zhao et al., 2004). The measured fracture toughness was greatly enhanced with the decrease of the SiC grains from 10µm to 20nm (from melt infiltration method to ball milling procedure). An increase from 8.2MPa.m$^{1/2}$ to 12MPa.m$^{1/2}$ was reported.

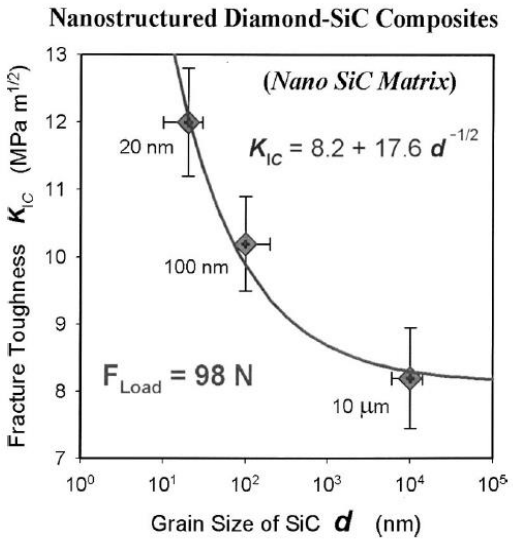

Figure 3: Relationship between fracture toughness of the diamond- SiC composite and SiC grain size (Zhao et al., 2004)

Figure 3 shows that the measured fracture toughness increases about 50% with decreasing grain size of the SiC from 10µm to 20nm. The achieved K_{IC} was 12MPa.m$^{1/2}$ for diamond-SiC composites. This value toughness was about 30% higher than that of tungsten carbide (8MPa.m$^{1/2}$). Zhao et.al successfully overcame the common inverse relationship between hardness and fracture toughness of most materials (Zhao et al., 2004). These produced diamond-SiC composites possess super-hardness and high fracture toughness simultaneously. Apart from the improved fracture toughness from 10 ± 3 MPa.m$^{1/2}$ to 12 MPa.m$^{1/2}$ of the ball milled diamond-SiC ceramics, the melt infiltration method presented greater chances of failing due to (i) Si melt failing to sufficiently fill the highly compacted

nanodiamond grains and (ii) residual diamond converted to graphite at high temperatures (Ekimov et al., 2000).

2.2.2.5. Low pressure infiltration of diamond composites

The production of low pressure infiltration diamond composites was introduced to ensure cost-effective production of dense composites and the flexibility to make diamond tools of different shapes and sizes. SiC-diamond composites are some of the commonly known composites created using a technique that involves the matrix binding the diamond crystals together. Secondary phases have the ability to improve formability and fracture toughness of such diamond-based materials (Mlungwane, Herrmann, & Sigalas, 2008). However, it is crucial to select secondary phases that are suitable for the achievement of desired properties. 3d transition metals have been reported to promote graphitisation at temperatures below 1000°C. SiC was selected as a binder due to its structural similarities with diamond, enabling the establishment of strong adhesion with diamond and thermal stability at temperatures above 1000°C. Also, SiC can be formed in situ from a reaction between diamond and molten Si. An additional advantage with using Si as an additive is that diamond is well wetted by the molten metal at temperatures above 1450°C. The infiltration process is beneficial because the liquid phase fills the pores in the diamond skeleton and produces a dense material (Qian et al., 2002). Mlungwane et al. (2009) successfully sintered diamond – SiC composites through infiltration process. The process was achieved through using the molten Silicon as a liquid phase additive due to its ability to adequately wet diamond at a contact angle of 20° after melting. This reaction is highly successful in large diamond preforms (5-250µm, 7-63µm particle size) (EP1019337, 1998) and (Gordeev et al., 2001). It was reported that the formation of SiC during infiltration is accompanied by volume expansion of the solid phase – this can lead to blockages, and is especially pronounced in fine grained diamond preforms (Sangsuwan et al., 1999) which are highly sought after by manufacturers of high performance composites. Therefore, in order to eliminate this occurrence in the study Mlungwane et al. employed a process that first infiltrated a fine diamond particle powder preform with phenolic resin. The resulting compact was first heat treated to set the resin and subsequently pyrolysed at 1000^{o}C. The latter step converted the phenolic resin to carbon, which coated the diamond particles. This preform was then placed on top of a metallic Si plate. The temperature was raised to a temperature above the melting point of Si. The molten metal infiltrated the preform, reacted with the carbon and swiftly made SiC. Because of the small particle size used, the pores were small. Thus the diffusion path needed to be traversed by the reacting C and Si (in order to form SiC) atoms was small, thus allowing for the whole mass of the molten Si to be converted to SiC. Initial granulation of the diamond particles, prior to forming the preform, ensured that sufficient intergranular pore paths were available to ensure complete molten Si infiltration up to distances of 5mm. (Mlungwane et al., 2009) and (Mlungwane et al., 2008).

2.2.2.6. Si_3N_4 – based diamond composites

Si_3N_4-based materials are attracting a great deal of attention because of their range of applications where low density, high hardness, high wear resistance and good thermal shock resistance are required (Klemm, 2010). These materials are recognized as potential candidates for high-temperature structural components (Peng, 2004) and (Klimczyk & Urbanovich, 2009). However, the strong covalent bonds between Si and N, and a low self-diffusivity coefficient interfere with the sintering processes. Sintering aides such as SiC, TiN, TiB_2, TiC, BN, WC, ZrO_2 and carbon nanotubes have previously been used to improve mechanical, electrical and chemical properties of bulk Si_3N_4 ceramics (Huang, Swarnakar, Vanmeensel, & Vleugels, 2013). Thus, alternative approaches were attempted and high densities were reached with the use of such sintering aids (Hampshire, 2007). In addition, Si_4N_3 is used as a non-oxide additive for diamond sintering processes. Huang et al. sintered Si_3N_4 and diamond – Si_3N_4 composites at 1550°C - 1750°C under maximum pressure of 100MPa with a heating rate of 200°C/min using spark plasma sintering technology. Si_4N_3 is commonly used as ceramic matrix for sintering of diamond due to the small difference between the thermal expansion coefficients of these two materials, i.e. 0.8 - 1.0 x 10^{-6}/°C for silicon nitride and 3 - 3.5 x 10^{-6}/°C for diamond (Huang et al., 2013). This limits the thermal residual stresses during sintering. In addition, the combined hardness, thermal shock resistance and high fracture toughness of diamond and the β-Si_3N_4 ceramic matrix present a concerted mechanical advantage to the materials to be sintered.

Three mixture compositions were prepared: (i) monolithic Si_3N_4 with 4wt% Al_2O_3 - 5wt% Y_2O_3 and (ii) 30vol% of 2µm diamond grade ad-mixed into Si_3N_4 with 4wt% Al_2O_3 - 5wt% Y_2O_3 LPS aid and (iii) 30vol% of 30µm diamond grains ad-mixed into Si_3N_4 with a 4wt% Al_2O_3 - 5wt% Y_2O_3 LPS aid.

A comparison revealed that the monolithic Si_3N_4 Al_2O_3 - Y_2O_3 composites reached the highest relative density, highest Vickers hardness and relatively low fracture toughness values. The SPS densification curves showed that the monolithic Si_3N_4 composites reached full densification at 1550°C when applying 60MPa. Rapid densification was initiated at 1200°C, with a maximum shrinkage rate at 1350°C; beyond 1650°C, with a dwell time of 1 min, no further densification occurred.

However, the composites prepared with 30vol% 2µm and 30vol% 30µm diamond powders sintered with the aid of 4wt% Al_2O_3 and 5wt% Y_2O_3 LPS sintering aids had substantially reduced relative density, especially the 2µm diamond grade. The maximum shrinkage rate was reached at 1350°C and densification continued throughout the 4 min dwell time. The significant density decreases at 1750°C for the 30vol% diamond Si_3N_4 composites, were due to the graphitisation and increase of volume by 50%. Diamond additions retarded densification, hardness was compromised due to the graphitisation of the interfaces and K_{ic} improved due to the graphitic interfaces.

2.2.2.7. Diamond – WC-Co composites

Some diamond composites are prepared using cemented carbides matrix and sintered at low pressures. Cemented carbides are used because their mechanical properties can be manipulated over a broad range by changing the content of the binding Co phase and the WC grain size (Grzonka et al., 2015). Experimentally, WC (1.9µm)-10wt% of Co powder (1.4µm) was wet ball milled for 15 hours. Thereafter, the WC-10wt%Co powder and 20wt% of diamond (10µm) were dry ball milled for 2 hours. These powders were sintered between 970°C-1270°C under 41MPa pressure with a 3 minutes dwell time. The SPS sintering technique was used to reduce the exposure time of diamond to high temperatures without the compromising graphitisation process. Diamond particles were coated with a SiC layer to avoid contact with molten Co during sintering (Moriguchi, Tsuzuki, & Ikegaya, 2001). These diamonds, dispersed within the cemented carbides matrix, resulted in composites with high hardness of 16GPa and the fracture toughness was 50% higher than conventional cemented carbides materials. The fracture toughness was confirmed by the crack propagation behaviour (Moriguchi et al., 2007).

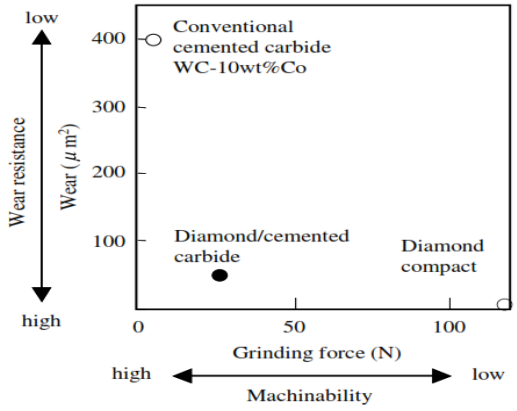

Figure 4: Relationship between wear resistance and machinability with changing the composite diamond and cemented carbide composition (Moriguchi et al., 2007)

Cemented carbides with diamond particles coated with a SiC layer exhibited five times higher machinability than diamond compacts, as shown in figure 4. In conclusion, the cemented diamond-dispersed carbides were produced with superior properties than conventional cemented carbides.

Table 3 shows the mechanical properties of diamond non-oxide ceramic composites with their respective key mechanical properties i.e. hardness and fracture toughness. These properties were tested under different conditions; the sources are contained within the table for referencing and further study of the experimental procedures followed to achieve all the properties listed below.

Table 3: Diamond particle composites sintered with hard ceramics as sintering aids

Composite material	Sintering conditions	Hardness (GPa)	Fracture toughness (MPa•$m^{1/2}$)	Reference
Diamond-SiC	1400°C - 2000°C, .7.7 GPa ~1527°C, 5 GPa	51 GPa 60 – 80 GPa	10 MPa.$m^{1/2}$ 8 – 12 MPa.$m^{1/2}$	(Ekimov et al., 2000) (Zhao et al., 2004) (Zhu, Lang, & Ma, 2012)
Low pressure diamond SiC	1450°C - 1550°C, 50MPa 1400°C - 150°C, pressure less infiltration	11GPa (Knoop micro-hardness) <35GPa		(Mlungwane, 2009)
Diamond-Si_3N_4	1550°C - 1750°C, 100 MPa	8 GPa – 16 GPa	3 – 10 MPa.$m^{1/2}$	(Huang et al., 2013)
Diamond-WC -Co	1350°C, 100 MPa	16 – 23 GPa	~15 MPa.$m^{1/2}$	(Moriguchi et al., 2007) (Michalski & Rosiński, 2008) (H. C. Kim, Jeong, Shon, Ko, & Doh, 2007)

Diamond-SiC composites reached the highest hardness followed by the diamond dispersed cemented carbides and diamond-Si_3N_4 composites with the lowest hardness. Diamond WC-Co composites defied the inverse relationship between hardness and fracture toughness due to the high values reported in table 3.

2.2.3. Mechanical properties of diamond composites

2.2.3.1. Hardness

Hardness is a measure of a material's resistance to plastic deformation. Indentation hardness testing investigates the mechanical properties of materials in general and, in the case of composite ones such as diamond composites, gives an indication of their microstructural features (Gong, Wu, & Guan, 1999). This property is influenced by the volume fractions of the various constituent phases, the relative density of the composite and the grain size distributions. High hardness of diamond composites can be lowered or compromised by the (i) sintering parameters that expose diamond to oxidation and therefore graphitisation, and (ii) thermal stability of the binder phase. Vickers is the most commonly used indentor geometry for measuring a material's hardness (Gong et al., 1999). Diamond-8.9wt%Co was consolidated *in situ* on a WC-10wt%Co substrate and sintered at 1300°C, 1400ºC and 1500°C and at a pressure of 5.8GPa under vacuum for 1 hr. Sample A, sample B and sample C were produced at these conditions respectively. Sample A reached a hardness of 2500kg/mm^2 and samples B and C both

reached similar hardness values of~ 7000kg/mm^2. At 1400°C and 1500°C diamond partially converted into graphite and dissolved in the molten cobalt; it then precipitated out of the cobalt melt as diamond leading to strong interfacial bonding between the diamond grains themselves as well as to the cobalt phase on solidification. Sample A was examined by Raman spectroscopy and no graphite was observed. Therefore, no surface graphitisation occurred at 1300°C, 5.8GPa which could cause poor interfacial bonding and low hardness. Further sintering tests were performed at 1400°C/5.8GPa, with diamond sizes of 0-1µm -8.9wt%Co and 5-12µm-8.9 wt%Co to investigate the effect of diamond grain size on surface graphitisation. It was proven that the highest hardness values were possible at these conditions and that the eutectic point of diamond-cobalt falls slightly below 1400°C. Therefore, sufficient graphitisation can be achieved to facilitate carbon transfer during sintering. Coarse diamond powder (5-12µm) reached hardness of 2500kg/mm^2 and fine diamond grade (0-1µm) reached a high hardness above 7000kg/mm^2. The extreme differences in hardness between the diamond-WC-Co size range powders may be due to the difficulty of coarse diamond powder to transform to graphite during sintering interrupting the reconversion of the graphite into diamond through a solution re-precipitation process that results in strong diamond-diamond bonds (Akaishi et al., 1982). Therefore, hardness is affected by the size of the diamond particles; fine diamond particles react readily to reconversion reactions that form stronger diamond-diamond bonds. However, Katzman and Libby successfully liquid phase sintered 20vol% cobalt (Co)-diamond (1µm - 5µm) at 6.2GPa and 1590°C and the sintered compact reportedly possessed a high hardness (Katzman & Libby, 1971). In addition, the liquid phase sintering above the Berman Simon line gives inter-grown diamond grains through the solution re-precipitation process. The composite produced from this process is then a very hard-tough-strong PCD.

2.2.3.2. Fracture toughness, K_{1C}

Fracture toughness, K_{1C}, describes the ability of a material containing a crack to resist further fracture (Droty, Dauskardt, Kant, & Ritchie, 1995). One of the ways used to measure K_{1C} is by using Vickers/Knoop indentation-based methods or the Hertzian test, using a blunt diamond indenter (Field, 1983). Diamond is known for its extreme hardness but possesses low fracture toughness. This inverse relationship is also applicable to various other hard materials such as WC. Incorporating secondary binder phases (e.g. metals) into the sintering process may result in radically improved toughness if the new phase is ductile. Thus, metallic binders within the diamond composites may improve fracture toughness. In addition, fracture toughness is grain-size dependent. This relationship has been demonstrated in several investigations. Rice et al. (Rice, Freiman, & Becher, 1981) and (Rice, 1984) assumed that changes in the fracture surface energy could be attributed to thermal expansion mismatches between diamond and cobalt. The large difference creates and propagates cracks in the

diamond/cobalt interface. Additional factors which influence fracture toughness include impurities, amount and size of the second phase and amount of plastic deformation in diamond grains. PCDs have low impact resistance due to the extremely high stiffness and low strain to failure of diamond causing fracturing and spalling during machining. To alleviate this brittleness, metallic (and subsequently cermet) backing was incorporated into the synthesis of PCDs (US4604106, 1985). PCDs are designed to make drill bits for oil and gas drilling and are therefore required to possess good fracture toughness to avoid incurring costs during the drilling operation.

2.2.3.3. Wear resistance

Wear resistance is the ability of a material to resist removal of material from the surface by sliding or rolling contact against a counter surface. Wear is classified by wear mechanism and these mechanisms include adhesive wear, abrasive wear, wear caused by surface fatigue and wear caused by tribological reactions (Axén, Hogmark, & Jacobson, 2000). The wear behaviour of PCDs is very complex due to the presence of a binder catalyst and randomly oriented diamond crystallites of different particle sizes. This complexity makes PCDs suitable for use in turning, sawing and drilling operations. Random crystallographic orientation arrangements within PCDs result in a very isotropic abrasion-resistant material. Removal rates obtained using a cast iron scaife are very low compared to removal rates using a bonded wheel (Hitchiner, Wilks, & Wilks, 1984). Shock resistance and wear resistance increase with a decrease in grain size, reports Kingery (Kingery, Bowen, & Uhlmann, 1976) and (Horton & Horton, 1985), respectively. However, under extremely high wear conditions, coarse-grained PCDs were more wear resistant than finer grained PCDs. Fine grained composites are more resistant to abrasive wear.

2.2.3.4. Erosion resistance

Because of their superior erosion resistance, diamonds have been recognised as potential bearing materials for space aircraft applications. Techniques such as the CVD have been applied because they make it possible to deposit diamond films on large substrates (Feng, Tzeng, & Field, 1992). Studies have shown that all forms of diamond have been used in erosive environments, and erosion resistance of bulk diamond and PCDs are the highest recorded. However, the erosion resistance of CVD diamond continues to improve (Nazare & Neves, 1999). The two diamond forms (CVD and PCD) presented in table 4 highlight some important differences in behaviour between the free-standing CVD diamond and single crystal diamond, when subjected to the erosion conditions listed.

Table 4: Erosion by quartz particles of 300-600μm diameter (Nazare & Neves, 1999)

	Single crystal diamond	Free-standing CVD diamond
Removal mechanism	Multiple intersections of ring cracks	Intersection of ring cracks plus grain pull-out and chipping
Example erosion rate at 114 m s^{-1}/mg kg^{-1}	0.04 ±0.01 for {100} face	2.3 ±0.1*
Velocity exponent, n ($E=kV^n$)	1.0 ±0.05	3.3 ±0.3*

*Note that the erosion of CVD diamond varies with sample quality, grain size and growth orientation.

Rain erosion has been a major concern for aircraft and missile manufacturers since World War II. Rain erosion during flight can cause damage to aircraft over time. In addition, diamond is being considered as an "IR" window material in aircraft and missile applications. PCDs are also a potential material for these applications, especially in areas where transparency is not a concern. Applications using diamond are then designed to curb the erosive effects on aircraft. The impact of these particles on moving blades, valve constrictions, pipe joints and bends, as well as other surfaces, is severe and costly. However, due to diamond erosion resistance these damages can be alleviated.

2.2.4. Thermal properties of diamond composites

Synthetic diamond has a high thermal conductivity of ~2200W/(m.K) that assists thermal management during tool application. Diamond also has a low thermal expansion coefficient of ~1.11×10^{-6} K^{-1}. These properties significantly affect the performance of the composites, with considerable impact from the secondary binder phases within the diamond composites. Diamond composites are used in applications that generate high temperatures and therefore these thermal properties are critical to the operational performance of diamond composites (Kidalov S.V., 2009). Table 5 shows various materials that are commonly used as binders during sintering of diamond composites, with their respective thermal properties. These thermal properties affect the overall properties of the diamond composites.

Table 5: Thermal properties of diamond and other hard materials at room temperature(Kidalov & Shakhov, 2009)

Material	Thermal conductivity, λ, W/(m•K)	Thermal expansion coefficient, $\alpha \cdot 10^6$, K^{-1}
Synthetic Diamond (c)	1000-2200	1.1.
Silicon (Si)	153	3.8
Aluminium Nitride (AlN)	280-400	3.8
Copper (Cu)	380	16.5
Silver (Au)	420	19.8
Aluminium (Al)	240	22
Tungsten carbide (WC)	110 *	5.5 *
Cobalt (Co)	100 *	4.9 *
Silicon carbide (SiC)	155**	5.6**
Titanium carbide (TiC)	110**	7.7**

*- (Morrell R., 2015)

** - (MATBASE)

2.2.4.1. Thermal conductivity of diamond composites

Natural diamond has a thermal conductivity of ~2200W/(m.K) due to strong covalent bonds and low phonon scattering. Diamond composites possess relatively low thermal conductivity, compared to synthetic diamond, because binders affect this property by decreasing it, based on Maxwell's model (Kidalov S.V., 2009). Binders can also reduce thermal conductivities with increased interfacial area and low thermal conductance between the binder and diamond particles (Mizuuchi et al., 2015). Maxwell's model assumes the filler (diamond) has a spherical shape and that the volume fraction of particles in the binder is not large. It also disregards the thermal resistance generated at the filler-binder boundary interface and non-spherical filler particles (Kidalov S.V., 2009). However, Maxwell's formula is valid only for a maximum of 25vol% of the filler (Pietrak K., 2015) and therefore is applicable only in the cases of low diamond volume fraction. Outside the stated scenarios, The Hasselman-Johnson (Eq 2.1) model has been used to evaluate the thermal conductivity for various materials, including metal-matric composites, ceramics, and foods (Hasselman D.P.H., 1987). This model emphasized that the effectiveness of thermal conductivity depends on the filler volume fraction and its particle size (Mizuuchi et al., 2015).

$$k = k_m \left(\frac{2\left(\frac{k_d}{k_m} - \frac{k_d}{ah_c} - 1\right)V_d + \frac{k_d}{k_m} + \frac{2k_d}{ah_c} + 2}{\left(1 - \frac{k_d}{k_m} + \frac{k_d}{ah_c}\right)V_d + \frac{k_d}{k_m} + \frac{2k_d}{ah_c} + 2} \right)$$

Equation 2. 1. (Mizuuchi et al., 2015)

Where:

k = thermal conductivity of the composite

k_d = thermal conductivity of dispersions (diamond)

k_m = thermal conductivity of the matrix

a = radius of the dispersed phase

h_c = boundary conductance.

However, if perfect bonding between diamond particles and the Al matrix is assumed, h_c becomes ∞ and equation 2.1. becomes the Maxwell-Eucken equation below:

$$k = k_m \times \left(\frac{2(\frac{k_d}{k_m} - 1)V_d + \frac{k_d}{k_m} + 2}{(1 - \frac{k_d}{k_m})V_d + \frac{k_d}{k_m} + 2} \right)$$

Equation 2.2: (Mizuuchi et al., 2015)

Where: V_d volume fraction of the dispersions. This equation is used to evaluate the effect of consolidation for the Al-matrix composites. Mizuuchi et al. compared the thermal conductivity of monomodal diamond composites to bimodal diamond composites using a Si dispersed Ag matrix. It was found that the monomodal diamond composites experienced an increase in thermal conductivity with increasing the diamond volume fraction up to 50vol% (Mizuuchi et al., 2015). However, the thermal conductivity decreased with a diamond volume fraction higher than 50vol% due to decreased relative packing density. A different behaviour was observed in bimodal diamond composites. In bimodal diamond composites, thermal conductivity increased with increasing diamond volume fraction. Bimodal diamond composites of an increasing diamond fraction (55vol%, 60vol%, 65vol% and 70vol%) experienced increasing thermal conductivities of 455W/(m.K), 530W/(m.K), 581W/(m.K) and 578W/(m.K) respectively. In comparison, 50vol% bimodal diamond composites exhibited higher thermal conductivities than 50vol% monomodal diamond composites, due to higher packing efficiency in the former. The 35vol%, 40, 45 and 50vol% of the diamond volume compositions reached thermal conductivity of 407, 458, 503 and 552W/m K respectively.

2.2.4.2. Thermal expansion coefficient

The thermal expansion coefficient (CTE) is the fraction by which a material expands per degree of temperature. The coefficients of thermal expansion depend on bond strength between atoms that constitute the materials (Kyocera International Inc, 1994). Materials with high bond strength typically have low a thermal expansion coefficient e.g. SiC, diamond and Si_3N_4 and materials such as stainless steel, possess weaker bonds between atoms and therefore result in a higher coefficient of thermal expansion than ceramics. The thermal expansion coefficient of a composite material is calculated by the Kerner equation (Kerner E.H., 1956) and Turner model (Turner P.S., 1946). The Kerner model is more applicable to actual case studies, because it considers the shear effects at the boundaries between the binder and the filler particles and therefore has been used widely for theoretical evaluations of CTEs of composite materials.

The Kerner model uses equation 2.3. to calculate the coefficient if thermal expansion of the composite.

$$\alpha_c = \alpha_m \cdot V_m + \alpha_d V_d + V_d V_m(\alpha_d - \alpha_m) \times \frac{K_d - K_m}{V_m K_m + V_d K_d + (3K_d K_m / 4G_m)}$$

Equation 2.3 (Kerner E.H., 1956)

Where:

α_c = coefficient of the composite

α_d = coefficient of the dispersions (diamond 2.3×10^{-6} K^{-1}),

α_m = coefficient of the matrix,

V_m = volume of the matrix,

K_d = bulk modulus of the dispersions (3.6×10^{11} Pa),

K_m = bulk modulus of the matrix and the

G_m = shear modulus of the matrix

2.3. Sintering

Sintering is a process that thermally transforms powder particles into dense, solid structures through mass transport mechanisms. This technique influences the microstructure of the final materials, their density and their mechanical properties. The beneficial uses of sintering include fabrication of complex, high performance shapes such as medical implants, powder metallurgical parts and bulk ceramic

components for different applications in industry. Materials that can be sintered are metals, ceramics, composites, glasses, alloys etc. Sintering models include variable parameters such as particle size, surface area, temperature and pressure, time and sintering atmosphere (S.-J. L. Kang, 2004) and (German, 2010).

2.3.1. Sintering driving forces

The driving force of sintering is the curvature of the particle system and the reduction in the overall interfacial energy of the powder compacts, where the overall interfacial energy is defined as the product of specific surface (γ) energy and total surface (A) area of the compact. The total reduction in the overall interfacial energy can be expressed as:

$$\Delta(\gamma A) = \Delta\gamma A + \gamma\Delta A$$

Equation 2.4. (German, 2010)

The change in the interfacial energy that occurs during sintering is caused by densification and the changes in surface area energy are due to grain coarsening and replacement of the grain interfaces from solid-air to solid-solid.

2.3.2. Mechanisms of sintering

The atomic densifying pathways during sintering include surface diffusion, lattice diffusion (from the surface), vapour transport, grain boundary diffusion, lattice diffusion (from the grain boundary) and plastic flow (by dislocation motion) as illustrated in figure 5, which are enhanced during sintering for the particle centres to move closer to one another, form bonds and reach full densification.

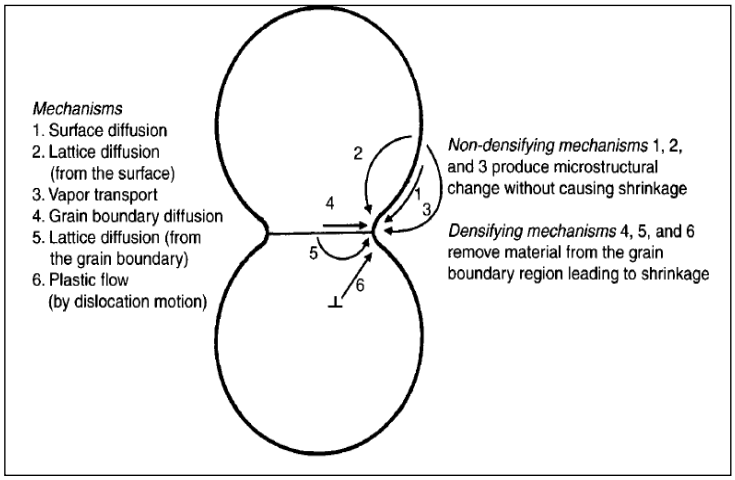

Figure 5: Illustrations of mass transport mechanisms that occur between two particles during sintering (Sōmiya et al., 2003)

These mechanisms allow neck growth, shrinkage and particle deformation to occur, enhancing densification, especially in the production of ceramics with high density (Sōmiya et al., 2003). The final stage begins at approximately 93-95% of theoretical density, when porosity is already isolated. Ideally, at this stage, all pores should be eventually eliminated.

2.3.3. Liquid phase sintering

Liquid phase sintering (LPS) is a consolidation technique that occurs when a powder sample is sintered in the presence of a wetting material that forms a liquid at sintering temperature. Ideally, the liquid phase should exhibit complete wetting of the solid phase. The solid grains should at least be partially soluble in the liquid in order to facilitate material transfer and pull the solid grains together (S.-M. Lee & Kang, 1998) and (German, Suri, & Park, 2009). The liquid phase has an influence on microstructural development, phase composition and properties and serves several essential roles such as accelerating the densification rates, facilitating mass transport, reducing grain growth and lowering the sintering temperature. Microstructural changes during the liquid phase sintering occur rapidly due to the fast material transfer by the liquid (S.-J. L. Kang, 2004).

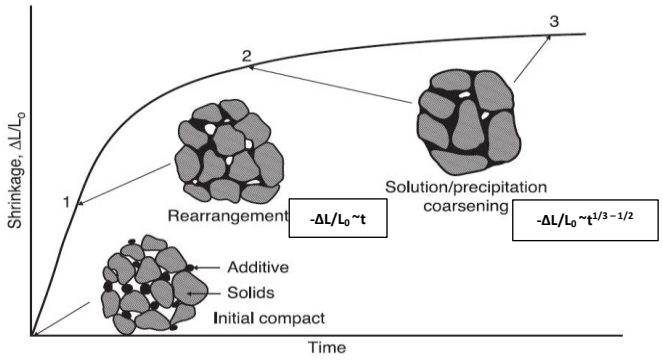

Figure 6: Depiction of the sequence stages that occur during liquid phase sintering (German et al., 2009)

For complete densification to be achieved, the following three steps must occur:

(i). Liquid phase forms through heating of a powder mixture. Particle rearrangement of the solid grains is driven by the capillary forces that are generated by the capillary pressure difference between coarse and fine channels of solid particles respectively (S.-J. L. Kang, 2004). Initial densification occurs at this stage due to the liquid inducing re-arrangement, improving packing efficiency and filling up pores. The amount of densification is small

(ii). Increase of the liquid phase volume fraction encourages rapid material transfer by solution reprecipitation, increasing density and particle rearrangement facilitated by liquid flow also contributes to densification (S.-J. L. Kang, 2004). Solution-reprecipitation is dominant when the solid is soluble in the liquid. The final sample is expected to have smaller/no pores between the solid additives as seen in figure 6. The pores diminish in size and number with time during sintering. However, among systems with low intersolubility densification is achieved with regrouping of particles and solid state skeletal densification (German et al., 2009). These stages cover most of the densification with only 5-10% porosity remaining (Sōmiya et al., 2003)

(iii). In the final stage of densification, and depending on the wetting, the formation of a dense and solid skeleton could take place (Boland, 2014). The rise of isolated pores and voids also marks the start of the final stage (Sōmiya et al., 2003). Further densification, usually much slower, occurs where elimination of isolated pores occurs. On cooling, the liquid solidifies forming a microstructure with tailored properties.

Pressure application enhances mass transfer by mechanically moving particle centres close to one another. After LPS, the microstructure contains a dense, solidified network of grains. The volume fraction, particle size, shape and distribution affect properties such as hardness, strength and elastic modulus of the material sintered. This technique is used for sintering hard materials that cannot be fabricated by other manufacturing techniques (German et al., 2009).

2.3.3.1. Sintering of rigid inclusions

Particulates, whiskers and platelets are included as sintering components to enhance the properties of materials. However, these inclusions can, at times, introduce inhomogeneities in powder systems and cause severe problems such as lowering of densification rate and anisotropic shrinkage. Retardation is more severe in polycrystalline matrices than in glass matrices (Rahaman, 2003). Hard components that are commonly regarded as rigid inclusions are an essential component in the fabrication and production of superhard materials-containing composites to achieve high hardness. However, hard components sometimes behave as rigid inclusions during densification, and a high volume fraction of these incompressible particulates leads to lower densification rates and production of materials with poor properties (Rahaman, 2003). Differential densification between the coarser and finer phase, coupled with interactions between the particles in the coarser phase, can severely inhibit densification. A mixture of the coarser and finer particles was seen to result in an increase in packing density (finer particles fill in the interstices of the larger particles). Therefore, the shrinkage required for complete densification is reduced. The width of the particle size distribution benefits the densification during the early stages of sintering, due to the presence of the fine powders with higher driving force for sintering. Later stages of sintering depend on the packing of particles of the green body. Packing controls shrinkage, particularly at the early stages. Two types of particle rearrangement exist: (i). homogenous packing – small pores of narrow size distribution. High final density can be achieved, regardless of the width of the initial particle size distribution, emphasizing the importance of pore structure. (ii). Heterogeneous packing – increase in width is expected to have detrimental effects on differential densification and grain growth (due to enhanced driving force arising from size difference) so that density decreases. Homogenous packing is ideal for optimum densification because packing density variations in the green body are passed as heterogeneities that limit the engineering properties. Pressure applied cannot be transmitted uniformly because of the friction between the particles, die walls and particles themselves. Stress variations lead to density variations. Mechanical compaction provides far less control in the manipulation of the green body microstructure. Sintering methods such as SPS, Hot Isostatic pressing (HIP) and Hot Pressing (HP) have also been observed to reduce the stresses, as well as using a matrix with low viscosity at the sintering temperature, or a liquid phase sintering system with a high amount of liquid (Herrmann et al., 2012). The amount of the hard component (e.g. c-BN or diamond) that can be used in composite dense materials is limited to 30vol%. Higher volume fractions of 50vol% - 70vol% can be attained with dense materials using multimodal hard components, or the hard component partially dissolves in the matrix and reacts with it to precipitate the thermodynamically metastable phase. Apart from liquid phase sintering that was considered as a technique that also alleviated the stresses generated during differential densification, the infiltration method was found to produce dense materials with even higher diamond volume fraction, 80vol% - 90vol% without the cost of ultra-high

pressure application due to the presence of the liquid that relaxed or alleviated the stresses generated by anisotropic shrinkage, (Ihle, Herrmann, & Adler, 2005), (Mlungwane et al., 2008) and (Gordeev et al., 2001).

2.3.3.2. Liquid phase sintering of non-oxides ceramics with oxide additives

The Y_2O_3-Al_2O_3-SiO_2 system is used as a liquid phase sintering aid to produce structural ceramics such as Si_3N_4, SiC and SiAlON etc. (Arita I., Wilkinson D.S., Purdy G.R., 1992). Both, SiC and Si_3N_4 possess strong covalent bonds that are rendered useful in many technological applications. However, these strong covalent bonds interfere with the sintering f these ceramics.

Therefore, it is important to find alternative sintering methods that will improve sintering of these strong ceramics and produce high performance materials. In this section, we will look at the liquid phase sintering processes facilitated by the yttria alumina silica system (low temperature melting phase) to produce dense materials from the SiC and Si_3N_4 ceramics.

Si_3N_4 – oxide additives

Si_3N_4 is difficult to sinter by itself because of the strong covalent bongs between Si and N. Therefore, sintering oxides are required to consolidate Si_3N_4 ceramics (Yang, Ohji, & Niihara, 2004). Y_2O_3 is a common additive which reacts with the SiO_2 layer that is sometimes found on the surface of Si_3N_4 particles or SiO_2 that is added as an starting material forms a silicate melt or an oxynitride liquid that promotes rapid sintering to achieve high densities (Ribeiro & Strecker, 2004). The liquid phase sintering of Si_3N_4 process involves dissolution of the alpha phase (α-Si_3N_4) into the liquid and subsequent precipitation of the beta phase (β-Si_3N_4) through the solution-precipitation process (Mitomo & Mizuno, 1986). The reconstructive α-to-β phase transformation provides the driving force for densification (Kingery, 1959). (D.-D. Lee, Kang, Petzow, & Yoon, 1990) investigated and reported that the phase transformation has no effect on the densification of the Si_3N_4 ceramic. The transformation of α-Si_3N_4 to β-Si_3N_4 requires a lattice reconstruction. This type of process occurs when the transforming material is in contact with a solvent (Hampshire, 2007). The greater solubility of the unstable material drives it into solution and precipitates into the less soluble, more stable form. The metal-silicon-oxynitride liquid phase induces phase transformation during sintering under 1400°C temperatures. β-Si_3N_4 grows in the longitudinal direction as prismatic hexagonal rod-like crystals that impinge on each other forming an interlocked microstructure (Hampshire, 2007). The successful liquid phase sintering of Si_3N_4 with Y_2O_3-Al_2O_3 sintering system lead to many groups successfully densifying α-Si_3N_4 and β-Si_3N_4 with these additives(Can, 2006).

Yang et.al conducted a study that employed a fixed Y_2O_3:Al_2O_3 ratio of 5:2 with varying 3.5-14wt% total additive content. The ratio was fixed at 5:2 to maintain the chemistry of the grain-boundary glassy phase (Yang et al., 2004). Three varying mixtures of the oxide additives (in units of wt%) 2.5Y-1.0Al, 5.0Y2.0Al and 10.0Y4.0Al were balled milled with the Si_3N_4 powder for 24h then cold/dry pressed at 200MPa. Pressureless sintering was performed in a graphite resistance furnace at various temperatures ranges of 1300°C-1900°C with a heating rate of 10°- 20°/min. Densification was started at 1450°C and phase transformation began at temperatures above 1500°C. The liquid phase content greatly affected the densification behaviour because the densification was enhanced with increasing additive content. However, phase transformation was unaffected by the additive content. Density declined at temperatures above 1650°C and that is a region where the phase transformation reached completion. However, this occurrence was prominent in lower amounts of sintering additives. From this study, it was observed that densification started at lower temperatures than phase transformation, densification was active only at the beginning of the phase transformation and densification was enhanced by an increased liquid phase additive while phase transformation remained unaffected. Much like our study, this sintering process solely depends on particle rearrangement and solution-precipitation both enhanced by liquid phase formation at grain boundary. The solution-precipitation process does not enhance densification. Phase transformation and grain growth occurred due to solution-precipitation mechanism that was controlled by the interfacial reaction. Additive content had no significant effect on the densification – however, Y_2O_3 had some effect due to its character as a primary network modifier in a Y-Si-O-N glass. Density decreased with increasing sintering temperatures after phase transformation was complete – this was caused by the β-Si_3N_4 grain growth.

Mitomo et.al conducted a pressureless and gas pressure sintering study to investigate the level of densification of Si_3N_4 achieved by each method (Mitomo & Mizuno, 1986). In this study, 5wt% Y_2O_3 and 2wt% Al_2O_3 were employed to sinter Si_3N_4 ceramics at 1750°C-1800°C (pressureless) and 1800°C-1900°C (gas pressure sintering) temperatures. These powders are ball milled and placed in a furnace with carbon rods. Nitrogen pressure applied was 1 atm - 10 atm. Pressureless sintering was performed under 1 atm and gas pressure sintering was performed at 10 atm.

Pressureless sintering of the Si_3N_4 composites

First densification was observed at about 1400°C attributed to the particle rearrangement and solution reprecipitation occurred at 1600°C-1750°C supported by the rapid densification rate observed. The densification of material progressed with the dissolution of α-phase and reprecipitation of β-phase. Density of 71.7% was achieved. Densification stopped at 1800°C although on-set of another densification process could be seen. Larger weight loss resulted in much lower density. Crystalline

phases were detected at the reported temperatures as shown in table 1. Materials sintered at 1750°C and 1800°C achieved similar densities but very different microstructures. Pore growth is exaggerated at 1800°C due to grain growth and the skeleton development that hindered further densification.

Table 6: Pressureless/Gas pressure sintering methods with crystalline phases produced through each method

N_2 pressure (atm)	**Sintering temperature (°C)**	**Crystalline phase**
1 atm (Pressureless sintering)	1750 1800	$Si_3N_4.Y_2O_3$ $Si_3N_4.Y_2O_3 > Y_5(SiO_4)_3N$
10 atm (Gas pressure sintering)	1800 1930 1950 1980	$Y_5(SiO_4)_3N$ α-quartz α-quartz α-quartz – $Y_2Si_2O_7$

Gas pressure sintering of the Si_3N_4 composites

Thermal decomposition was depressed and therefore the density achieved was higher. High density materials (>97%) were obtained at 1930°C-1980°C with maximum density of 99.4% at 1950°C. Density of the material sintered at 1980°C was lower due to the weight loss. Presence of apatite ($Y_5(SiO_4)_3N$) phase was observed at 1800°C and only oxides (quartz or $Y_2Si_2O_7$) at higher temperatures. Breakdown of the densification processes into two processes: liquid phase sintering performed at temperatures below 1750°C (Process I) and liquid phase sintering performed above 1750°C (Process II). A comparative analysis between these processes was presented by Mitomo et.al. Contributions to densification of each of these processes was analysed. Process I contribution were highest at 1750°C it was the only process conducted at that temperature. Process II achieved further densification. Process II contribution increased up to 1950°C and decreased at 1980°C due to the grain growth. Process II contribution was high at this temperature because stability of the materials depends on the N_2 pressure. Abnormal grain growth is related to densification of process II. Elongated β-Si_3N_4 grains improved the fracture toughness of the materials. High strength materials with bending strength >900MPa were fabricated by the gas sintering method. Therefore, Si_3N_4 should be sintered with 5wt% Y_2O_3 and 2wt% SiO_2 at 1930°C-1980°C under gas pressure sintering in 10 atm N_2.

Sintering of SiC using the oxide additives

Liquid phase sintering of SiC as a means of densifying SiC ceramics was invented by Omori et.al (Omori & Takei, 1982). Methods of sintering of SiC are categorised into two groups. The first group is the bonded silicon carbide materials which are not dense. The high porosity-silicon carbide types (~20vol% open porosity) include Ceramically-bonded Silicon Carbide (CSiC), Recrystallised Silicon Carbide (RSiC) and Reaction-Bonded Silicon Carbide (RBSiC). The second group are the sintered, dense silicon carbide materials. The low porosity-silicon carbide types (less than 2%) include Solid-State Silicon Carbide (SSSiC), Liquid-Phase Sintered Silicon Carbide (LPSSiC) and Silicon-infiltrated Silicon Carbide (SiSiC). We will focus on the low porosity type's examples to align with this study.

The yttria and aluminum hydroxide reactants successfully sintered SiC by pressureless sintering at 2100°C. These additives facilitated densification via liquid phase sintering (Omori & Takei, 1982). SiC has been recognized as a potential material for gas-turbine, turbocharger rotor components, heat exchangers and load bearings exposed to temperatures up to 1500°C, due to their mechanical properties such as low density, high thermal shock resistance, and high resistance to corrosion and oxidation (Negita, 1986). However, their low fracture toughness diminishes the applicability of these ceramics. Due to the strong Si-C covalent bonding and low self-diffusion coefficient, these ceramics have a high hardness of 20-27GPa (Can, 2004) but are difficult to sinter. Solid state sintering of SiC favours coarsening mechanisms, so it is difficult to sinter SiC to full densification. In addition, solid state sintering occurs at much higher temperatures (2000°C – 2100°C) than liquid phase sintering (1800°C - 1900°C) (Can, 2004). Liquid phase sintered silicon carbide (LPS-SiC) at room temperature has double the strength of SSiC ceramics (Sciti D., 2000). The introduction of sintering aids was motivated by this difficulty and their use resulted in the production of ceramics with higher hardness and toughness.

Y_2O_3-Al_2O_3 and AlN-Y_2O_3 are the best-known additives for successfully sintering of SiC. SiC sintered with the AlN-Y_2O_3 system was shown to suppress the decomposition reactions that occurred during sintering by application of a nitrogen overpressure (EP0419271 A2, 1990). Therefore, using the oxides can improve densification of the SiC ceramics and potentially minimise the undesirable chemical reactions that occur during sintering due to their inertness. There are three eutectic phases between Al_2O_3 and Y_2O_3, with the lowest one found at 1760°C between Al_2O_3 and $3Y_2O_3.5Al_2O_3$ (YAG) (She & Ueno, 1999). Kim et al. liquid phase sintered α-SiC phase of 0.6µm with 6:4 mixtures of Al_2O_3 and Y_2O_3 using the hot pressing under argon atmosphere. Sintering was done at 1800°C, 35MPa for 30min (D.-H. Kim & Kim, 1990). The recovered SiC specimens had relative densities ranging between 96% and 99%. Fracture toughness was observed to increase with increasing the Y_2O_3-Al_2O_3 liquid phase volume fraction with an intergranular fracture mode, confirming crack deflection by the liquid phase. The thermal expansion coefficient mismatch between the liquid phase and α-SiC generated residual

strains surrounding the second phase particles. Therefore, the cracks were deflected and fracture toughness of the SiC ceramics was improved. Median deflection angles increased with increasing liquid phase volume fraction exhibiting improved fracture toughness. Y_2O_3-Al_2O_3 has also been reported to cause decomposition reactions during liquid phase sintering of SiC, which compete with sintering processes. Additions of carbon alleviated the decomposition reactions and formed a SiC material with 26GPa micro-hardness (van Dijen & Mayer, 1996). Additions of a powder bed consisting of a course mixture Al_2O_3 and SiC powder have proven to reduce decompositions reactions during sinterings (Winn & Clegg, 2004). Also, this powder bed was able to improve densification from 92% to 98% claiming it was due to diffusion of Al_2O_3 into the samples.

She and Ueno showed that sintering shrinkage of Al_2O_3- and Y_2O_3- doped SiC increased with increasing Al_2O_3-Y_2O_3 content (She & Ueno, 1999). In addition, the contact angle was 4° at 1870°C indicating good wetting between SiC and Al_2O_3-Y_2O_3 and therefore high densification (Taguchi, Motta, Balestra, & Ribeiro, 2004). The SiC infiltrated with Al_2O_3/Y_2O_3 produced ceramics with high hardness of ~20GPa and fracture toughness of ~4.5MPa $m^{1/2}$ (Taguchi, Ribeiro, & Balestra, 2008).

2.3.3.3. Surface wetting

Surface wetting of solid grains by a liquid phase determines the densification during sintering. This process is governed by the interfacial reactions that occur between the solid grain and the liquid during sintering. Young's contact angle, $\boldsymbol{\theta_Y}$, is the degree of wetting measurement between the solid-vapour-liquid system (Sobczak N., Singh M., Asthana R., 2005). Figure 7 illustrates the difference in the contact angle between the wetting and non – wetting environment.

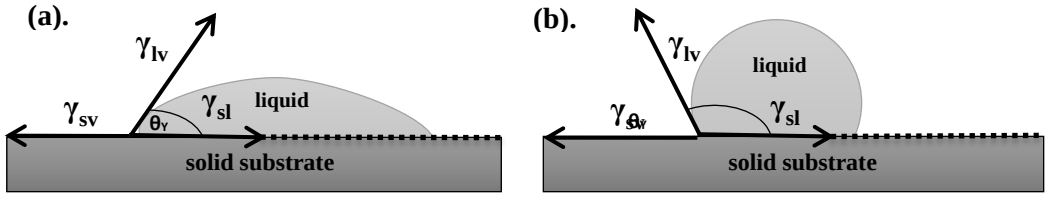

Figure 7: Triple line diagram showing interfacial energies with (a). low contact angle due to complete wetting and (b). a large contact angle due to low wetting

The driving force Fd (*t*) for wetting is given by the equation below:

$$\mathbf{Fd}(t) = \gamma_{sv} - (\gamma_{sl} + \gamma_{lv}\,\mathbf{Cos}\theta(t))$$

Equation 2. 5. (Kumar G., 2007)

Where:

θ_Y = Young's contact angle

$\boldsymbol{\gamma_{ab}}$ = indicates interfacial energies between the solid (s), liquid (l) and vapour (v) phases, that form an interface at the triple point

At equilibrium, Fd(*t*) = 0 and therefore Young's equation can be defined as:

$$\gamma_{sv} = \gamma_{sl} + \gamma_{lv}\cos\theta$$

Equation 2.6. (Kumar G., 2007)

The work of adhesion, $\boldsymbol{W_{sl}}$, between the solid and liquid is defined by the Young - Dupre's equation given below:

$$W_{sl} = \gamma_{sv} + \gamma_{lv} - \gamma_{sl}$$

Equation 2.7. (Kumar G., 2007)

The derivatives of the Young's equation (eq. 2.6) and Young - Dupre's equation (eq. 2.7) were formulated under the assumptions of a spreading liquid during non-reactive wetting (Kumar G., 2007). The work of adhesion, $\boldsymbol{W_{sl}}$, is a parameter that characterises the thermodynamic stability of the interfaces between different materials, and predicts the material's potential to bond with another (Sobczak N., Singh M., Asthana R., 2005). The liquid/substrate wettability of surfaces is illustrated in Figure 9.

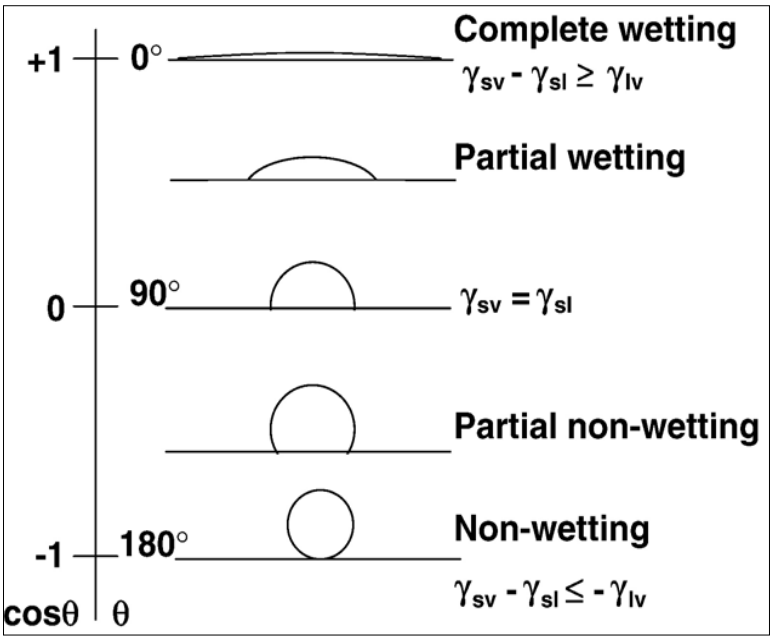

Figure 8: Illustration of the liquid/substrate wettability relationship and the resultant contact angle, θ_Y. (Kumar G., 2007)

The liquid is considered a wetting agent when is forms a contact angle of less than 90° upon contact with the solid substrate. Figure 8 shows the changes in the contact angle with the changing interfacial energies. Complete wetting is achieved when the contact angle is close to zero (Kumar G., 2007). The level of reactivity on the substrate surface can remove wetting barriers thus improving wetting. However, the newly formed product can also be a wetting barrier (Dezellus O., 2010).

2.4. Spark plasma sintering

Spark plasma sintering (SPS) is a rapid sintering method that uses a pulse-activated direct current and uniaxial pressure application that ensure processed materials reach full densification under lower sintering temperatures and reduced grain growth (Xie, Ohashi, Song, Mitsuishi, & Furuya, 2005). The sintering process takes place under vacuum conditions (or controlled atmosphere) and all the heated parts are kept in a water-cooled chamber during the operation (Guillon et al., 2014). The SPS method has also shown improved overall results in the sintered composites and microstructural behaviours, examples of improved properties achieved using the SPS method, cleaner grain boundaries in sintered ceramic materials (Risbud, Groza, & Kim, 1994), a remarkable increase in super plasticity of ceramics (Shen, Peng, & Nygren, 2003), improved bonding quality (Munir, Anselmi-Tamburini, & Ohyanagi, 2006) and reduced impurity segregation at grain boundaries (X. . Chen, Khor, Chan, & Yu, 2004). High heating rates are easily attained due to either internal heating of the sample (if the sample is electrically

conductive) or indirectly through the heating achieved by passing the current through the graphite tooling.

The rapid sintering cycles allow operating control over unwanted reactions/by-products in highly reactive systems. The direct heating allows the application of very high heating and cooling rates and dominance of densification mechanisms over grain coarsening mechanisms (Suarez et al., 2013). The SPS technique also enhances densification through minimised grain coarsening and enhanced particle-to-particle bonding (Mamedov, 2002). SPS technology began in the late 1930s, when a sintering process using electrical energizing energy was introduced in the US. Spark sintering based on the pulsed current applied sintering technique was researched and patented in Japan, in 1960. The SPS technique applications were delayed due to the lack of technology at the time, limited fields, equipment cost and sintering efficiency (Tokita, 1999). Johnson et al. studied plasma sintering of ceramic oxides and reported that using rapid heating rates minimized surface diffusion and increased densification rates (Williams & Johnson, 1982). The final and successful development of the SPS was a result of combined discoveries from previous studies conducted by a number of researchers. Resistance/spark sintering was developed in Korea (Choi, Kim, & Lee, 1992), pulsed electrical discharge sintering with pressure in USSR (Raichenko, Kolchinskii, & Levina, 1976) and plasma sintering in Brazil (Muzart, Batista, Franco, & Klein, 1997). Research into electric field activated sintering commenced in the mid-1980s and early 1990s, leading to development of the second generation of equipment. Development of the spark plasma sintering process increased as third generation equipment was introduced in Japan. The value of this equipment was recognised due to the development of large DC pulse generators of 2000 to 20000A (Tokita, 1999).

2.4.1. Principles of a SPS furnace

The SPS technique has new distinctive features that have shown advantages over conventional sintering techniques such as hot pressing (HP) and hot isostatic pressing (HIP). The SPS system can easily consolidate various types of materials because of the uniform heating applied to the samples being sintered (Tokita M., 1999). Powder is placed in a graphite die and heating is achieved by passing a current through the graphite die (in the case of non-electrically conducting charge) and simultaneously applying pressure to the powder. SPS systems also exhibit advantages over other conventional sintering techniques due to the ease of operation and accurate control of sintering energy as well as high sintering speed and high reproducibility (Suarez et al., 2013).

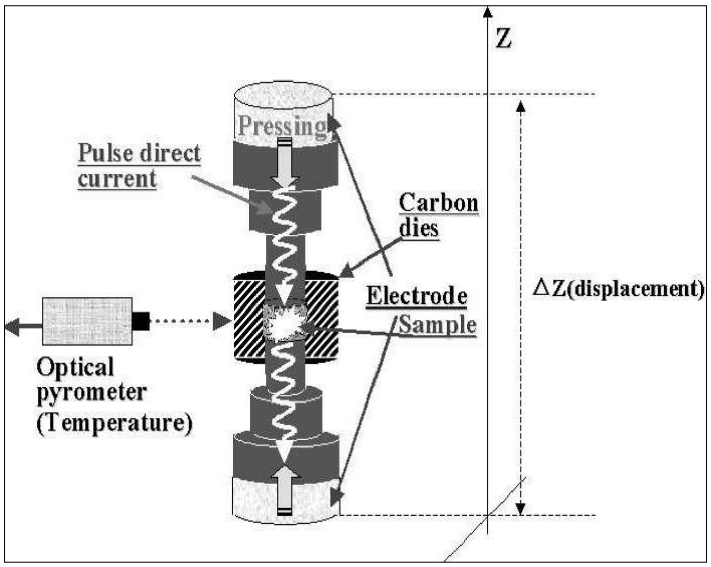

Figure 9: Schematic diagram of the SPS furnace (Yamamoto et al., 2005)

The SPS set-up of the operating parts shown in figure 9 includes a vacuum chamber, punch electrodes, graphite dies, position measuring unit, the DC-pulse sintering powder generator, atmospheric conditions control mechanism, temperature unit, applied pressure display unit, and the vacuum chamber parts that are located close to one another, eliminating the temperature gradient that may occur between samples and the electrodes (Tokita M., 1999). Additionally, the SPS furnace directs the pulse discharge, created by the application of a voltage of about 30V and a current of about 60-1000A, through the electrically conducting graphite pressure dies to the sample, enhancing surface diffusion mechanisms, enlarging contact areas between particles and promoting full densification. The sintering time is determined by the type of material to be sintered. Heat transfer pathways are determined by electric conductivity of a material. Conductive materials are heated by the Joule effect. For non-conductive powders, the heating occurs through the heat transfer from the die and the punches. SPS technique functions through the particle surface activation of the powders and increased diffusion rates on the contact zones of the powder particles caused by the applied pulse current. Electrical resistance experienced during sintering is alleviated with the use of electrically conducting pressure graphite dies, lined with a graphite foil coated with hBN (hexagonal Boron Nitride - insulating material) that, if the powder is electrically conducting, directs the current through the powder, creating the highest possible current density and disintegration of grain boundaries for neck growth and contact areas. Application of pressure enlarges contact areas between grains and reduces the diffusion distance ensuring stress-free neck growth (Mamedov V., 2002).

2.4.2. Spark plasma generation and joule heating

The SPS system achieves high quality sintered compacts at short sintering times with the aid of (i) spark plasma, (ii) spark impact pressure, (iii) Joule heating and (iv). electrical file diffusion effect. During the

SPS process the surface particles are easily purified and activated, promoting material transfer at macro and micro levels (Tokita M., 1999). Heating is achieved by spark discharges in gaps between the powder particles, generated by instantaneous pulsed direct current, which is applied through the electrodes, to the top and bottom punches of the of the graphite die. These discharges purify and activate the surface particles generating a self-heating phenomenon between the particles which will complete mass-transfer and heat-transfer mechanisms instantaneously (Gao, Hong, Miyamoto, & Torre, 2000).

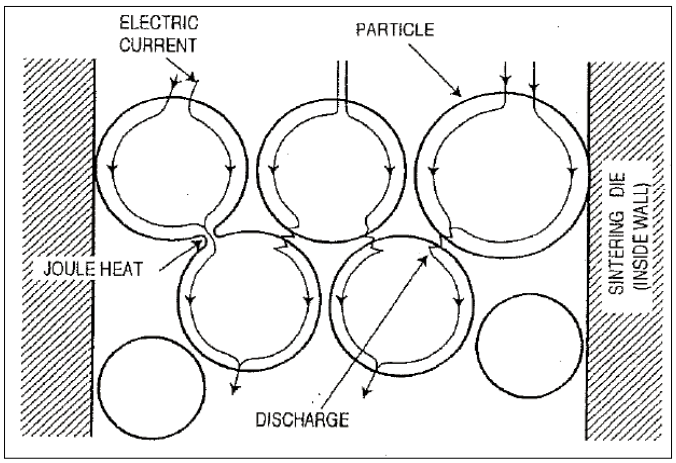

Figure 10: Illustration of the pulsed current flow through loosely packed powder particles (Suarez et al., 2013)

The repeated application of an ON-OFF DC current pulse between the powder particles results in the current being transferred and dispersed through the particles as shown in figure 10, resulting in high densification rates at low power consumption (Fuji Electronic Industrial Co, Ltd,). Joule heating is thus achieved (Rodger, Wells, Moffett, & Bailey, 2001). The counter effect of current flowing through local, resistive points creates a rise in temperature of several to ten thousands of degrees celcius momentarily. (Fuji Electronic Industrial Co, Ltd,).

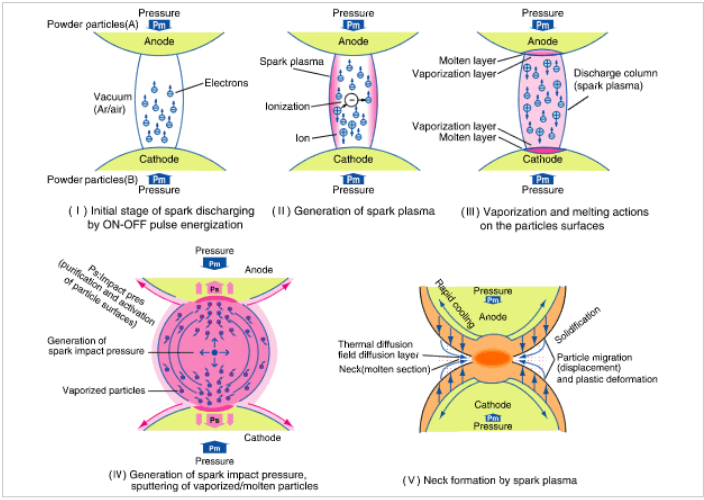

Figure 11: Diagram clearly outlining the sequence of surface diffusion reaction s that occur leading to neck formation (Fuji Electronic Industrial Co, Ltd,)

A sequence of processes that occur during the spark plasma generation until neck formation are illustrated in Figure 11. As temperatures approach critical level - when the temperature causes melting on the particle contact zones, surface diffusion is slowed down (Mamedov V., 2002). These high temperature conditions melt and vaporise the surface of the particles and the necks are formed around the contact area between the particles (Tokita M., 1999).

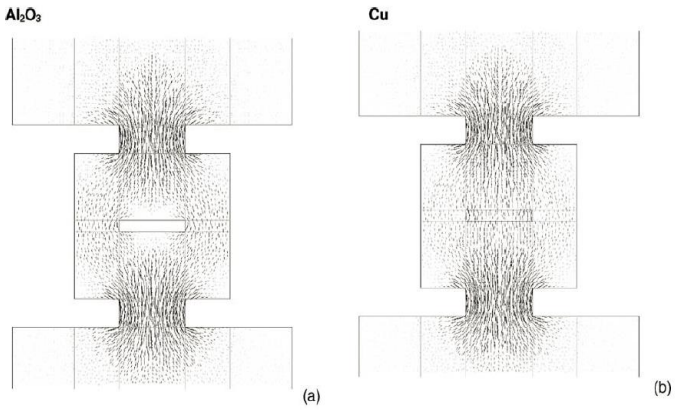

Figure 12: Diagram representing the flow of electrical current through two samples with different electrical conductivities (Anselmi-Tamburini, Gennari, Garay, & Munir, 2005)

Current flow through conductive and non-conductive materials

Anselmi-Tamburini (I) et al. conducted an investigation on current and temperature distribution differences between two materials with different electrical conductivities, using fully dense alumina (non-conductive) and fully dense copper (conductive) during sintering by the SPS (Anselmi-Tamburini et al., 2005). Electrical fields create paths that behave differently as they travel through conductive and

non-conductive materials. Copper temperature rose through direct joule heating of that material, whereareas the temperature of the alumina sample rose by heat being conducted into it from the surrounded graphite tooling, the latter warming up because of Joule heating. (Mamedov V., 2002) and (Guillon et al., 2014). This behaviour can be observed in Figure 12.

2.5. Project Motivation

Diamond composites are derivatives of diamonds, with a second phase/s comprising additional phases, be they metallic or ceramic in nature. Such materials are typically used as sintering aids. Conventionally, PCD materials are produced under HPHT conditions with the aid of diamond-diamond bonding. However, in this study we will bind diamond crystals using an yttrium aluminosilicate matrix under low pressures. Additionally, bimodal diamond powders will be used in order to improve diamond packing efficiency. Pressure is an expensive parameter, though in this work there will be attempts to sinter fully dense materials at pressures 30MPa – 50MPa with sintering temperatures 1200°C-1400°C. The achievement of full densities at low pressure, with the aid of controlling liquid phase compositions and the sintering conditions, will ensure hard and wear resistant PCD materials are manufactured at low costs. In this work, it is proposed to make and study a different type of PCD in which the diamond particles are not fused together via liquid phase sintering, but rather are bound together at relatively low temperatures with the help of a binder. Material made using this method obviates the need to sinter at HPHT conditions thus saving significantly on manufacturing costs.

The matrix resulting from the solidification of the sintering aid will introduce hard, crystalline properties to the composites. Crystalline phases are generally harder than the corresponding amorphous phases. These residual intergranular phases will improve hardness and are also expected to improve fracture toughness. The latter is expected to happen because of the difference in the thermal expansion coefficients of the two main constituents (diamond and the liquid phase) of the composites being proposed for this work (Hyatt & Day, 1987).

2.6. Choice of Liquid Phase sintering Aid and the quantities used in preparing the composites

In this study, the Y_2O_3-Al_2O_3-SiO_2 phase diagram was used to fully understand the LPI and LPII additives behaviour under the reported sintering conditions.

Phase diagram and the liquid phase additives

YAS glasses were selected as liquid phase additives for this study due to their high transition temperatures (giving high thermal stability to the resulting composite) and their ability to accelerate sintering of hard ceramics under reduced temperatures (Arita I., Wilkinson D.S., Purdy G.R., 1992). In addition, these glasses were selected to facilitate solid particle rearrangement under the capillary gradients created by the liquid phase. Particle rearrangement can then take place at lower temperatures, and this can improve densification kinetics (Maître et al., 2008). Successful sintering under low pressures was greatly aided by the liquid phase in facilitating particle rearrangement, to increase the contact area between the diamond and the liquid phase, in order to achieve full densification. The use of a bimodal diamond particle distribution increased the coordination number and minimised the shrinkage required to achieve full densification. The particle distribution enhanced densification rates through the high number of connected grain boundaries. The compositions and temperatures were selected using the phase diagram in order to yield equilibrium liquids (Kwon & Messing, 1990).

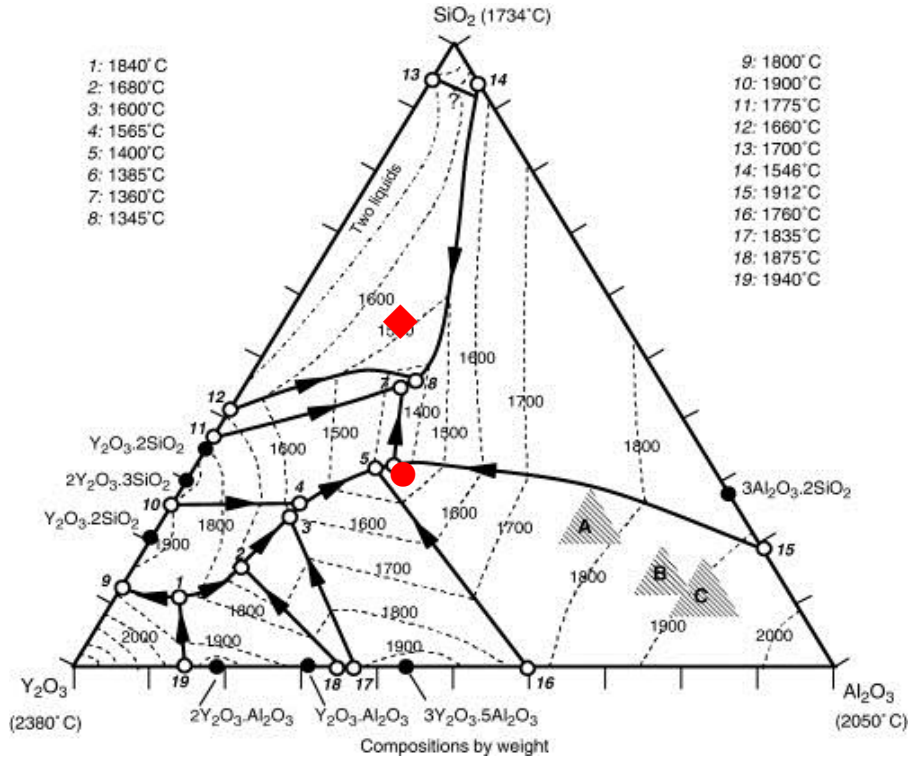

Figure 13: Ternary phase diagrams of the Y_2O_3-Al_2O_3-SiO_2 system (Cock, Shapiro, Todd, & Roberts, 2005) The compositions of LPS aids used in this study are indicated as LPI (●) and LPII (◆)

The diagram in Figure 13 shows the behaviour of the two liquid phases of varying Al_2O_3-Y_2O_3-SiO_2 mixture compositions. There are six possible quasi-binary phases that were reported to form via the YAS glasses: $Y_2Al_4O_9$ (YAM), $YAlO_3$ (YAP), $Y_3Al_5O_{12}$ (YAG), Y_2SiO_5, $Y_2Si_2O_7$ (C and D modifications) and $3Al_2O_3.2SiO_2$ (mullite) (Kolitsch U., Seifert H.J., Ludwig T., Aldinger F., 1999). These glasses have good stiffness and have shown good resistance to oxidation and radiation.

The LPI composition 40wt%Y_2O_3-25wt%Al_2O_3-35wt%SiO_2 formed a eutectic liquid at lower temperatures (~1350°C), and therefore was selected as a promising liquid phase sintering aid that would produce dense composites without exposing diamond to graphitisation. However, this proved to be difficult to achieve due to LPI's inability to sinter dense composites. Therefore, we formulated an additional liquid phase aid (LPII: 25.02wt%Y_2O_3-18.83%Al_2O_3-56.15wt%SiO_2) that would generate sufficient liquid at higher temperatures. The LPII composition formed a eutectic liquid at ~1550°C. Should one use this composition to make diamond-oxide LPS sintering aid composites, the materials derived will possess good thermal stability properties, particularly because the liquid phase compositions are eutectic (Maître et al., 2008). The phase diagram also shows what distinct phases can be formed at thermodynamic equilibrium at the given pressure and temperature.

A sample labelled YAS-6 from the Hyatt et.al study with a 42wt%Y_2O_3-25%Al_2O_3-33wt%SiO_2 composition was reported to possess high density, hardness and refractive index due to the high content of Y_2O_3. It was clear that an additive of similar oxide content would successfully produce a sample with high density and high hardness to fulfil the objectives of this study (Hyatt & Day, 1987).

The LPII additive oxide composition was used in the Wu et al. study (Wu et al., 1990). A sample labelled as YAS-1 in the study, with an oxide content of 25.02wt%Y_2O_3-18.83%Al_2O_3-56.15wt%SiO_2 and a Y/Al molar ratio of 3/5 was prepared by these authors. This Y/Al molar ratio was observed to produce dense materials which are a beneficial feature for this study. Therefore, it was an attractive liquid phase composition for fulfilling the objectives of this study in producing dense diamond composites. This sample was chosen to compare with LPI, and identify the oxides with favourable effects on the properties of the diamond composites.

In sintering monomodal diamond composites, we encountered experimental problems as shown in figure 27 below. The problems were caused by the high liquid volume generated by melted LPI during sintering – therefore, the liquid escaped from the graphite dies. The monomodal diamond composites also used in trial and error sintering runs to help identify the sintering regions that produced the highest densities. When the liquid phase additive volume fraction was reduced from 75vol% to 40vol% we successfully sintered diamond composites without the dies breaking. This then informed the decision to only sinter using 40vol% liquid phase volume fraction of both LPI and LPII additives. At conditions beyond 1500°C/30MPa – graphite dies used to make bimodal diamond composites with started breaking. Therefore, we concluded the bimodal diamond composites experiments at 1500°C/30MPa. The reason for this occurrence was not identified during the study.

Chapter 3

EXPERIMENTAL PROCEDURE

This chapter describes the experimental procedures followed in order to produce the powders that make up the various liquid phase sintering aids, the steps involved in mixing these with the various diamond powders, the sintering process and finally the characterization and evaluation of the sintered compacts. All the steps required to accomplish the processes mentioned above are given below.

3.1. Starting materials and their characterisation

All the raw materials used in this project, the particle size distributions and suppliers of the as- received powders are listed in Table 7.

Table 7: Particle size distribution of raw starting materials and their respective suppliers (location)

POWDER	D(0.1) µm	D(0.5) µm	D(0.9) µm	Supplier
Alumina	0.122	0.202	1.792	Sumitomo, South Africa
Yttria	1.756	4.370	14.861	Sigma Aldrich, South Africa
Silica anhydrous	9.745	28.301	84.546	Sigma Aldrich, South Africa
Diamond M0-1	0.165	0.390	0.924	Element6, Micron+, India
Diamond M3-6	1.733	2.866	4.774	Element6, Micron+, India
Diamond M20-30	13.518	18.590	26.654	Element6, Micron+, India

Initial powder materials were analysed using a particle size analyser to confirm particle size distribution, X-Ray Diffraction (XRD) in order to confirm phase composition, Scanning Electron Microscopy (SEM) to confirm particle size distribution examine particle morphology and detect impurities. Information thus collected is presented in Chapter 4.

Sample nomenclature of the diamond composites

The naming system denotes:

d = monomodal diamond composite

D = bimodal diamond composite

LPI= liquid phase additive **I** (40wt%Y_2O_3-25wt%Al_2O_3-35wt%SiO_2)

LPII= liquid phase additive **II** (30.78wt%Y_2O_3-13.65wt%Al_2O_3-55.58wt%SiO_2)

Sintering conditions are denoted as:

1300-30 = sintering temperature of 1300°C under 30MPa.

Therefore, a monomodal diamond composite of 60vol% diamond, sintered using the LPI additive at 1400°C under 50MPa will be shown as d60LPI/1400-50. A bimodal diamond composite with 50vol% diamond, sintered using LPII at 1400°C under 50MPa will be shown as D50LPII/1400-50.

3.2. Experimental apparatus

Table 8: Equipment used during the project

Equipment	Model, supplier and location
Particle size analyser	Malvern Mastersizer 2000
Planetary ball mill	FRITSCH Pulverisette 6
Rotary Evaporator	Heidolph Laborata 4010 digital
Sieving machine (sieve pots)	Retsch AS 200
Turbula mixer	WAB Turbula System Schatz
Spark Plasma Sintering furnace	HP D5 FCT Systeme GmBH
TGA/DSC dual equipment	Netszch 449 F3 Jupiter Simultaneous thermal analyser
Sandblaster	Adendorff Machinery Mart
Density measurements balance scale	Sartorius ED224S Extend
Drying oven	LABOTEC Ecotherm
Fracture equipment/ computer program	Tinius Olsen, Type: DBBSTOL-50kN
Grinding/Polishing machine	SPECTRUM SYSTEM 2000, Leco
Sample mounting machine	Struer CitoPress-10
X – ray Diffractometer	D2 - Phaser Xray Diffractometer
Scanning Electron Microscope	Carl ZEISS Sigma, Oxford x-act EDS detector
Hardness Tester (bulk)	FUTURETECH FV – 80, Vickers Hardness Tester

3.3. Powder processing

Powder processing consists of two stages that serve the purpose of (a) reduction of particle size range, and (b) disperse the diamond into the liquid phase oxides before sintering. The planetary ball mill and the turbula mixer apparatus are known to create uniform powders out of the extremely different particles such as refractory oxides and synthetic diamond (Bauman, Ćurić, & Boban, 2008). Therefore, these instruments were utilised during powder processing in order to achieve efficient milling and homogeneity of a multicomponent powder system.

3.3.1. Milling of the oxides

The Al_2O_3, Y_2O_3 and SiO_2 (YAS) powder mixtures of the compositions investigated here were milled using a planetary ball mill (FRITSCH Pulverisette 6) for 3 hours at a speed of 200 rpm. The oxide powders were milled using 200ml of hexane solvent with the aid of ϕ 2mm alumina balls. All the milling parameters details are listed in Table 9. The oxide powder to the 2mm alumina balls mass ratio was 1:5. Adequate mixing was a priority over particle size reduction.

Table 9: Milling parameters

Milling pot	250ml, WC
Milling balls	2mm ϕ alumina balls
Solvent	Hexane (200ml)
Mass of powder	20g
Milling time	3 hours
Milling speed	200rpm

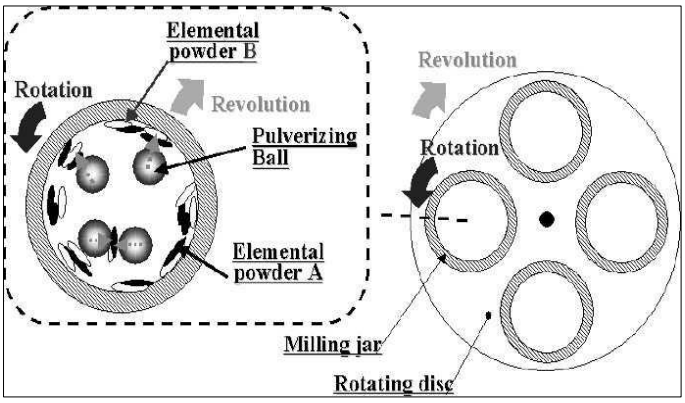

Figure 14: Planetary ball milling mechanism (Yamamoto et al., 2005)

The planetary ball milling process created collision and friction between the milling balls and the powders milled. The pot is placed onto of a rotating disc as shown in figure 14 to enhance the possibility of collision between the inner walls of the pot, tungsten milling balls and the material itself for enhanced milling.

3.3.1.1. Drying and sieving

The milled slurry, together with the milling balls, was collected into a 250ml round bottom flask, and the suspension was dried using a ROTVAP. Drying was performed at 65ºC (the boiling point of the solvent is significantly lower under vacuum) and at a rotating speed of 60rpm. Powder was then stored

in an oven (below 60ºC) overnight to dry completely. Traces of WC contaminants were detected by the XRD and were caused by erosion of the inner lining of the milling pot by balls during milling. The dried milled powder was transferred into a sieve pan and clamped to the sieve shaker. A four-layer sieving system was formed by the lid at the top, a top sieve with a 150µm aperture to trap large agglomerated powder particles, millings balls and any possible contaminants, and the bottom sieve with a 70µm aperture. All the fine particles filtered through the 70µm sieve were collected into the sieve pan.

3.3.2. Mixing of the diamond powder with oxide additives

The diamond and the oxide liquid phase additives were mixed with a turbula mixer according to the mixing parameters summarized in Table 10. This method of mixing integrates and homogenises the powders of different densities and particle size distributions without damaging diamond, and required no drying step. High volumes of powders can be mixed very efficiently at short mixing times with lower wear of the alumina balls caused by the diamond particles.

Table 10: Turbula mixing parameters

Mass of media	**Oxide composition II: 14.5g** **Oxide composition I: 20g**
Mixing balls	ϕ 20mm alumina balls
Mixing pot	Sealed container
Mixing speed	67rpm
Mixing time	2 hours

The turbula mixing was carried out in a tightly sealed plastic container for 2 hours at 67rpm. This process eliminates the possibility of contamination. Milling balls are sieved out of the powder mixture at the end of the mixing process using a sieve with a mesh size of 70µm.

3.3.3. Particle size analysis

Particle size analysis measurements were obtained using a MALVERN Master Sizer 2000 with the wet dispersion unit. The standard operating procedure (SOP) set 3 measurements in order to assure accuracy of results. Powder (1g) was prepared into a paste using distilled water. For measurements, the slurry was then poured into sample chamber and dispersed using the ultrasonic displacement, stirrers and dispersant called sodium hexametaphosphate.

3. 4. Spark plasma sintering (SPS) furnace

Sintering of diamond composites is carried out in the spark plasma sintering (SPS) furnace which is computer controlled. Milled diamond composite powders, mixed with those of the LPS sintering aid, weighing 4.5g - 4.8g were loaded into cylindrical graphite dies with an inner diameter of 20.9mm lined with graphite foil. Graphite electrode punches are used to apply the sintering pressure as well as the current pulses to the graphite tooling of which of course they form part. The top punch has a hole with a closed bottom that facilitates sample temperature measurements using an optical pyrometer. This allows for the control of the temperature at the centre of the specimen (Rahaman M., 2007). The graphite punches and powder sample are separated by a thin layer of graphite foil coated with hexagonal boron nitride (hBN). This insulates the exterior of the sample holder and prevents the sample from interacting with the graphite rams (Vleugels Pr., 13 August 2010). The sintering is conducted inside a vacuum chamber at high temperature (1300ºC - 1500ºC) and medium pressure conditions (30MPa – 70MPa), with a dwell time of 5min, to ensure complete densification. A Heating rate of 100ºC/minute and a cooling rate of 400ºC/minute were administered during sintering of all the samples. Graphite foil used to line the SPS die adhered to the sample upon removal from the dies. This was removed using a sandblaster gun connected to a vacuum which creates a pressure release of sand particles which abrade the sample surfaces, peeling off and eroding the graphite foil. It was crucial to remove the graphite foil before analysis to avoid density measurement errors and contaminants detected by PXRD or SEM.

3.5. Characterization of sintered composites

3.5.1. Density measurements via Archimedes' principle method

Archimedes' principle density measurement method was utilized to measure the density of the sintered diamond composites. The density was determined as follows:

A specimen was boiled in distilled water for 3 hours and cooled at room temperature before the specimen was removed and placed onto a metal plate suspended through thin wires from a Sartorius EDS244S Extend balance scale. The disc and specimen were submerged into a bowl containing distilled water. The boiled suspended weight (W2) of the specimen–was measured in water. Immediately thereafter the moisture of the specimen was removed with a tissue paper to weigh the wet sample in air, (W_3). The boiled sample was then dried in an oven for 24 hours, cooled down to room temperature and the dry weight (W_1) was measured in air (Hodgman C.D., 1957). The bulk density and open porosity were calculated with the equations shown below:

$$Bulk\ density\ of\ the\ sample\ (\rho) = \frac{W_1 \rho_w}{(W_3 - W_2)}$$

Equation 3.1

$$Theoretical\ density\ = \frac{1}{\left(\frac{m_C\%}{\rho_{Diamond}} + \frac{m_{YAl2O3}\%}{\rho_{Y2O3}} + \frac{m_{Y2O3}\%}{\rho_{Y2O3}} + \frac{m_{SiO2}\%}{\rho_{SiO2}}\right)}$$

Equation 3.2

Where:

$\rho_{diamond}$ = 3.51 g/cm^{-3}

ρ_{Al2O3} = 3.98 **g/cm^{-3}**

ρ_{Y2O3} = 4.85 **g/cm^{-3}**

ρ_{SiO2} = 2.65 **g/cm^{-3}**

mass fraction (**m_n%**) of each constituent

$$Relative\ density = \frac{Bulk\ density\ of\ the\ sample}{Theoretical\ density} \times 100\%$$

Equation 3.3

$$Volume\ fraction\ of\ open\ porosity\ \ (\boldsymbol{Po}) = \frac{(W_3 - W_1)}{(W_3 - W_2)} \times 100\%$$

Equation 3.4

Where:

ρ = bulk density

ρ_w = density of water

W_1 = dry weight

W_2 = suspended weight

W_3 = wet weight

$\boldsymbol{P_o}$ = open porosity volume fraction

3.5.2. Powder X-ray diffractometer (PXRD)

An X-ray diffractometer was used to confirm the phase composition of the raw materials and identify the phases formed in the composites during sintering. The powder and cross section were prepared and

loaded into the goniometer (samples stage). $Co_{K\alpha}$ radiation was used over a 110° angle, with no rotation from 10° to 120° for 17min with step size of 0.028°.

3.5.3. Thermogravimetric analysis (TGA) - Differential Scanning Calorimetry (DSC) systems

The TGA/DSC analytical technique was used to study the mass changes and determine the sample energy changes (absorbed/released) during transformation as a function of temperature. The equipment measures both heat flow and mass difference. TGA/DSC generates two different curves: the mass loss curve and the heat flow curve. TGA/DSC are commonly used together because these techniques produce results that complement one another and aid in the analysis of the material's behaviour under heating conditions (Perkin Elmer Inc, 2017). The heat flow from the furnace to the sample is measured relative to the heat flow to the reference material. Sample and reference crucibles are identical except that the reference is usually empty (See Figure 15). Both crucibles are surrounded by a heated chamber/furnace.

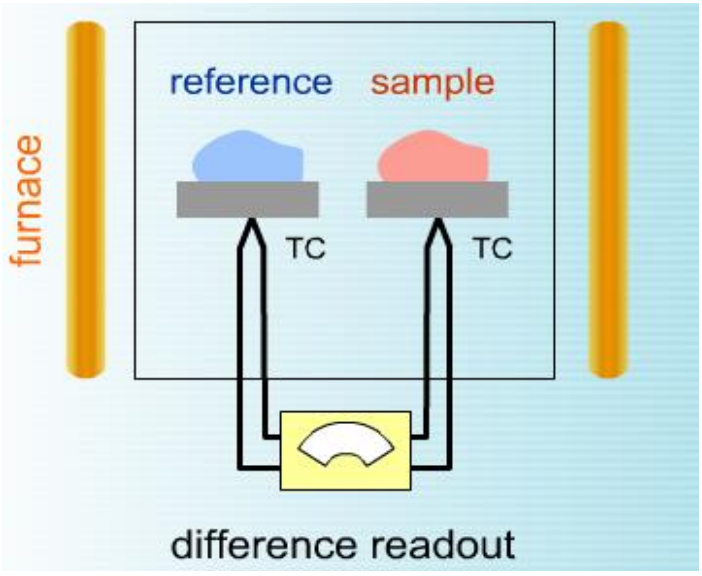

Figure 15: Schematic diagram of the sample and reference pans surrounded by the furnace, with the thermocouples reading the changes in temperature

The sample is placed in a crucible or pan, which sits directly on top of the sensor. The sensor detects the heat flow and its acute sensitivity can detect even µW transitions. The crucibles used must possess excellent thermal conductivity and be in optimum contact with the sensor. There is a thermo-state balance that minimizes environmental influences. A thermobalance is attached to the sample, continuously measuring and recording its mass. This is used to monitor the sample mass changes caused by decomposition or oxidation (should the experiment take place in air instead of an inert atmosphere).

The thermobalance prompts the user to empty the balance pan, zero the balance and place a calibration weight with the instrument.

3.5.4. Scanning Electron Microscope (SEM)

A SEM was used to study microstructural features, including intergranular phases, grain size and grain growth, possible reaction regions, phase morphology and to analyse elemental compositions by the spot and area mode, using an Energy Dispersive Spectrometer (EDS) detector. The analysis was carried out at a working distance of 10mm with a voltage of 10-20kV. Two detectors were used: a secondary electron detector to examine the topography of the microstructure at low voltage and working distance of ~5mm for clear images, and a backscatter diffraction detector (NTS BSD) to examine the various phases found in the sample, detected by the contrasting colours ranging between white grey and black, with heavier elements appearing brighter.

Lapping and polishing

Sintered diamond composites were fractured into halves using the automated fracture equipment, Tinius Olsen: Type: DBBSTOL-50kN, with the 3-point jig. Compacts recovered from the SPS sintering furnace are treated to smooth and refine the surfaces in order to capture images with high magnifications. A grinding and polishing method performed at Element Six, Springs is outlined in the table below:

Table 11: Material removal method used during samples preparation

Method	Plate	Liquid Suspension	Duration
Lapping	Cast iron wheel	Diamaxx - 45 µm	60 min
Polishing	Diamond wheel	No suspension	45 min

Both lapping and polishing were performed manually.

Lapping

Lapping is a machining process in which two surfaces are rubbed together with an abrasive between them, manually or using a machine. This process creates a flat surface on the material being lapped. In the case of this work, the lapping plate against which the samples were rubbed was cast iron, while the third body was diamond powder. Sintered samples had rough surfaces due to sandblasting damage incurred during the graphite foil removal. The surface of the sample was levelled by manually lapping for 60 minutes with an aid of a 45µm diamond suspension.

Polishing

Polishing is performed to produce scratch-free, smooth surfaces. This is achieved by rubbing the sample with cloths containing fine abrasive particles, moving from coarser to finer abrasives until a smooth surface finish was achieved. In this study and because of the presence of diamond in the materials made, instead of cloths, diamond wheels were used to ensure the samples had a mirror smooth surface finish, suitable for the subsequent SEM imaging and accurate hardness measurements. Polishing was performed with no suspension for 45 minutes.

3.6. Hardness tests

In this study, the unit of hardness measure is Vickers hardness. The sintered polished cross sections were subjected to a load of 10kgf with a diamond indenter for 30seconds, using the FUTURETECH FV-80 bulk hardness tester. The diamond indenter makes an angle of 136° between opposite sloping surfaces indented by the specific load. The diagonal indentations were measured using the SEM equipment. Five measurements were done on each sample to confirm the accurate value and the average was calculated. Figure 16(a) shows the relation between the diamond indent and the material's slopping surfaces. Upon performing the indentations, the indent diagonals labelled *d1* and *d2* shown in figure 16(b) are measured using an optical microscope, or a scanning electron microscope, in order to calculate the Vickers hardness.

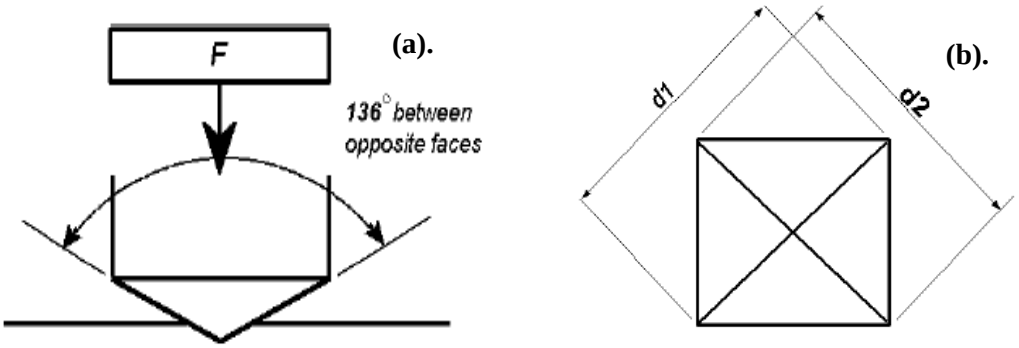

Figure 16: Schematic representing the angle between the slopping surfaces and indenter, and an image of an indented surface with diagonals labelled d1 and d2. (Reinhorn A.M., 2000)

The following equation was used to calculate the Vickers hardness value:

$$HV = 1.854 \times \left(\frac{F}{d^2}\right)$$

Equation 3. 5

F = load applied to the samples by the indenter (kgF)

d = arithmetic mean of the two indenter diagonals, d_1 and d_2 in mm

HV = Vickers hardness

To convert HV to MPa one has to multiply by 9.807 and to convert HV to GPa one has to multiply by 0.009807. Multiphase samples have unequal hardness in each phase, thus making such measurements unreliable, depending on sample homogeneity and scale of microstructural features.

Chapter 4

EXPERIMENTAL RESULTS

This chapter will outline the experimental results obtained from milling the oxide additives, mixing the liquid phase sintering aid/binder with diamond powder via the turbula mixer and liquid phase sintering of diamond composites under different conditions using the SPS furnace. The characterisation of the materials studied was conducted using XRD, TGA/DSC and SEM/EDS.

4.1. Raw material characterisation

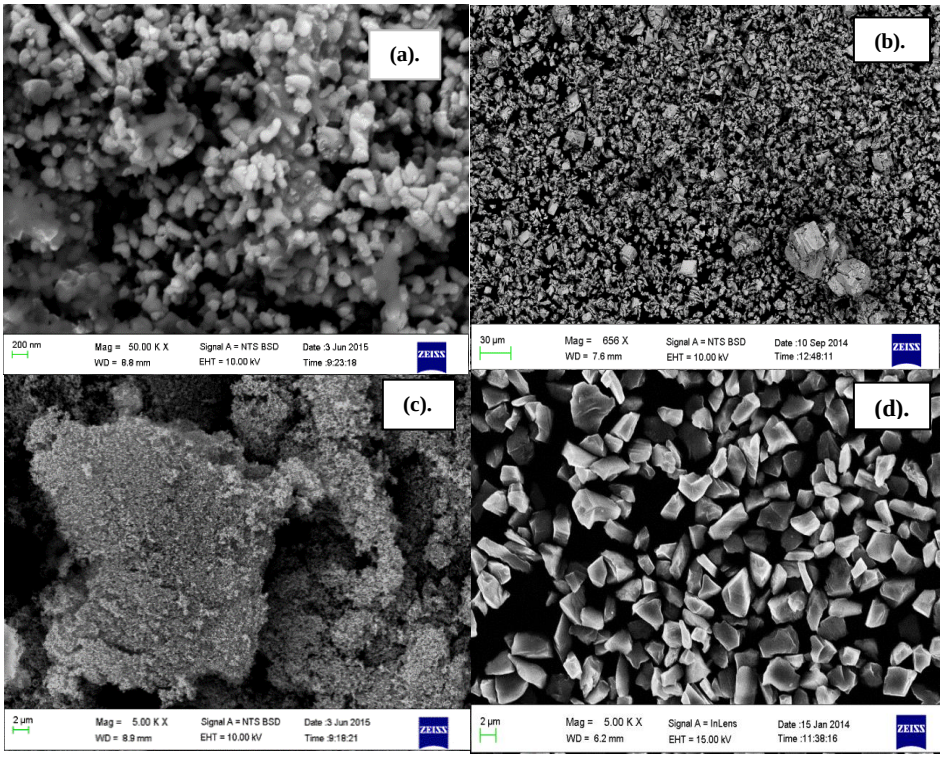

Figure 17: SEM micrographs of the as-received raw materials (a). alumina, (b). yttria, (c). silica and (d). diamond

Figure 17 displays the raw materials observed under SEM. The micrographs clearly show the morphology of the raw materials.

Table 12: A list of particle size distributions of the raw powder materials characterised using the Malvern Particle size analyser

Specimen	$D_{0.1}$ (µm)	$D_{0.5}$ (µm)	$D_{0.9}$ (µm)

Diamond (M 3-6)	1.73	2.87	4.8
Diamond (M 20-30)	13.52	18.5	26.6
Alumina	0.12	0.20	1.79
Yttria	1.76	4.37	14.86
Silica anhydrous	9.7	28.3	84.5
Additive comp. I	3.557	13.246	31.171
Additive comp. II	0.862	10.730	30.301

Table 12 displays the particle size distribution of the raw materials, oxide ceramics and diamond crystallite grains. The characterisation of anhydrous silica required repeated measurements due to the amorphous nature of this material and the range of the particle size distribution. The mixture composition of each additive is as follows: **Additive comp. I, LPI**: 40wt%Y_2O_3-25wt%Al_2O_3-35wt%SiO_2 and **Additive comp. II, LPII**: 30.78wt%Y_2O_3-13.65wt%Al_2O_3-55.58wt%SiO_2.

4.2. Powder processing

The synthetic diamond powder was mixed with oxide ceramic powders of varying volume compositions in order to consolidate a starting material to be used for preparing sintered diamond composites. The bimodal diamond composites in this study were made using 30wt% (~2μm) and 70wt% (~20μm) synthetic diamond powder. The dispersion and homogeneity of the additives are shown in Figure 19. The oxide additives were selected as binders for this study due to their properties of creep resistance, chemical inertness and their compatibility with hard ceramic materials such as diamond, Si_3N_4 and SiC. (Kolitsch, Seifert, Ludwig, & Aldinger, 1999). The properties of these additives were a key prerequisite for the production of the diamond composites with the desired properties.

Thermogravimetric analysis (TGA) and Differential Scanning Calorimetry (DSC)

The TGA/DSC analytical technique was performed to better understand the diamond liquid phase mixture compositions and their thermodynamic behaviour during heat treatment. This technique provided a dual function – (i) a TGA function to analyse mass loss of a sample during heating, the change in mass (moisture loss or gas release etc.), and (ii) DSC function measures the heat flow during an endo- or exo-thermic reaction as a function of time and temperature. An increase/decrease in heat flow is equal to the amount of heat released/absorbed during a reaction. These graphs also inform us about the physical and chemical changes of the mixture composition during the different stages of heating. Each of the two samples weighed 30mg.

Sample I consisted of: 60vol%C/12vol%Y_2O_3-9vol%Al_2O_3-19vol%SiO_2 (LPI) and sample II consisted of 60vol%C/8vol%Y_2O_3-4vol%Al_2O_3-27vol%SiO_2 (LPII). These graphs are shown in Figure 18 and Figure 19 respectively. The heating rate was 20°C/min. The measurement readings commenced at ~40°C and at this stage there was a loss of volatile components such as moisture, mixing solvents and heat transfer between the sample, the pan and the DSC sensor. The thermodynamic reactions in figure 18 and figure 19 were interpreted and labelled using the red exothermic arrow pointing down (top right corner of each graph). The designation of exothermic reactions was confirmed by an expert technician that handled the equipment used to run the TGA/DSC runs.

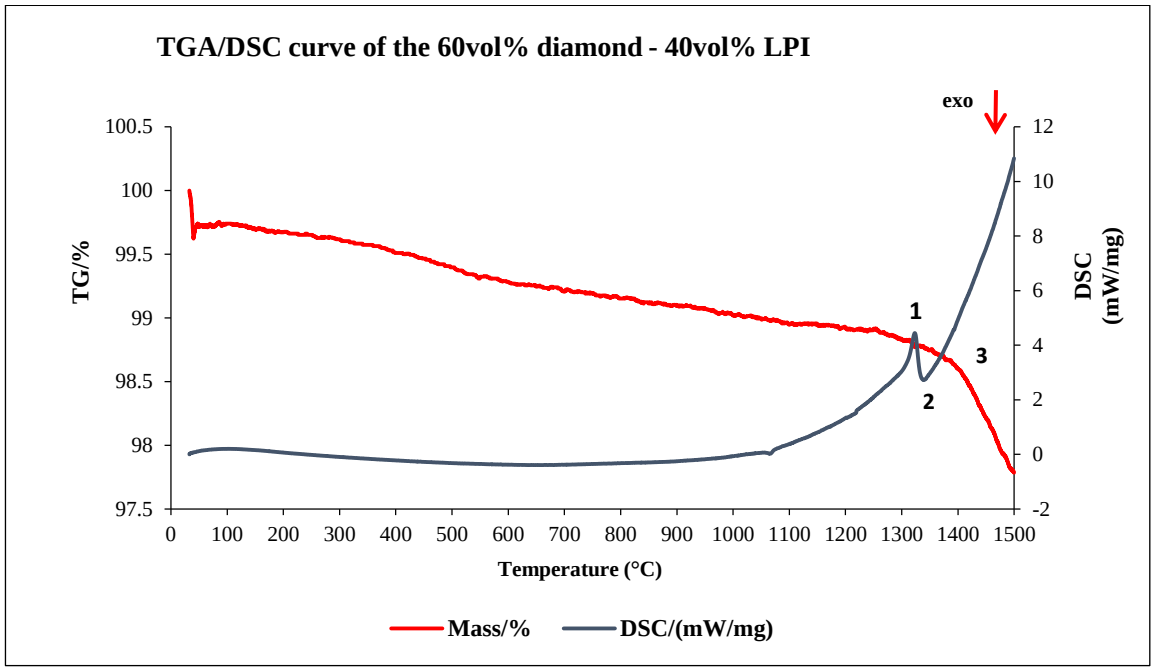

Figure 18: A TGA/DSC curve of the 60vol.%C/40wt%Y_2O_3-25wt%Al_2O_3-35wt%SiO_2 heated up to 1500°C

Figure 18 shows the thermodynamic reactions that occurred during the heating of the LPI mixture composition. The sequence of reactions was as follows: **1**. Eutectic melting, as indicated in Figure 13, **2** baseline shift, and **3**. possible reduction of SiO_2 by the C in the graphite tooling, as explained below. The melting of the composite powder was followed by crystallisation and final melting proceeded as the mass loss continued, until the process was completed.

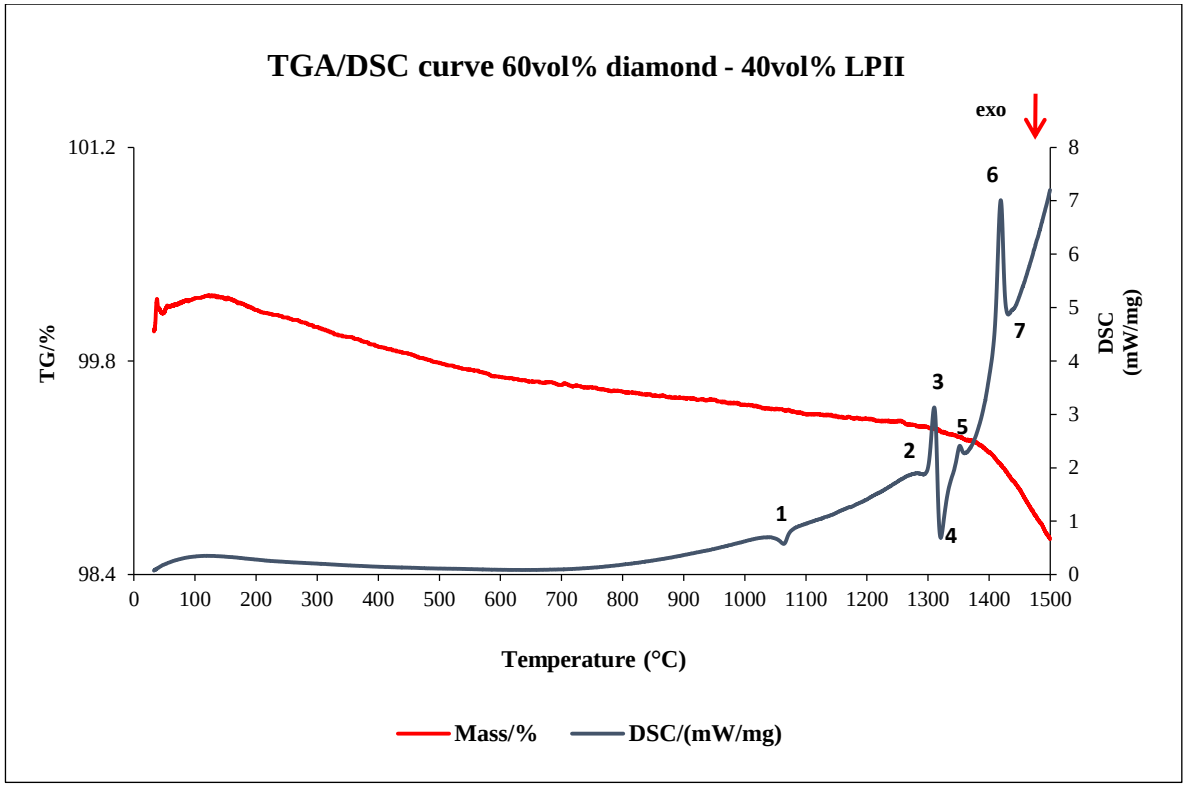

Figure 19: A TGA/DSC curve of the 60vol.%C/30.78wt%Y_2O_3-13.65wt%Al_2O_3-55.58wt%SiO_2 sample heated up to 1500ºC

Figure 19 shows the sequence of thermodynamic reactions that occurred during the heating process. The reactions occurred as following: **1**. crystallisation, area between **1** & **2** – melting (endothermic), **2**. crystallisation, **3**. Eutectic melting, **4**. secondary crystallisation, **5**. endothermic to short exothermic cycle reaction, **6**. melting of the crystallised intermediate phases; and **7**. tertiary crystallisation of the melt. This occurred during the decomposition phase displayed by the TGA curve. It was observed that melting occurs over long temperature ranges. Crystallisation occurs at a definite temperature. The LPII mixture contained a high silica component and silica is known to be a network enhancer and a crucial component in the crystallisation process. This may be the cause of the three crystallisation peaks. Mass loss observed in figures 18 and 19 may indicate the reaction of SiO_2+3C =SiC+2CO – or formation of SiO and CO – this could partially (local) shift the composition to lower SiO_2 values and hence increase the crystallisation. This is possibly more emphasised in the LPI phase.

4.3. Sintering of monomodal composites

The monomodal diamond composites were sintered using the LPI 40wt%Y_2O_3-25wt%Al_2O_3-35wt%SiO_2 binder additive only. Three diamond compositions were sintered with mono-sized diamond compositions: 25vol%, 35vol% and 60vol% as shown in Table 13.

Table 13: Relative density and hardness values of the monomodal diamond composites liquid phase sintered using the SPS method

Sample ID	*T* (°C)	*P* (MPa)	*d* (g cm^{-3})	d_{rev} (%)	P_O (%)	HV_{10} (kg/mm^2)
d25LPI/1200-70	1200	70	3.081	79.0	9.10	619 ± 15
d25LPI/1300-70	1300	70	3.537	90.7	0.06	938 ± 10
d35LPI/1300-70	1300	70	3.590	92.8	0.05	625 ± 49
d35LPI/1600-50	1600	50	3.498	90.5	0.06	817 ± 116
d60LPI/1300-30	1300	30	2.254	62.9	38.84	221 ± 28
d60LPI/1400-30	1400	30	3.324	92.7	6.61	380 ± 19
d60LPI/1500-30	1500	30	3.205	89.4	9.83	348 ± 27
d60LPI/1600-30	1600	30	2.552	71.9	21.32	168 ± 4

Sample d25LPI/1300-70 achieved the highest Vickers hardness with d35LPI/1300-70, and d60LPI/1400-30 reaching the highest relative densities among the monomodal diamond composites, as shown in Table 13. The experiments done with the monomodal diamond powder were exploratory in nature, designed to identify the optimal sintering range that would produce high densities. The rather wide range of mixture compositions is a result of powder sample bursts well outlined in section 4.3.3. Depending on sintering temperature and diamond volume fraction, the liquid phase aids would generate excessive amount of liquid at the sintering temperature, resulting in graphite tooling bursts. This was found to be the case largely for monomodal composites for sintering temperatures exceeding 1400ºC and/or 50vol% of liquid phase sintering aid. The reported analysed samples represent those that escaped powder bursts either through their mixture compositions and/or sintering conditions. A wide variety of mixture compositions presented in table 13 are therefore a result of selecting the samples that survived the bursting problem with a goal of identifying compositions that will lead to high densities.

4.3.1. Densification of monomodal diamond composites

The densification curves shown below show the behaviour of the diamond composites during sintering. These curves indicate regions of different activities resulting in densification as well as the rate of such densification.

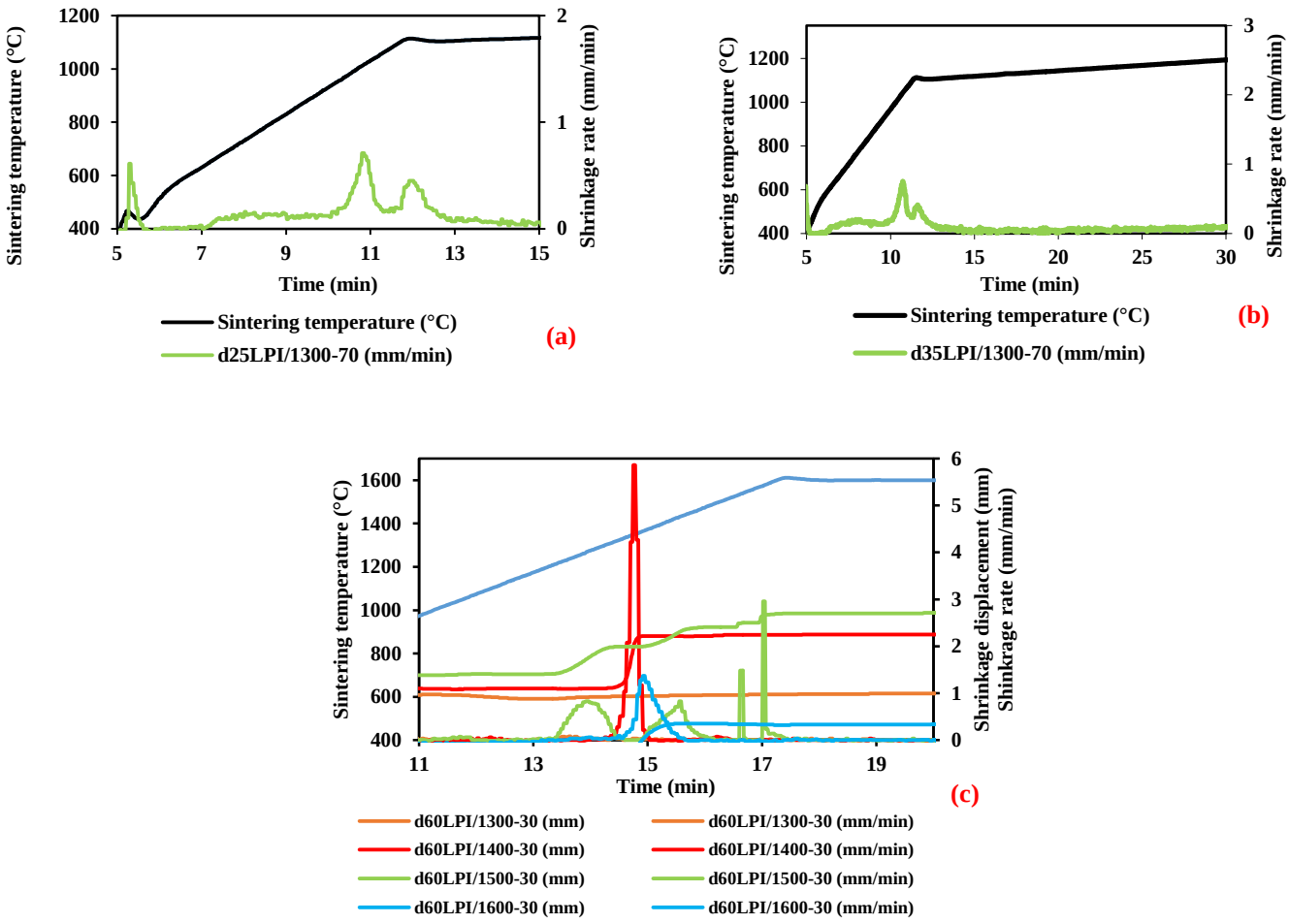

Figure 20: Densification graphs of the (a). 25vol% (90.7%, 938HV), (b). 35vol% (92.8%, 625HV) and (c). 60vol% (92.7%, 380HV), (89.4%, 348HV) and (71.9%, 168HV) monomodal diamond composites

The shrinkage rates indicated in Figure 20 show the speed with which the pistons move towards (or away from) one another as sintering progresses. Shrinkage rates of the 60vol% diamond composites were faster than those of the 25vo% and 35vol%, but the liquid phase initiation and particle rearrangement occurred at higher temperatures for the high diamond composition samples than it did for the low diamond content samples. The difference in the diamond content influenced the grain boundary phases and the resulting mechanical properties. Graphs in figure 20a and figure 20b sintering temperatures (primary vertical y-axis) and sintering times (x-axis) axis's were cropped to ensure we present a clear and enlarged view of the shrinkage peaks. However, the highest sintering temperature for these composites is 1300°C as indicated table 13. The shrinkage peaks in these two composites appeared at above 1000°C, indicating that particle rearrangement occurs at that temperature. The shrinkage achieved is small, as indicated by the low piston displacement speeds attained for these two materials. These two shrinkage peaks correspond to the small peak in the DTA trace of figure 18. This maybe a glass transition temperature for the SiO_2 phase, which was amorphous in the as-received phase

(established by XRD analysis of the as-received powder). The shrinkage peaks in figure 20c indicate that particle rearrangement in that composition took place at ~1350°C and highest density was achieved by d60LPI/1400-30. This transition corresponds to the eutectic of LPI, as indicated in the phase diagram of Figure 20. At 60vol% unimodal diamond particle content, this phase is above its percolation point, contrary to the composites examined in Figures 20a and b. Therefore, when the glass transition of the SiO_2 phase is reached, no discernible piston displacement takes place. However, when at that temperature reaches the eutectic one for the LPI composition, enough liquid of low enough viscosity is generated to allow significant particle rearrangement to take place. Composites sintered at temperatures above 1400°C experienced decline in density and vickers hardness measurements as shown in table 13.

4.3.2. Microstructural evolution of monomodal diamond composites

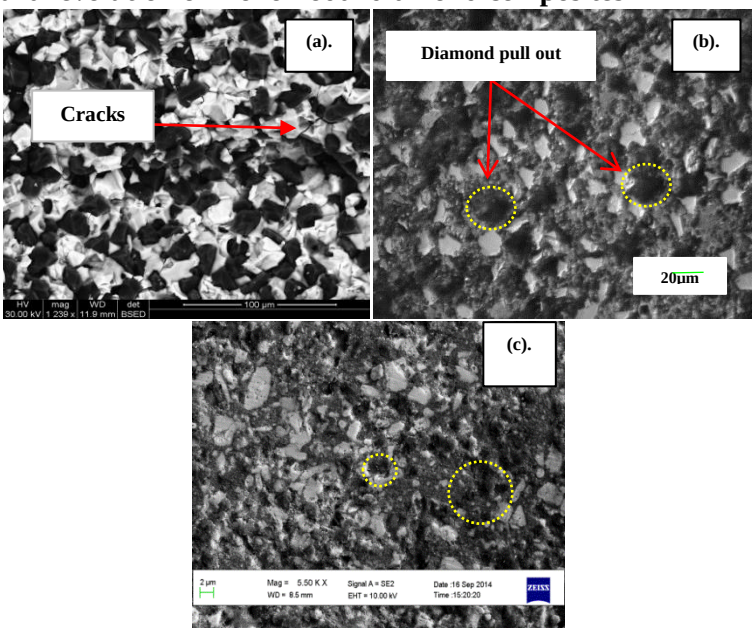

Figure 21: SEM micrographs of (a). fractured surface of d60LPI/1500-30 with visible micro-cracks, (b). polished surface d35LPI/1300-70 sample with diamond pull out cavities and (c). polished surface of the d35LPI/1600-50

All the samples exhibited uniform distribution of the diamond particles. Micro-cracks observed in Figure 21a are probably the result of thermal stresses between diamond grains and the glassy matrix induced by the mismatched thermal expansion coefficients. Diamond pull-out was observed in Figures 21b and 21c. These microstructural defects, viz. cracks and diamond pull-out, signify poor adhesion between diamond and the matrix, and may be responsible for the low hardness values.

4.3.3. Phase analysis of monomodal diamond composites

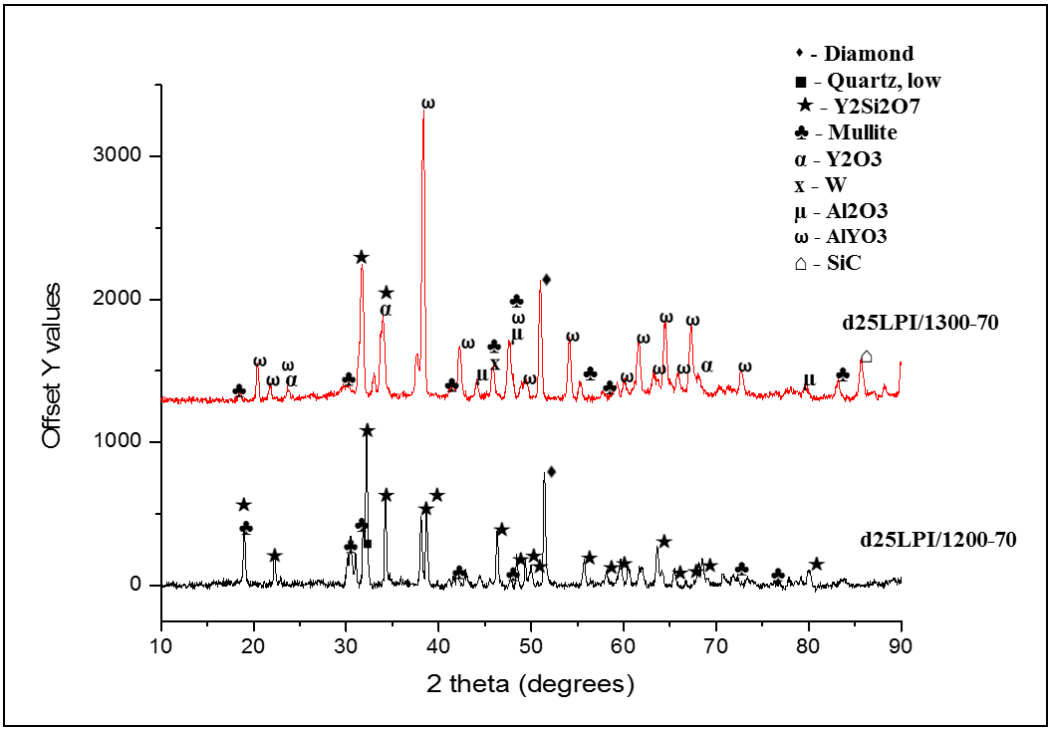

Figure 22: XRD patterns of the 25vol% monomodal diamond composites liquid phase sintered with LPI: 40wt%Y_2O_3-25wt%Al_2O_3-35wt%SiO_2

Figure 22 shows the XRD traces of the 25vol% monomodal diamond composites, sintered with LPI. Keivyite (Y) - $Y_2Si_2O_7$ was the most dominant phase in the sample sintered at 1200ºC, while $AlYO_3$ was prominent in the sample sintered at 1300ºC. $AlYO_3$ intergranular phase possibly impacted the d25LPI/1300-70 composite's hardness (Table 12) due to YAP's 8.5 Mohr's hardness and the anisotropic thermal expansion coefficient (Diehl & Brandt, 1975).

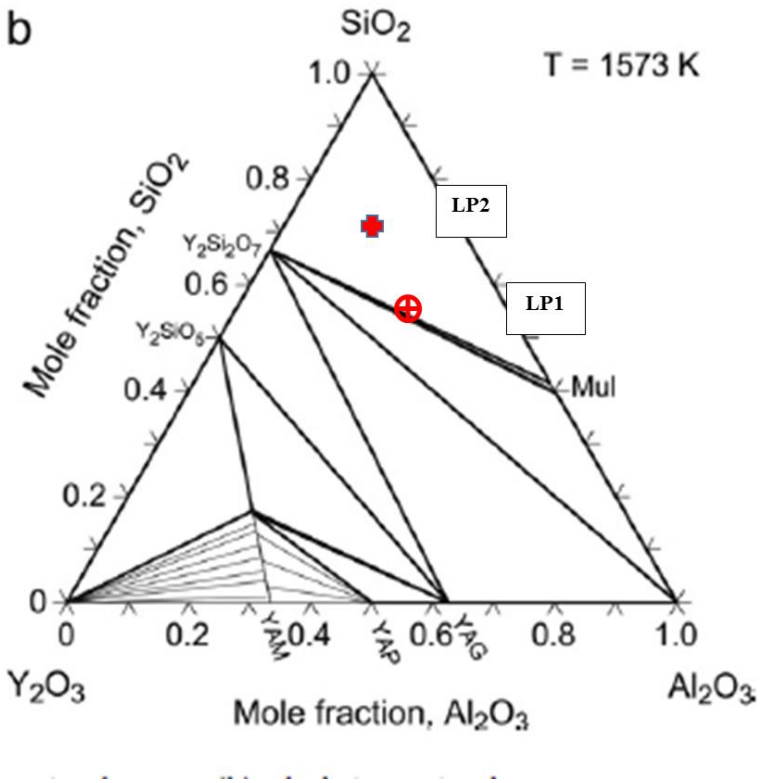

Figure 23: Al_2O_3-Y_2O_3-SiO_2 phase diagram at 1300ºC, after Mao et al. 2008

Newer calculations (Figure 23) conducted by Mao et.al reported that at LPI is in the peritectic and Al_2O_3 and γ-$Y_2Si_2O_7$ will crystallise (Mao, Selleby, & Fabrichnaya, 2008). Only in the second step during cooling second Al_2O_3 will react with the melt forming mullite. The phases present in samples d25LPI/1200-70 and d25LPI/1300-70 are caused by the fact that the sintering temperatures were low, thus not allowing for reactions and subsequent homogenisation to be competed. YAG and $Y_2Si_2O_7$ are the main phases of the d35LPI/1300-70 and d35LPI/1600-50 samples. As the sintering temperature increases, the reduction of SiO_2 becomes more prominent, pushing the composition to lower SiO_2 content in the phase diagram of Fig 23, thus causing the generation of the YAG phase.

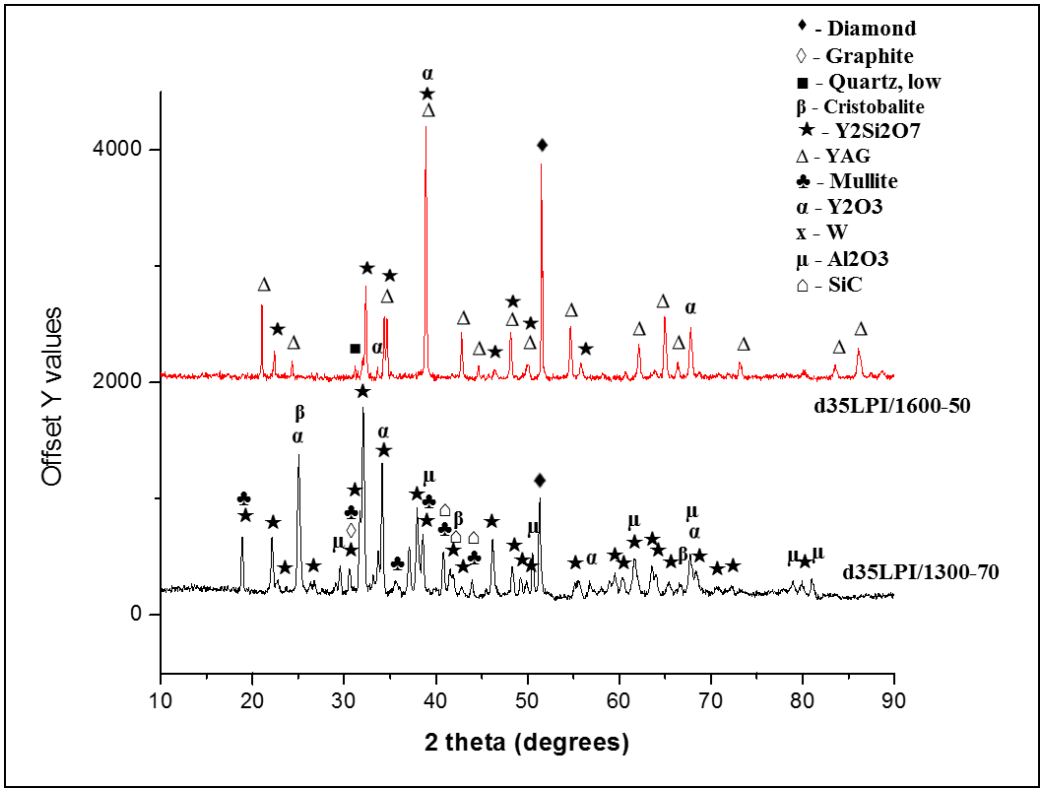

Figure 24: XRD patterns of the 35vol% monomodal diamond composites liquid phase sintered using LPI: 40wt%Y_2O_3-25wt%Al_2O_3-35wt%SiO_2

Figure 24 shows that the sample d35LPI/1300-70 still had a number of the starting components present, as well as a mixture of other phases. Because the sintering temperature was too low, no melting took place and the reactions were not completed. d35LPI/1600-50 had YAG and $Y_2Si_2O_7$ as the main phases present; this enhanced the hardness measured to 817 ± 116kg/mm², as shown in Table 12 The composition of the sample sintered at 1600°C can again be explained in the same way as that of the 25vol% diamond sample, sintered at the same temperature and discussed above (i.e. reduction of the SiO_2 phase).

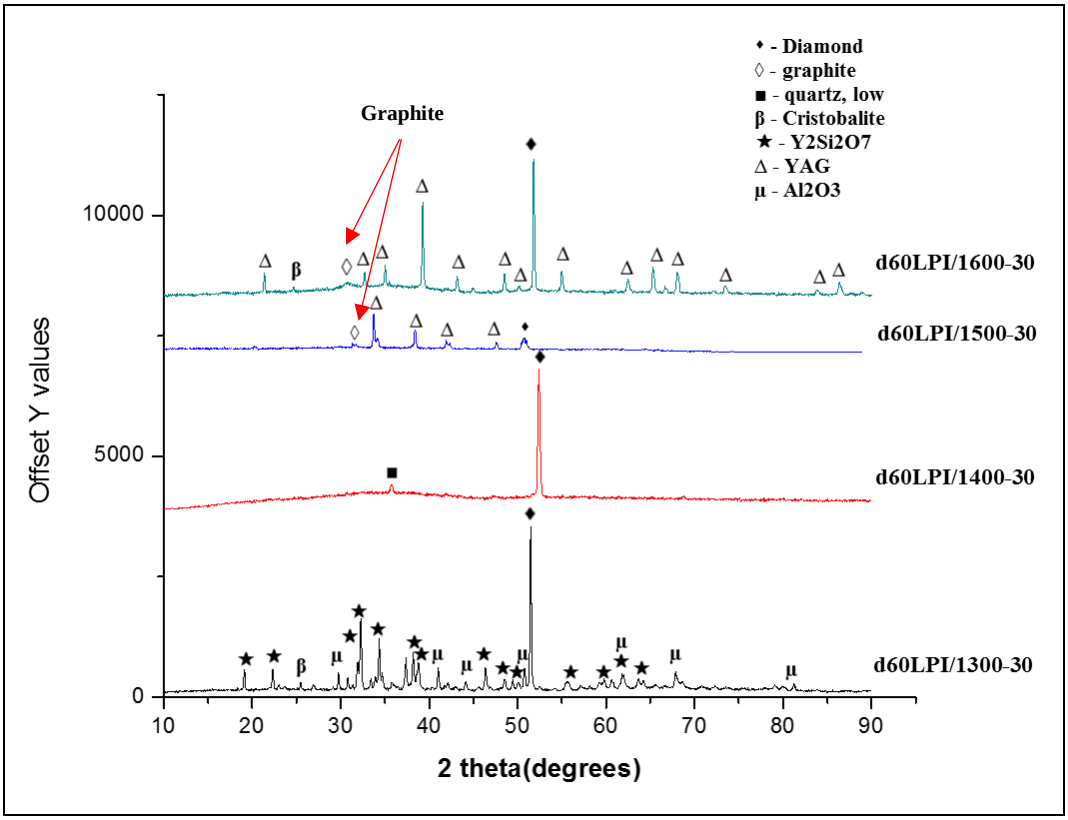

Figure 25: XRD patterns of the 60vol% monomodal diamond composites liquid phase sintered using the LPI: 40wt%Y_2O_3-25wt%Al_2O_3-35wt%SiO_2 additive

Figure 25 shows the XRD patterns of the 60vol% diamond containing samples, sintered with the LPI sintering aid. It can be seen that those sintered at temperatures higher than 1300°C show some presence of graphite, which must have been generated on the surface of the diamond particles during sintering. As a result, the hardness values declined among 60vol% monomodal diamond composites increasing sintering temperature. The patterns in figure 25 show that at 1300°C there's no equilibrium, at 1400°C the grain boundary phase was still amorphous, at 1500°C and 1600°C – strong reduction of SiO_2 occurred and therefore, the crystallisation of YAG started.

Table 14: Listed phases formed during sintering monomodal diamond composites liquid phase sintered with LPI – binder phase

Sample ID	Phases detected by the XRD
d25LPI/1200-70	Diamond, quartz, Keivyite (Y) - $Y_2Si_2O_7$, mullite
d25LPI/1300-70	Diamond, $AlYO_3$, mullite, Keivyite (Y) - $Y_2Si_2O_7$
d35LPI/1300-70	Diamond, graphite, cristobalite, SiC (Moissanite – 3C), Keivyite (Y) - $Y_2Si_2O_7$, mullite
d35LPI/1600-50	Diamond, YAG, quartz, Keivyite (Y) - $Y_2Si_2O_7$
d60LPI/1300-30	Diamond, $Y_2Si_2O_7$, Al_2O_3, cristobalite
d60LPI/1400-30	Diamond, $AlYO_3$, diamond, YAG, mullite, graphite, cristobalite
d60LPI/1500-30	Diamond, YAG, graphite
d60LPI/1600-30	Diamond, YAG, cristobalite, graphite

Table 14 confirms all the phases detected by the XRD patterns shown in figures 22, 23 and 24. Keivyite (Y) - $Y_2Si_2O_7$ was common among low diamond compositions, as expected from the phase diagram and the YAG phase was present in samples fired at 1500°C or higher. $AlYO_3$ was identified in composites that had relatively higher hardness values in both low and high diamond composition samples.

Table 15: Comparative data between averaged densities and averaged hardness measurements for the 25vol%, 35vol% and 60vol% monomodal diamond composites sintered with LPI binder

Monomodal diamond	Average d_{rev} (%)	Average P_O (%)	Average HV_{10} (kg/mm^2)
25vol% and 35vol%	88.3	2.3	750 ± 155
60vol%	79.2	19.2	279 ± 101

Low diamond content composites outperformed the composites with the higher diamond content as presented in Table 15. This correlates with the lower densities attained for these composites. Such low densities can be attributed to the fact that at such high diamond volume fraction, this phase is well above its percolation limit, thus inhibiting densification through the particle rearrangement process. The latter is the only mechanism available in this series of experiments for the densification of these composites. One alternative method of improving densification is enhancing the packing efficiency and filling interspaces between the coarse diamond grains with finer diamond particles, instead of a softer binder phase. In addition, the density and hardness values presented in Table 15 highlight the role of the diamond content to the diamond composite's properties.

4.3.4. Limitations encountered with sintering of the monomodal diamond composites

It is evident that the monomodal diamond composites compositions had some inconsistency in the sintering conditions, particularly regarding the applied pressure. The reason for this is the occurrence of graphite tooling bursts during sintering. Several experiments were aborted because of this problem. As part of the strategy for addressing it, a detailed DTA trace was obtained for the 25vol% - LPI mixture. The run was done up to 1600^{o}C.

Possible causes considered based on the thermodynamic peaks presented in figure 26:

- Based on the DTA run performed on the monomodal diamond composite bound together by LPI sintered up to the conditions where the burst occurred, suggest that the rapid liquid phase generation may have caused this problem
- Crystallisation at ~550^{o}C resulted in volume expansion and may have catalysed fractures within the graphite dies that led to complete rupture of the dies

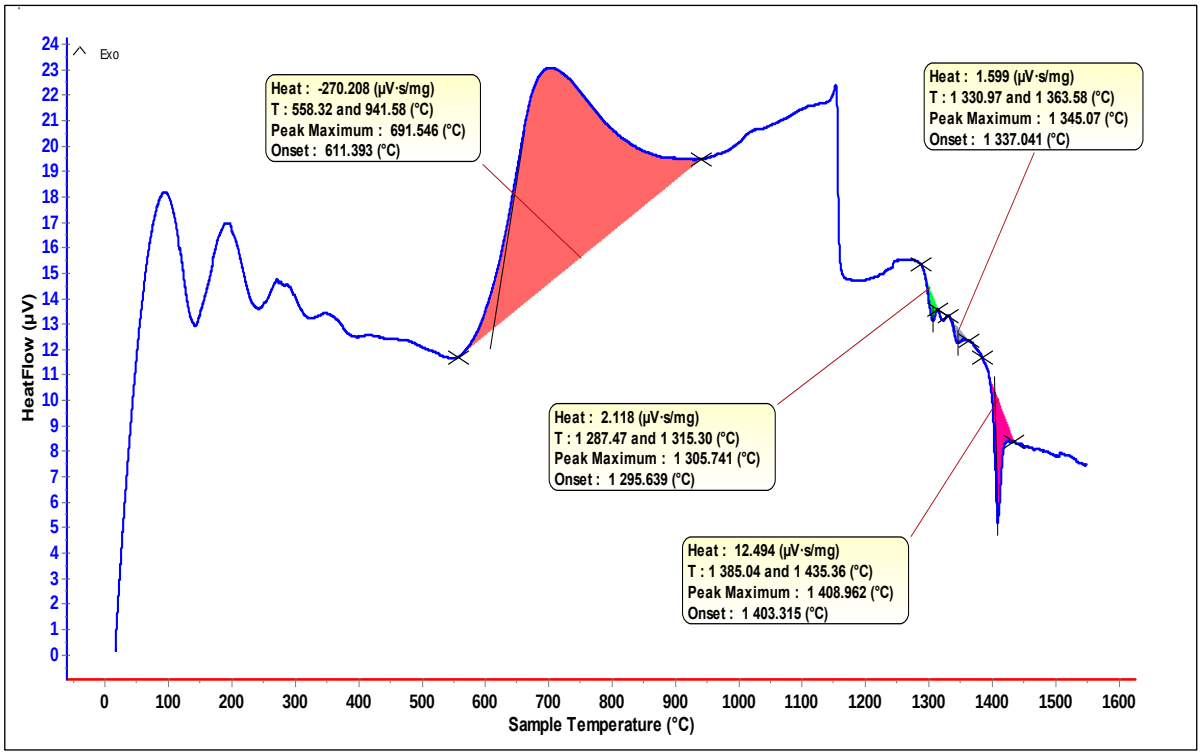

Figure 26: Diagram of the DTA graph of the 25vol% monomodal diamond powder plus LPI heated up to 1500°C

The 25vol% monomodal diamond sample behaviour was observed under the heating process via the DTA. Prominent points observed in Figure 26 were the exothermic (between 550°C – 990°C) and the endothermic (between 1300°C - 1400°C) peaks. It is highly likely that the graphite dies broke inside the SPS chamber due to the high liquid phase volume generated at these high temperatures. The damaged dies are shown in Figure 27b. The upwards facing arrow shown in figure 27 provided some assistance in interpreting the thermodynamic peaks. In other occurrences as seen in figure 27a, the melted liquid cooled and froze in between the graphite pistons preventing the extraction of the sintered composites. This problem requires further investigation and the exploration of possible techniques that can be employed to achieve sintering monomodal diamond composites at these conditions without experiencing graphite dies bursts. It is possible that high densities can be reached if such powder bursts can be prevented, thus allowing one to obtain strong, tough diamond composites.

Figure 27: An image of the graphite dies ruptured during a sintering process

The LPI diamond composite was selected as binder due to the ability to sinter at lower temperatures. However, the composites produced had low densities. Therefore, this motivated a demand for a new diamond/binder mixture that would be sintered under higher temperatures. LPII was formulated and bimodal diamond mixture was used in order to attain higher packing densities. Unfortunately, this problem also affected the bimodal diamond mixes when we attempted to sintered at 1500°C/50MPa using either LPI or LPII as sintering aides. Therefore, in the results presented on bimodal diamond composites we concluded the study at temperatures not exceeding 1590^{o}C or pressures higher than 30MPa.

4.4. Sintering of bimodal diamond composites

All the bimodal diamond composites, 50vol%, 60vol% and 70vol% diamond compositions were made from 30wt% (~3µm) and 70wt% (~20µm) bimodal particle size distribution. Two liquid phase additives, LPI: 40wt%Y_2O_3-25wt%Al_2O_3-35wt%SiO_2 and LPII: 30.78wt%Y_2O_3-13.65wt%Al_2O_3-55.58wt%SiO_2 liquid phase additives were used for their sintering. Because of the possibility of attaining higher diamond packing densities, the volume fractions of the diamond phase used in these experiments was 60 and 70vol%. In section 4.4.1 and 4.4.2, we study and highlight the impact of these additives on the densification, phase composition and mechanical properties of the bimodal diamond composites produced in this study.

4.4.1. 25wt%Al_2O_3-40wt%Y_2O_3-35wt%SiO_2 liquid phase sintering aid (LPI)

Table 16: Summary of the bimodal diamond composites liquid phase sintered using the LPI additive

Liquid phase (LPI) - 40wt%Y_2O_3-25wt%Al_2O_3-35wt%SiO_2					
SAMPLE NAME	**Diamond content**	**Al_2O_3**	**Y_2O_3**	**SiO_2**	**T.D.(g/cm^3)**
LIQUID PHASE I	**0**	25wt%	40wt%	35wt%	3.6054
MIXTURE I	60vol%	9.06vol%	11.89vol%	19.05vol%	3.5481
MIXTURE II	70vol%	6.79vol%	8.92vol%	14.29vol%	3.5386

Table 17: Mechanical properties of the 60vol% and 70vol% bimodal diamond composites liquid phase sintered using SPS with LPI as the sintering aid.

Sample ID	***T* (°C)**	***P* (MPa)**	***d* (g cm^{-3})**	**d_{rev} (%)**	**P_O (%)**	**HV_{10} (kg/mm^2)**
D60LPI/1300-30	1300	30	2.901	81.8	17.77	373 ± 34
D60LPI/1400-30	1400	30	3.189	89.9	4.56	572 ± 5
D60LPI/1500-30	1500	30	3.260	91.9	0.59	744 ± 16
D60LPI/1300-50	1300	50	3.085	86.9	10.87	384 ± 15
D60LPI/1360-50	1360	50	3.163	89.1	0.06	931 ± 6
D60LPI/1370-50	1370	50	3.455	97.4	0.04	1235 ± 20
D60LPI/1380-50	1380	50	3.452	97.3	0.30	1249 ± 57
D60LPI/1400-50	1400	50	3.439	95.9	0.02	1294 ± 26
D60LPI/1400-70	1400	70	3.359	93.7	0.06	1047 ± 19
D70LPI/1400-50	1400	50	2.9324	82.87	13.57	448 ± 60
D70LPI/1400-70	1400	70	2.9436	83.16	14.44	952 ± 50

The 60vol% diamond composites outperformed the 70vol% diamond composites, as indicated in table 17. It was expected that with a higher diamond content, the relative density would decline, because the diamond skeleton would exceed the percolation limit, even for a bimodal mixture, as discussed above.

This resulted in lower hardness values. Below, densification curves, XRD patterns and intergranular phases will be studied further to better understand the sintering behaviour and their effect on the mechanical properties of the diamond composites.

4.4.1.1. Densification

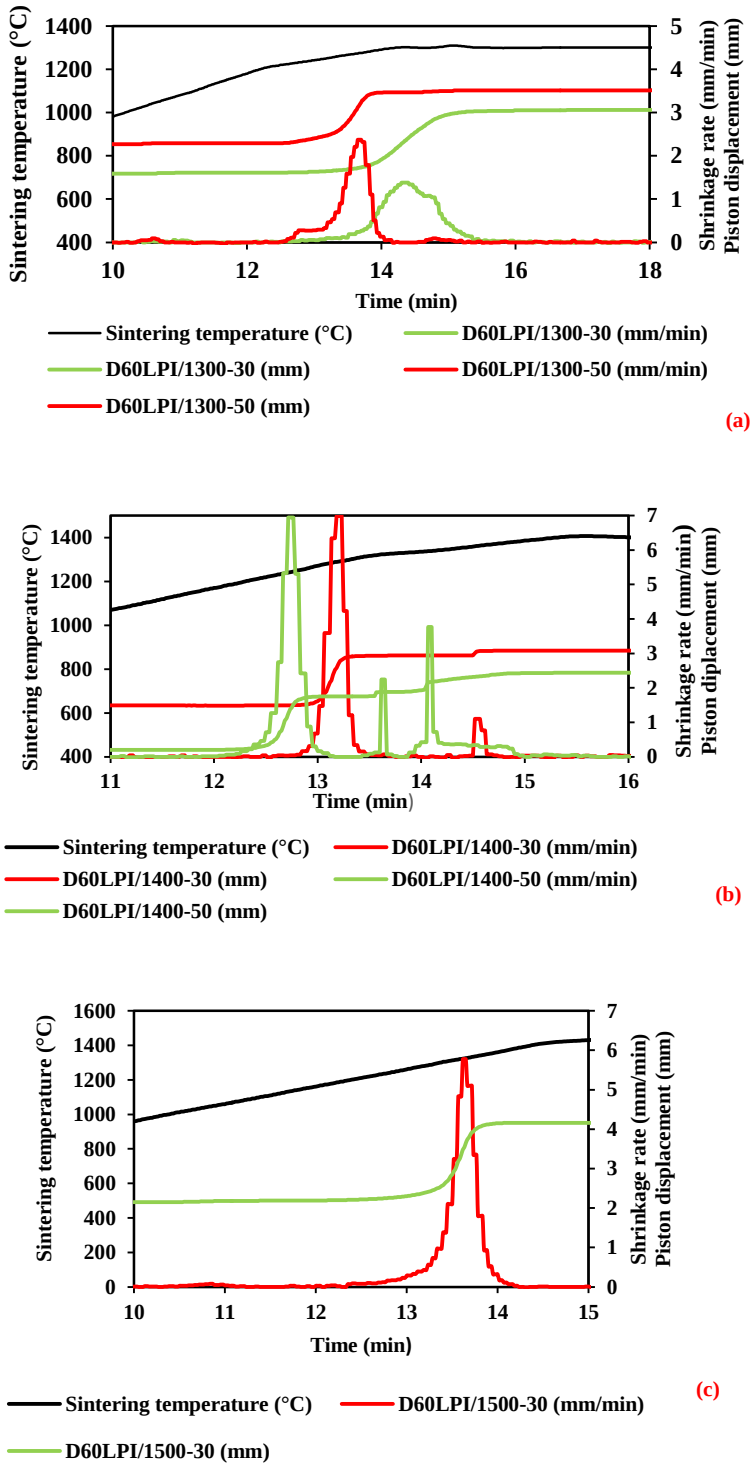

Figure 28: Densification curves of the LPI bimodal diamond composites

Figure 28 shows the densification curves of the 60vol% bimodal diamond composites. The shrinkage rate at sintering temperature of 1300°C did not exceed 3mm/min. The same rate increases to 7mm per minute at 1400°C, with a small decline to 6mm/min at 1500°C. In all cases, the shrinkage peak occurs in the vicinity of 1280°C that being the eutectic for the Al_2O_3-Y_2O_3-SiO_2 system, as shown in the phase diagram of figure 13. With increasing sintering temperature, the shrinkage rates increased rapidly from 2mm/min to 7mm/min and declined to 6mm/min at 1500°C. The increase from 1300°C to 1400°C can be attributed to the fact that 1300°C is too close to the eutectic. The subsequent decrease at 1500°C can be attributed to a wider range in time during which this displacement took place. It is also interesting to observe that, at higher applied sintering pressures, the shrinkage peak appears earlier in time, indicating the influence of stress on the initial plastic deformation of the binder phase being generated as the eutectic temperature is reached.

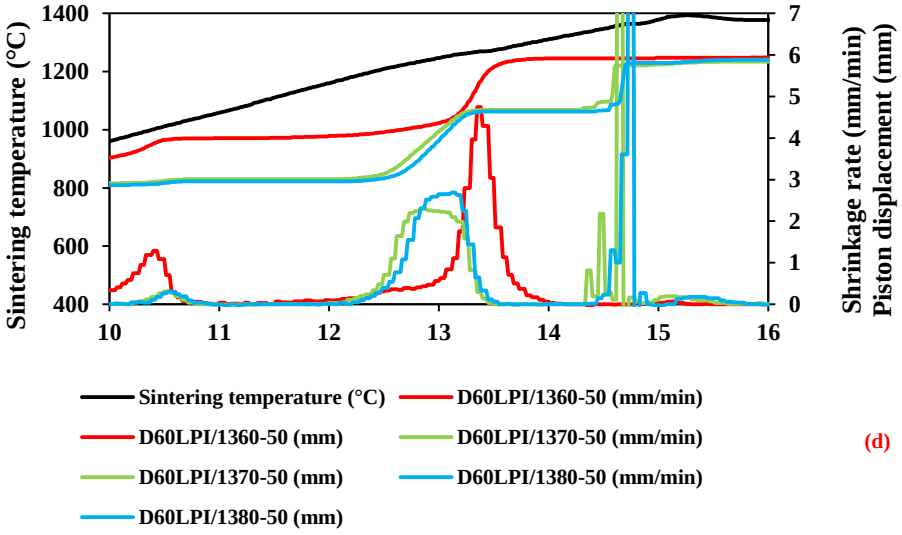

Figure 29: Densification curves of the LPI additive under the sintering conditions indicated

Figure 29 shows the densification curves of the bimodal diamond composites. As was to be expected, the shrinkage peaks are associated with the eutectic temperature of 1280°C. Because the up ramp rate was the same in all cases, the final temperature was sufficiently higher than that eutectic and the applied pressure was the same, these three runs can be considered to be the same within the error of the experimental arrangement used. The two curves, D60LPI/1370-50 and D60LPI/1380-50 show broad shrinkage rate peaks and these composites reached the highest densities of 97.37% and 97.29%, respectively.

4.4.1.2. Microstructures

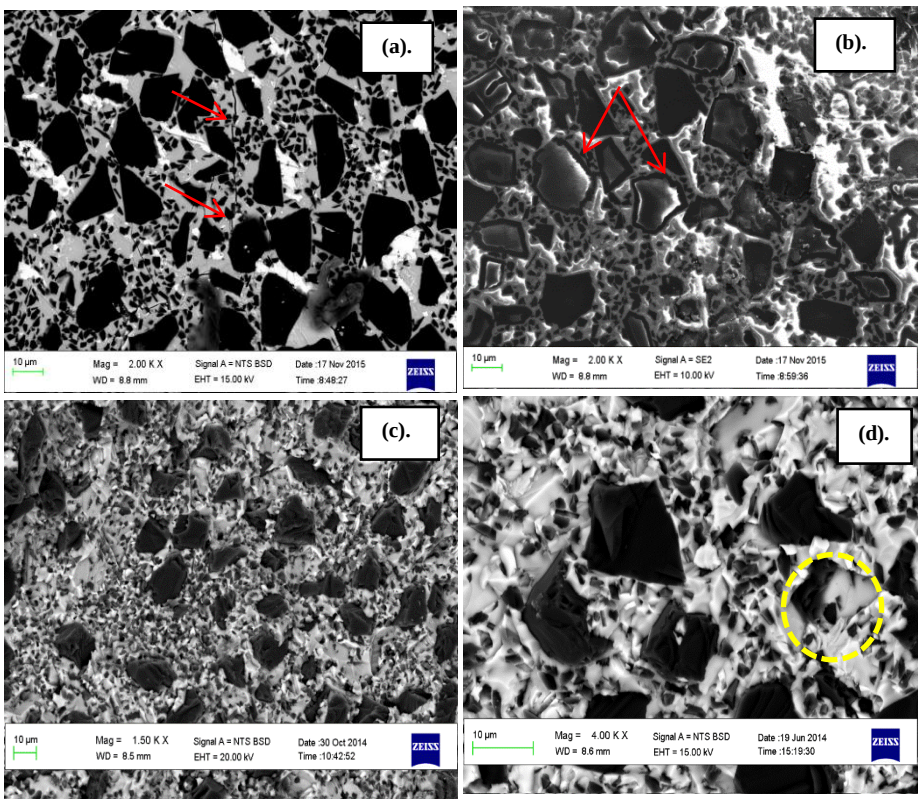

Figure 30: SEM micrographs of the (a). Backscatter, (b). Secondary image of polished D60LPI/1370-50 specimen, (c). Fractured D60LPI/1500-30 specimen with evenly dispersed diamond particles and (d). Fractured surface of the D60LPI/1400-70 specimen

Figure 30 shows polished microstructures of the specimens sintered using the LPI: 40wt%Y_2O_3-25wt%Al_2O_3-35wt%SiO_2 liquid phase sintering aid. The intergranular cracks are highlighted in Figure 30a. Diamond pull-out cavities are observed in Figure 30b. The second image of the D60LPI/1370-50 sample (Fig. 30c) shows the grain boundary around diamond crystals, or incomplete polishing. The central diamond area is more elevated than the periphery. No cracks were observed within the D60LPI/1400-70 except in the pull-out cavity.

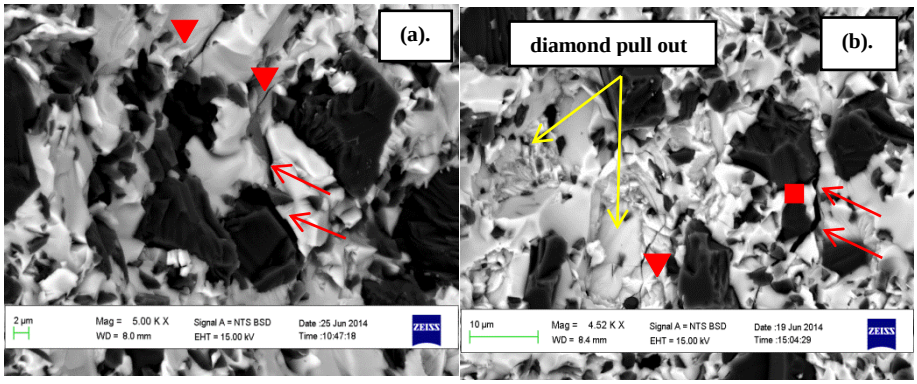

Figure 31: SEM micrographs of the (a). Fractured D60LPI/1400-50 specimen and (b). Fractured surface of the D60LPI/1400-70 specimen. (Cracks within the matrix (▼) and (■) cracks between the matrix and the diamond crystals)

Figure 31 shows the micrographs of the fractured D60LPI/1400-50 and D60LPI/1400-70 specimens. Yellow arrows indicate diamond pull-out cavities and the red arrows represent intergranular cracks passing through the matrix only (▼) and between the matrix and the matrix-diamond interface (■). The cracks within the matrix originated from the diamond pull-out. Local stresses are caused by sintering on cold down, due to mismatch in thermal expansion coefficients.

4.4.1.3. Phase analysis

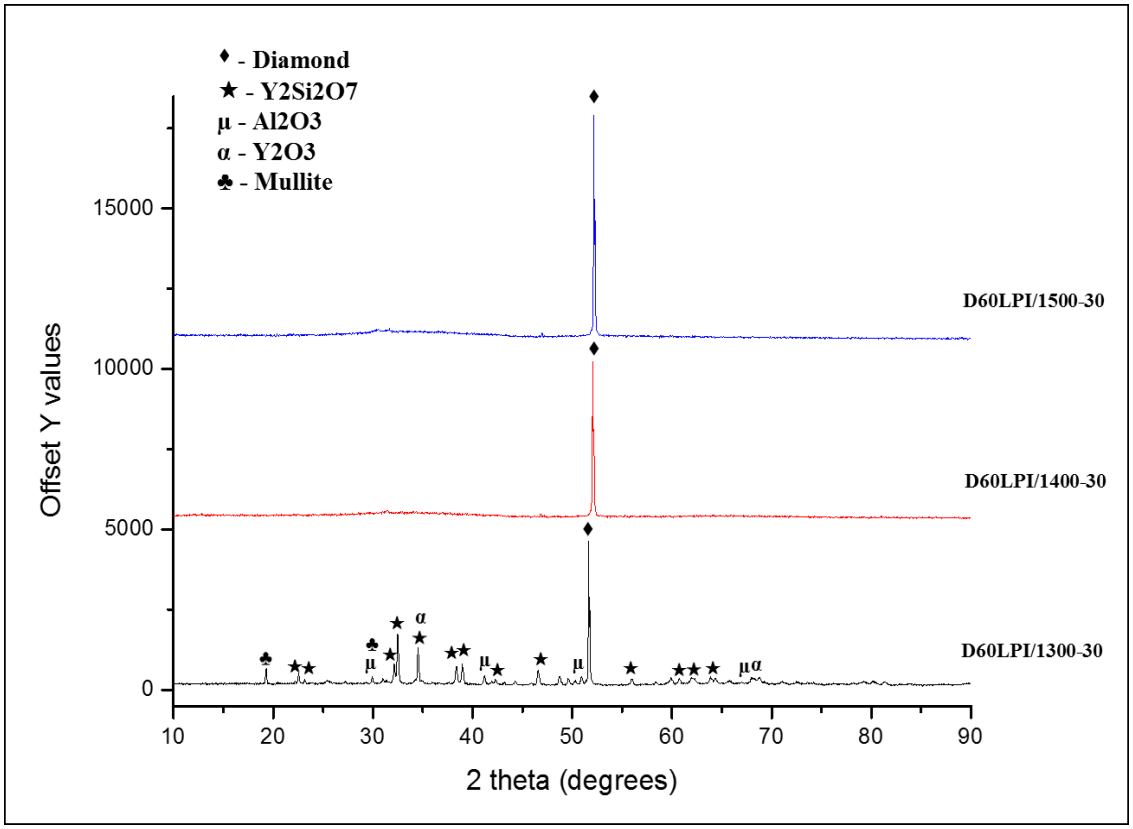

Figure 32: XRD patterns of the 60vol% bimodal diamond plus LPI sintered under 30MPa of applied pressure

Figure 32 shows the changes in amorphisation of the binder phase of the diamond composites with increasing temperatures, as predicted by the phase diagram of Figure 13. At the higher temperatures. LPI is in the primary area crystallisation of SiO_2. This is formed first, but hardly crystallises. The other phases do not have time to form within the sintering times employed.

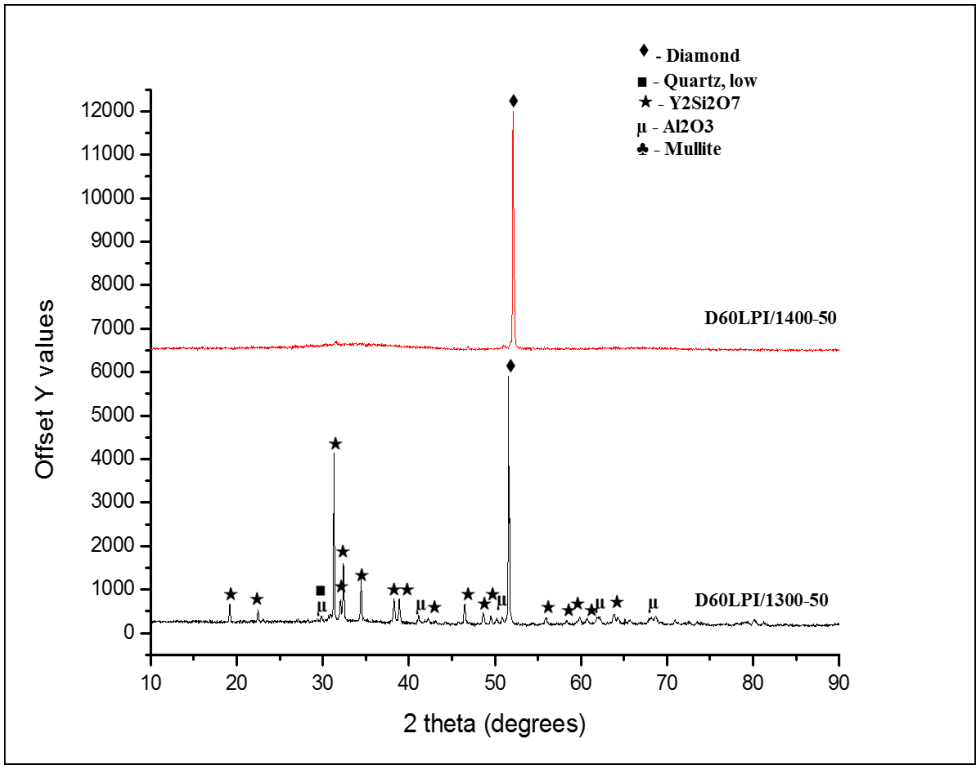

Figure 33: XRD patterns of the 60vol% bimodal diamond plus LPI sintering aid, sintered at 50MPa of applied pressure.

Figure 33 shows the XRD patterns of the diamond composites sintered at 50MPa of applied pressure. The high cooling rates have less effect on the diamond composites sintered at lower temperatures. Therefore, diamond composites sintered at lower temperatures formed crystalline solids. This trace is in agreement with the trace obtained for monomodal diamond composite made with LPI and sintered at the same temperature, as shown in Figure 25 above.

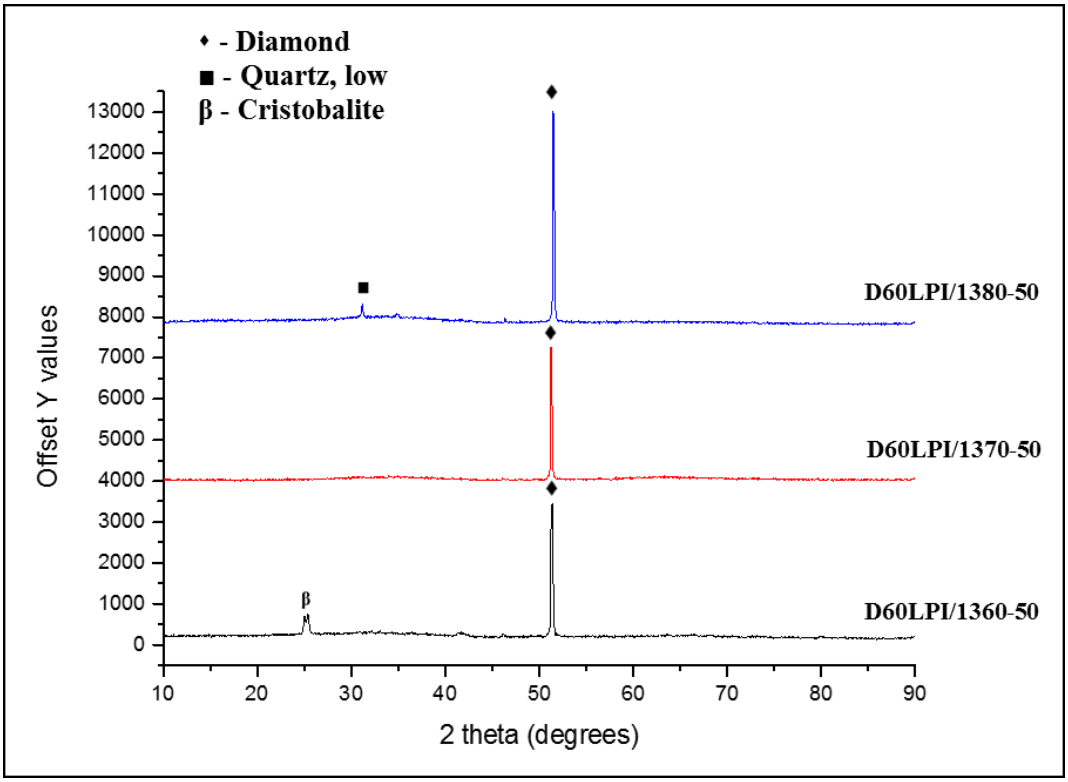

Figure 34: XRD patterns of the 60vol% bimodal diamond composites sintered at 1360°C, 1370°C and 1380°C under 50MPa

Figure 34 shows the XRD patterns of the 60vol% bimodal diamond composite composition sintered at 1360°C/50MPa, 1370°C/50MPa and 1380°C/50MPa respectively. The binder phase in these composites was amorphous, for the reasons explained above. The specimen with the lowest relative density contains cristobalite and the specimen with the highest relative density also had an amorphous secondary phase.

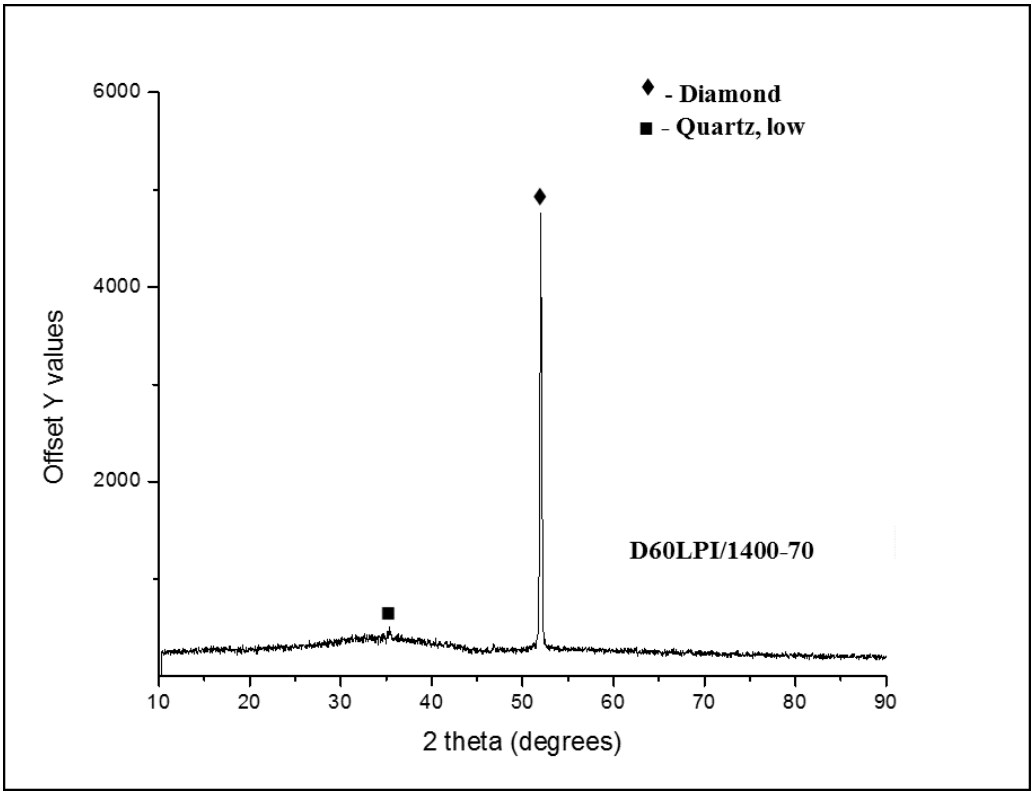

Figure 35: XRD pattern of the D60LPI/1400-70 specimen

Figure 35 shows the XRD pattern of the D60LPI/1400-70 specimen, where the binder is seen to be predominantly amorphous with quartz and diamond as the only crystalline phase within the composite.

Table 18: Intergranular phases confirmed in the diamond composites sintered using the LPI additive

Sample ID	Phases detected by the XRD
D60LPI/1300-30	Diamond, mullite, Keivyite (Y) – $Y_2Si_2O_7$, Al_2O_3 (Corundum) and Y_2O_3
D60LPI/1400-30	Diamond
D60LPI/1500-30	Diamond
D60LPI/1300-50	Diamond, $Al_2Y_4O_9$, (y) – $Y_2Si_2O_7$, cristobalite
D60LPI/1400-50	Diamond
D60LPI/1360-50	Diamond, cristobalite
D60LPI/1370-50	Diamond
D60LPI/1380-50	Diamond and quartz
D60LPI/1400-70	Diamond and quartz
D70LPI/1400-50	Diamond, cristobalite and quartz
D70LPI/1400-70	Diamond and quartz

The gradual temperature increases from 1300°C – 1400°C under 50MPa provided a broader view of the effect of temperature on sintering behaviours and mechanical properties.

Hardness measurements

- The hardness measurements were performed five times per sample

- No fracture toughness measurements were performed due to the status of the micrographs acquired after polishing

4.4.2. 30.78wt%Y_2O_3-13.65wt%Al_2O_3-55.58wt%SiO_2 liquid phase (LPII)

Table 19: Bimodal diamond powder weight fractions and liquid phase volume fractions using the LPII additive

Liquid phase (LPII) - 30.78wt%Y_2O_3-13.65wt%Al_2O_3-55.58wt%SiO_2					
SAMPLE NAME	**Diamond**	**Al_2O_3**	**Y_2O_3**	**SiO_2**	**T.D.(g/cm^3)**
LIQUID PHASE II	**0**	13.65wt%	30.78wt%	55.58wt%	3.2523
MIXTURE I	**50vol%**	5.58vol%	10.32vol%	34.10vol%	3.3812
MIXTURE II	**60vol%**	4.46vol%	8.26vol%	27.28vol%	3.4070
MIXTURE III	**70vol%**	3.25vol%	6.19vol%	20.46vol%	3.4327

Table 19 presents a list of mixtures that will be used to consolidate the diamond composites presented in Table 20. We will investigate the effect of these mixtures on the densification behaviours, microstructural evolution, XRD intermediate phases and Vickers hardness values. All the samples in Table 19 were fabricated using the LPII: 30.78wt%Y_2O_3-13.65wt%Al_2O_3-55.58wt%SiO_2 liquid phase additive. Because this composition has a higher melting point than LPI (as shown in Figure 13) the sintering temperatures used were higher than those used for LPI. The experimental design was as follows: Begin with 50vol% bimodal diamond at a sintering temperature of 1400^{o}C, applying the maximum pressure allowed by the SPS furnace, i.e. 70MPa. Then explore mainly the case of 60vol% bimodal diamond, as this was the one that gave the best densities when using LPI. Finish by exploring the case of 70vol% diamond, for the maximum pressure again. The reason for the latter is that we already know that at 70vol% densification by particle rearrangement is not easy to achieve as we already are above the percolation limit for this diamond powder mix.

Table 20: Summary of the bimodal diamond composites liquid phase sintered using LPII as sintering aid under the conditions listed

Sample ID	*Diamond comp.*	*T* (°C)	*P* (MPa)	*d* (g cm^{-3})	d_{rev} (%)	P_O (%)	HV_{10} (kg/mm^2)
D50LPII/1400-70	50vol%	1400	70	2.7221	87.9	0.10	539 ± 128
D60LPII/1300-30	60vol%	1300	30	2.9249	85.9	9.95	391 ± 2
D60LPII/1400-30	60vol%	1400	30	2.9475	86.5	7.97	490 ± 84
D60LPII/1500-30	60vol%	1500	30	2.9969	89.0	5.78	548 ± 13
D60LPII/1300-50	60vol%	1300	50	2.9633	88.0	7.83	477 ± 39
D60LPII/1400-50	60vol%	1400	50	2.9747	87.3	4.83	618 ± 15
D70LPII/1400-70	70vol%	1400	70	2.6716	75.2	17.99	218 ± 4

4.4.2.1. Densification

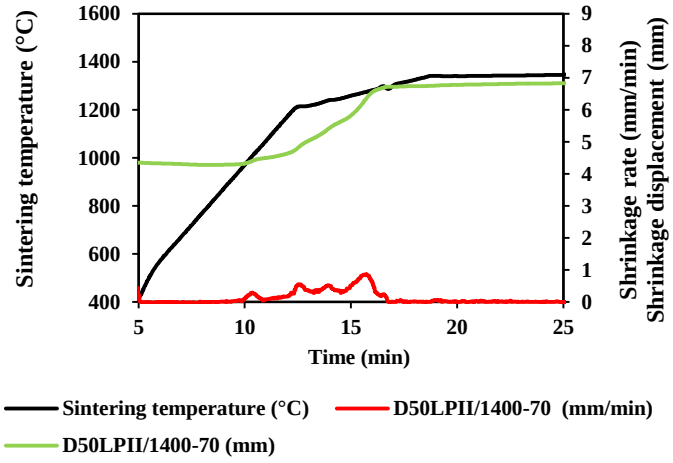

(a)

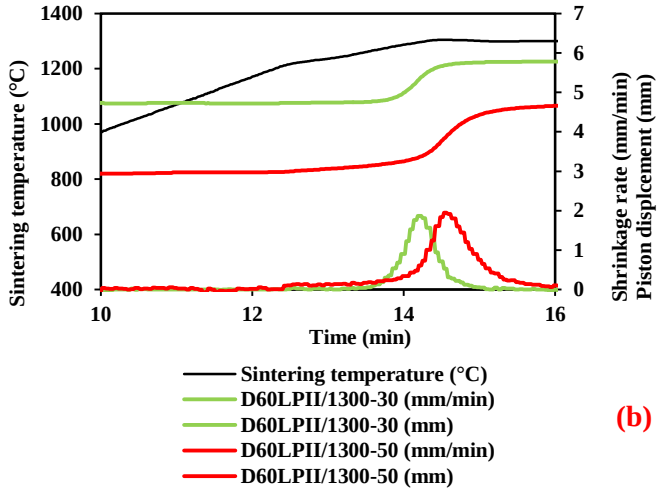

(b)

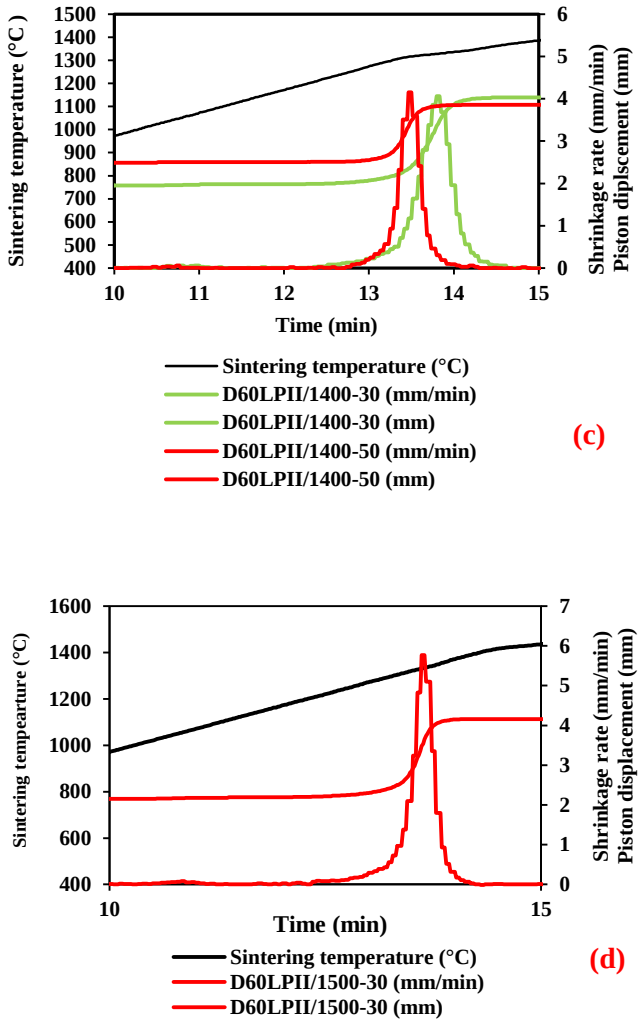

Figure 36: Densification curves of the (a). 50vol% diamond composite sintered at 1400°C under 70MPa, (b). 60vol% diamond composites sintered at 1300°C, (c). 1400°C and (d). 1500°C

Figure 36 above shows the densification graphs of the bimodal diamond composites, sintered with LPII sintering aid and binder. Sample D50LPII/1400-70 shows little piston displacement, possibly because of obstacle in the sample assembly arrangement. All other samples had a shrinkage peak again above the eutectic of 1280ºC. The displacement between the sample sintered at 1400°C and samples sintered at 1500°C remained at 4mm, in Figure 36b and Figure 36b respectively.

4.4.2.2. Microstructures

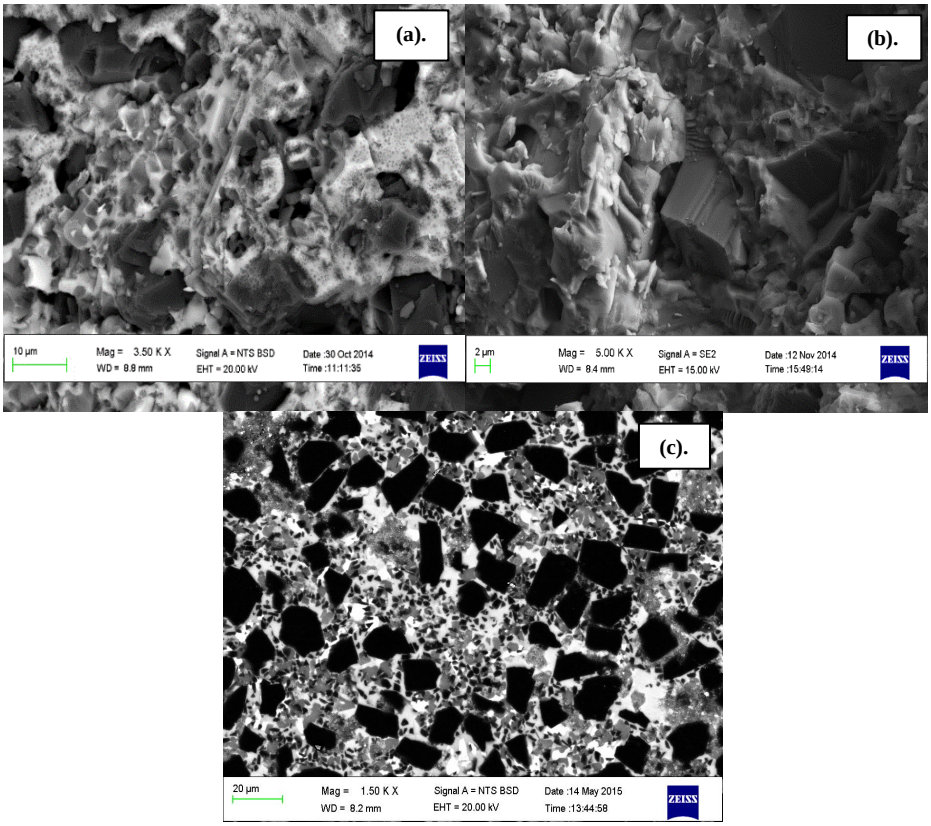

Figure 37: SEM micrographs of (a). Fractured surface D60LPII/1500-30 (89.0%) (b). fractured surface of D60LPII/1300-50 (86.98%), (c). polished D60LPII/1400-50 specimens

Figure 37 shows the micrographs of D60LPII/1500-30 (87.96% of TD) composite. From Figure 37c it can be seen that this composite had a dual phase binder. From the XRD analysis below, this is a solidified dual liquid amorphous phase. The diamond surface defects in Figure 37b suggest that a strong interfacial bonding between diamond particles and the liquid phase was formed. Figure 37c shows SEM micrographs of the polished surface of the specimen that reached the highest relative density among diamond composites sintered using LPII. No visible open porosity and no diamond pull-out.

4.4.2.4. Phase analysis

Figure 38 below, shows recent calculations of the Y_2O_3-Al_3O_3-SiO_2 phase diagram by Mao et al. 2008. From that it can be seen that LPII, when molten, is in a dual liquid phase region. This explains the findings of Figure 37 above, regarding the presence of a dual phase binder in Figure 37c, but also the XRD traces shown below.

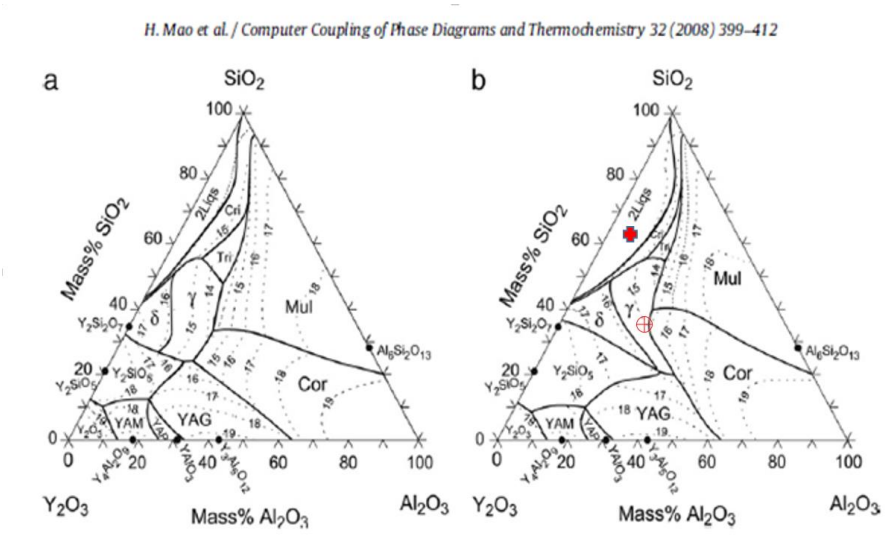

Figure 38: Phase diagram of the Y_2O_3-Al_3O_3-SiO_2 system, after Mao et al. 2008.

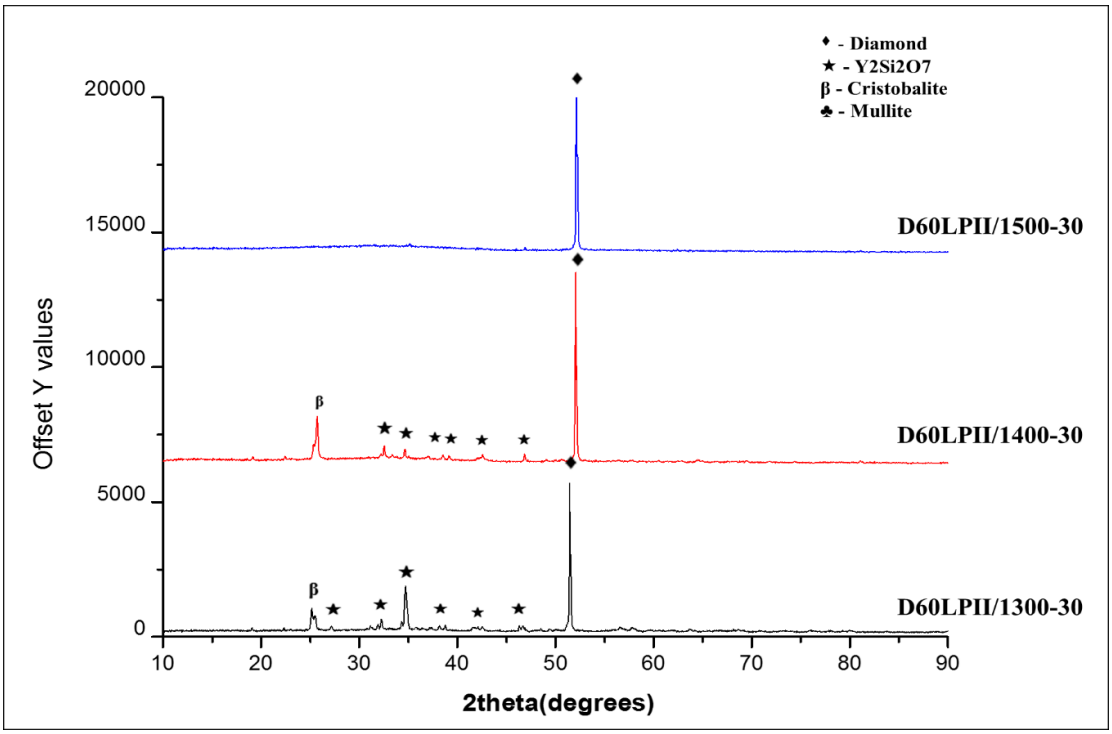

Figure 39: XRD patterns of the 60vol% diamond composites sintered with the 30.78wt%Y_2O_3-13.65wt%Al_2O_3-55.58wt%SiO_2 liquid additive, under 30MPa

Figure 39 shows the XRD patterns of the 60vol% bimodal diamond composites. The specimens were amorphised with increasing sintering temperatures. *(y)*-$Y_2Si_2O_7$ was the main phase on both the D60LPII/300-30 (85.85%) and D60LPII/1400-30 (86.51%) specimens. Specimen D60LPII/1500-30 (87.96%) was predominantly amorphous. Cristobalite was identified in the D60LPII/1300-30 and D60LPII/1400-30 specimens. These findings are in agreement with the findings in Fig 39b.

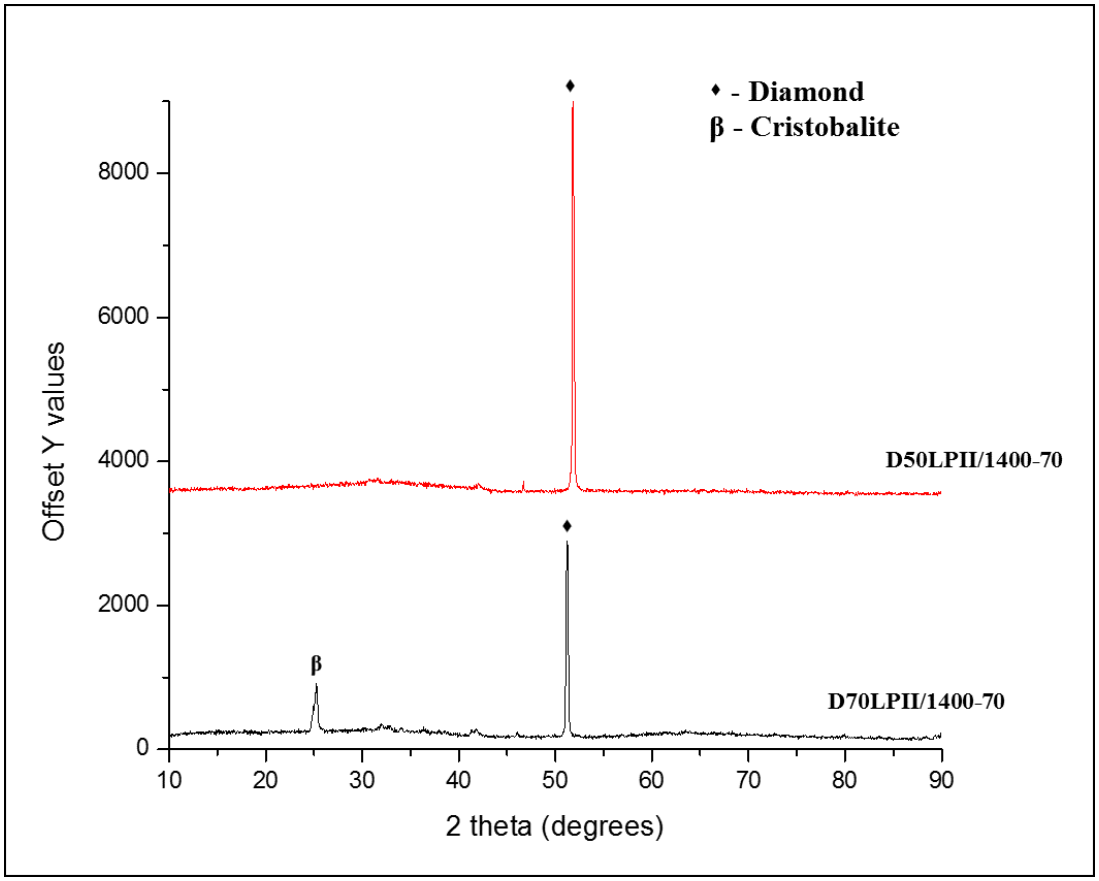

Figure 40: XRD patterns of the 50vol% and 70vol% bimodal diamond composites liquid sintered at 1400°C under 70MPa

Figure 40 shows the XRD patterns of the bimodal diamond specimens sintered at 1400°C. The specimen with 70vol% diamond shows the presence of cristobalite, as expected, while that with only 50vol% shows no crystalline phase. It may be that the presence of such high amounts of diamond inhibited the proper interaction of the starting components of the LPII in this particular composition. Vickers hardness (Table 19) declined by 50% from 539 kg/mm^2 to 218 kg/mm^2 with the increasing diamond content, when both D70LPII/1400-70 and D50LPII/1400-70 samples were sintered at 1400°C under 70MPa. This correlates well with the concomitant decrease in density from 87.9% to 75.2% of theoretical.

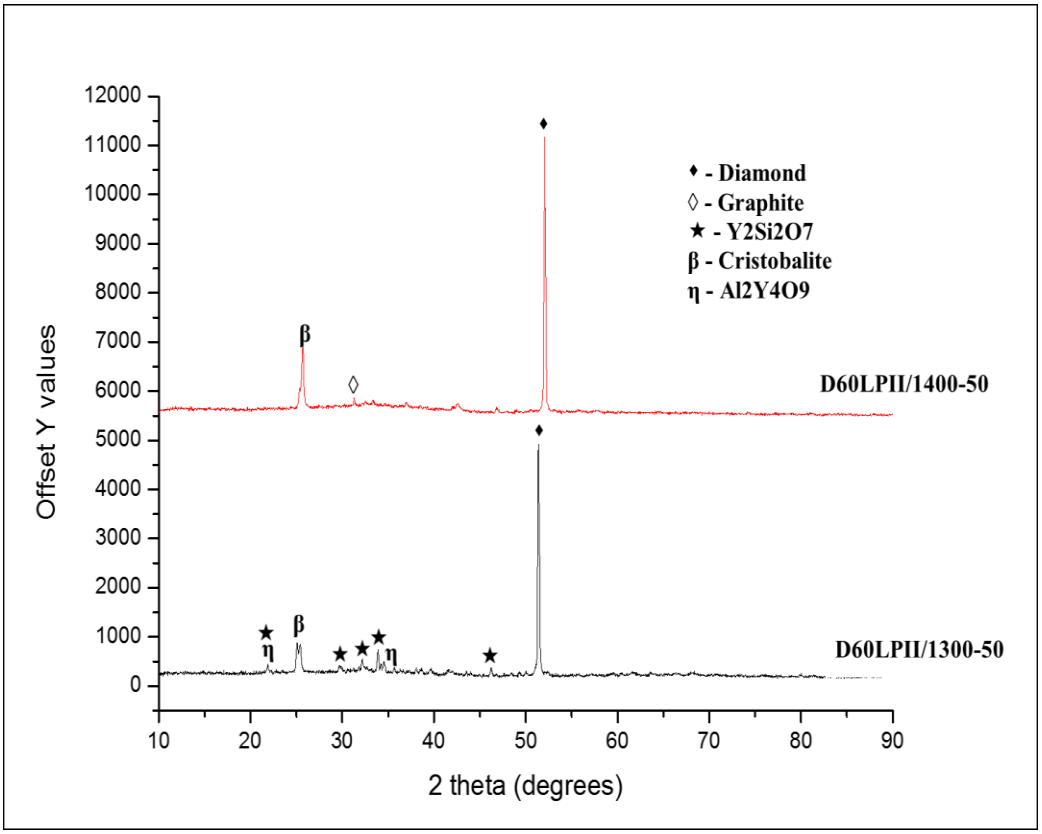

Figure 41: XRD patterns of the of the 60vol% bimodal diamond composites, D60LPII/1300-50 and D60LPII/1400-50 liquid phase sintered under 50MPa

Figure 41 shows the XRD patterns of the 60vol% bimodal diamond composites sintered under 50MPa. As explained above, the LPII starting components only react partially at low temperatures. This gives rise to the presence of Y_2SiO_7 and $Al_2Y_4O_9$ in the sample sintered only up to 1300ºC. At 1400ºC, the reactions are more advanced, with some crystalline SiO_2 in the form of cristobalite still remaining.

Table 21: Phases formed during the sintering of the specimens listed below

Sample ID	Phases detected by the XRD
D50LPII/1400-70	Diamond
D60LPII/1300-30	Diamond, cristobalite, (y)-$Y_2Si_2O_7$
D60LPII/1400-30	Diamond, cristobalite and (y)-$Y_2Si_2O_7$
D60LPII/1500-30	Diamond (amorphous)
D60LPII/1300-50	Diamond, $Al_2Y_4O_9$, (y) – $Y_2Si_2O_7$, cristobalite
D60LPII/1400-50	Diamond, cristobalite and graphite
D70LPII/1400-70	Diamond, cristobalite

Table 21 presents a summary of the intergranular phases formed during sintering. D60LPII/1500-30 was amorphous. As per the phase diagram of Figure 38, by Mao et al.

Of the materials sintered with bimodal diamond and LPII, the two materials with the highest densities, D60LPII/1500-30 (89%) and D60LPII/1400-50 (87.3%) had the highest hardness. Of the two samples,

the one sintered at the lowest temperature had the highest hardness, although sintered at a lower temperature.

Chapter 5

DISCUSSION OF THE EXPERIMENTAL RESULTS

A PCD composite was successfully bound without diamond to diamond bonding via LPS method under low pressures. The objectives of this study were categorized into two parts; (i). production of high density composites using only the particle rearrangement mechanism and (ii). achievement of high hardness through the selection of a reasonably hard matrix complementing a high diamond volume fraction in the attained composites. The Y_2O_3-Al_2O_3-SiO_2 matrix will be discussed first.

5.1. Production of dense diamond composites using the particle rearrangement method

Conventionally, liquid phase sintering is achieved through interfacial bonding to achieve full densification. To achieve full densification solely through particle rearrangement is largely dependent on the liquid phase and the particle size distribution of the powder being densified. The behaviour of the additives under SPS sintering is outlined in section 5.2. In addition to the proposed LPS additives, the diamond particle distribution was the second feature to be explored in order to achieve high densities. As reported in chapter 4, the bimodal diamond composites out-performed monomodal diamond composites using LPI as the sintering additive. Previous studies have shown that bimodal diamond particle distribution enhances the effect of the capillary difference between the course and fine channels of solid particles exaggerating particle rearrangement and subsequently improving densification via pore eliminations (S.-J. L. Kang, 2004). Mizuuchi et al. also demonstrated that bimodal diamond composites improved the packing density and thermal conductivity compared to monomodal diamond composites sintered using the same diamond and matrix volume fraction (Mizuuchi et al., 2015). Bimodal diamond composites also increased densities due to the increased coordination number, and therefore the shrinkage rates were higher because of smaller pores within high coordination number structures (Hirata, Hara, & Aksay, 2009). In bimodal sized composites, the degree of close packing is ideally low and densification was reported to occur uniformly. Bimodal diamond composites close large interspaces, large interspaces have low capillary force and therefore poor densification. Although the bimodal diamond composites exhibit good experimental results that are in line with the desired properties of the study, it is therefore possible for these composites to reach saturation and this is shown in Table 22.

Table 22: Vickers hardness values of the 60vo% and 70vol% bimodal diamond sintered under 50MPa and 70MPa of applied pressure

Sample ID	d_{rev} (%)	HV_{10} (kg/mm^2)
D60LPII/1400-50	87.31	618 ± 15
D70LPII/1400-70	75.19	218 ± 4
D60LPI/1400-50	95.95	1294 ± 26
D70LPI/1400-50	82.87	448 ± 60
D60LPI/1400-70	93.73	1047 ± 19
D70LPI/1400-70	83.16	952 ± 50

Table 22 shows the 60vol% and 70vol% bimodal diamond composites and highlight the change in the properties with increasing diamond content. The higher diamond volume compositions consistently displayed lower density values and lower hardness measurements. At such high volume fractions, the diamond phase exceeds it percolation limit, thus stopping the LPS aid from filing the voids between the diamond particles. Thus, beyond 35vol% diamond volume fraction, this inverse relationship between diamond volume fraction and density as well as hardness was found to apply in all samples tested in this work. The low quantity binder fails to penetrate the interspaces between diamond crystals to eliminate pores and therefore no inhibitors block the cracks, or re-direct them away from the diamonds to avoid compromising the strength of the composites (Tao, Zhu, Tian, Yang, & Yang, 2014).

5. 2. The Liquid Phase sintering aids

Liquid phase additives influence the state of densification through their liquid phase generation abilities at different sintering conditions. Two of the additives selected as aids for this study were studied using the SPS shrinkage rate and piston displacement curves. The mixture compositions of these two additives determined experimental outcomes and the properties of the composites. The selected additives generated liquids at temperatures above their eutectic to facilitate densification and alleviate residual/local stresses formed due to the mismatched CTEs. The intergranular phases formed as the results of sintering the additives can possibly improve fracture toughness if they are expandable (Noma, T. and Sawaoka, A., 1985). In a study conducted by Claussen et al., it was observed that the zirconia particle-dispersed alumina ceramics showed improved toughness due to stress induced micro-crack toughening (Claussen, Steeb, & Pabst, 1977). Therefore, phases such as graphite also provide toughening properties to the diamond composites because graphite acts as a barrier between the diamond crystals and the matrix. This barrier is more susceptible to cracks than diamond. Graphite evolution leads to volume expansion that causes stresses that close cracks, leading to fracture toughness improvement (Evans & Faber, 1981).

Two different LPS aid compositions, both within the Y_2O_3-Al_2O_3-SiO_2 were selected for this work. They are shown in Table 23 below:

Table 23: Compositions of LPI and LPII

	Y_2O_3wt%	Al_2O_3wt%	SiO_2wt%
LPI	40	25	35
LPII	30.78	13.64	55.58

From the composition of LPI, it follows that in the phase diagram by Mao et al. 2008, as shown in Figure 23 this LPS aid is in the peritectic between $Y_2Si_2O_7$ and mullite, $Al_6Si_4O_{13}$. Therefore, these two components, as temperature is raised, will crystallise first. According to more recent calculations (Figure 38, Mao et al. 2008) Al_2O_3 and γ–$Y_2Si_2O_7$ will crystallise first and only during cool down, as a second step, will Al_2O_3 react with the melt to form mullite. The remaining SiO_2 will stabilize the glassy phase. Samples sintered with LPI at temperatures below the eutectic, do not fully react; as a result, mixed compositions are obtained. This is seen for d25LPI/1200-70 and d25LPI/1300-70, in figure 22. At 1400ºC (Fig 25) complete melt is achieved and on cool down not enough time is given for the phases to crystallise, leaving only a small SiO_2 peak to appear. As temperature is raised, SiO_2 reacts with the graphite tooling, giving rise to the reaction $SiO_2+3C = SiC+2CO$, or even the reduction of SiO_2 to SiO which would be removed. In either case, the composition would move into the Al_2O_3-Y_2O_3 rich region of the phase diagram, giving rise to the formation of YAG, $Y_3Al_5O_{12}$, as seen in figure 24 for the d35LPI compositions. The same behaviour is observed for the 60vol% diamond containing samples, sintered with the LPI sintering aid (Fig 25). The same arrangement applies also for the binder phases of the bimodal diamond composites made with LPI, i.e. D60LPI/1300-50 and D6LPI/1400-50, Fig 33 and D60LPI/1360-1370-1380, Fig 34.

LPII was used in the case of bimodal powder. This composition is within the SiO_2 rich region. The products crystallising in this region would be SiO_2, $Y_2Si_2O_7$ and $Al_6Si_4O_{13}$. This is seen in figures 39, 40 and 41, where at low temperatures a set of mixed phases appear, to be replaced by amorphous phase at higher ones, as predicted by the phase diagram of figure 38. The amorphous phase thus generated would, given enough time, transform on cristobalite, mullite and $Y_2Al_2O_7$. This was largely suppressed by the rapid cooling rate of the SPS furnace. Of note is the appearance of a small graphite peak in the trace obtained for D60LPII/1400-50, figure 41. Also, the reader is referred to figure 37, where, in the micrograph of D60LPII/1400-50, one can see the presence of two glassy phases in the binder, as predicted by the phase diagram for LPII, Figure 38.

5.3. Sintering curves and densities attained

Figure 13 shows the phase diagram of the Y_2O_3-Al_2O_3-SiO_2 system, as published by Mao et al. 2008. The eutectic of this system is at 1280ºC. It is this temperature that largely determined the behavior of

the two LPS aids used here, as far as densification rates are concerned. The behavior of the binder phases with rising temperature is also reflected in the DTA/TG traces obtained for LPI and shown in Figures 18 and 19. From these figures two important features are observed: 1. there is a small peak at 1060ºC. This corresponds to the strain point of fused silica (SwiffGlass, 2015) and (De Jong, Beerkens, & van Nijnatten, 2000) and; 2. There is an endothermic peak at 1280ºC, that being the metastable eutectic point of the Al_2O_3-Y_2O_3-SiO_2 system.

In Figure 20 the piston displacement rate peaks of d25LPI/1300-50 and d35LPI/1300-70 both show a mild shrinkage at the vicinity of 1000ºC. This is possibly related to the amorphous silica particles reaching their strain point. In the same figure, d60LPI/1300-1600 show strong shrinkage just above the eutectic of 1280ºC, as discussed above. Figure 28 shows the shrinkage behavior of the D60LPI family of composites. In all cases the shrinkage peaks can be related to the above eutectic. Furthermore, the appearance of this peak shifts to lower temperature with increasing applied pressure, indicating that particle rearrangement involves a degree of plastic deformation of the binder phase, not just flow of a melt. The same effect can be seen for D60LPI/1360-1370-1380 composites, shown in figure 29. Figure 36 shows the shrinkage curves of the D60LPII family of composites made in this study. Again these peaks are associated with the metastable eutectic at 1280ºC. The figure for the D60LPII/1300 materials is small, indicating the resistance of the binder to deform at temperatures so close to the eutectic. The level of the shrinkage speed more than doubles as the sintering temperature crosses over to 1400ºC and above. The shrinkage speed of D60LPII/1400-50 is very low and must be related to an error in assembly of the cell.

It is important to notice that the shrinkage rates for the bimodal diamond mixes are consistently higher than the ones attained with the monomodal powders, vindicating in this regards the choice of bimodal powders as a means for attaining higher densifications.

5.3 Microstructure

The microstructures obtained in this work are represented here by Fig 21, 30, 31 and 37. Fig 21 shows the micrographs obtained for monomodal diamond sintered with LPI. All figures show the diamond phase well dispersed in the LPI matrix. Fig 21a shows the micrograph of the fracture surface ofd60LPI/1500-30. Of interest here is the fact that there is some clustering of the diamond particles, as there might be for such a high volume fraction. Also, importantly, cracks are detected, running through parts of the matrix. When the crack meets a diamond particle, it is not seen to be running through it, but rather on the diamond-matrix interface, appearing, bifurcated, on the other side. The XRD trace of this composite in figure 25 indicates the presence of graphite in it. Such a phase is usually formed on the surface of graphitizing diamond (Hickey, Jones, & Elliman, 2009); this would explain the behavior of this crack. Such clustering is not seen for Fig. 21 b and c, which show the micrographs of d35LPI 1300-70 and 1600-50 respectively. However, several diamond pull outs are observed. This is indicative that

the diamond-matrix interface is weak. It is possible that, even at 1300ºC, some graphitization appears on the surface of the diamond particles, weakening them and causing these pull outs to occur. Having said that, it is also important to mention that, because of the even dispersion of the diamond particles in the LPI matrix, it would seem that once the eutectic melt is formed, it wets the diamond particle surfaces quite well. The effect of wetting is even better seen in the micrographs of D60LPI/1370-50 in Figure 30. There, the large particles in this bimodal diamond composite are seen to be often touching, creating a bridging skeleton, in which the finer particles are located. However, instead of just filing the voids between the large diamond particles, they are seen to be diluted by the LPI matrix, which, by wetting these particles so well, seems to have pulled them apart. Diamond pull out is also seen to occur in these compositions, as indicated in Figure 31. Figure 30a also shows cracks in the D60LPI/1370-50 (Backscatter). These cracks also seem to bypass the diamond grains rather than run through them. This still supports the evidence of weak diamond-matrix interface. A weak diamond to matrix interface is also seen in Figure 30b, of D60LPI/1370-50 (Secondary imaging) specimen.

Figure 37 shows micrographs of the D60LPII family of materials. Of particular interest is Fig 37c, showing the polished surface of D60LPII/1400-50 material. The presence of a dual phase in the LPII matrix is clearly seen. The corresponding XRD trace in Figure 39 indicated that there should be present in that phase cristostallite, as well as $Y_2Al_2O_7$.

5.4. Densities and hardness attained

Tables 13, 17 and 18 summarize the results obtained in this work, in terms of densities and hardness. Table 13 shows the results for the d25, d35 and d60 composites, sintered with LPI. It can be seen that, as temperature is raised, density and hardness increase, as long as the sintering temperature does not exceed 1400ºC. The reason for this is that at higher temperatures the SiO_2 component is reduced by the graphite tooling (and possibly by the diamond itself) into SiC and CO. The gas evolution has been seen to generate small pores on the surface of these samples. This in itself explains the plateauing and subsequent decline of the density observed. The hardness of the d25LPI/1300-70 is seen to increase sharply with sintering temperature when compared to d25LPI/1200-70. This is explained by the fact that not only is the density significantly higher, but also, the binder phase is crystalline, being rich in mullite and Al_2O_3. The density of the 60vol% diamond composite is quite low when sintering at 1300ºC, because this volume fraction is well above the percolation limit. The density is seen to rise with increasing temperature for this family of composites, with a corresponding increase in hardness. However the hardness of d60LPI/1400-30 is only 380 Vickers, compared with the XRD trace in figure 25, it can be seen that this matrix is by and large amorphous, thus depriving this composite of the harness that comes with a crystalline matrix.

Table 17 shows the summary of the results obtained for the bimodal diamond composites, sintered with LPI as the sintering aid/binder. Density is seen to be higher than those of the monomodal diamond composites, indicating the improvement attained in packing density. The density and hardness are seen to increase with sintering temperature. Furthermore, increasing the applied pressure brings added benefits in terms of density, driving the hardness to the highest in this work, i.e. 1294 Vickers. The phases present, according to the trace of figure 34 is just diamond and some low quartz, with an amorphous background. Increasing the diamond volume fraction to 70% does not bring any added benefit in terms of density of hardness, clearly because the percolation limit for this composite is exceeded. Table 20 summarizes the results obtained for the bimodal diamond powder sintered with LPII sintering aid. Generally speaking, the densities attained are lower than those obtained for bimodal powders sintered with LPI. Thus, the fact that this composition is further from the eutectic did have a detrimental effect in the densification of these materials.

Finally, Table 24 shows the composites with which the highest densities and hardness were achieved.

Table 24: A list of samples that achieved relative density higher than 93% - bimodal liquid phase sintered using LPI

Sample ID	*T* (°C)	*P* (MPa)	d_{rev} (%)	HV_{10} (kg/mm^2)	*Intergranular phases*
D60LPI/1370-50	1370	50	97.4	1235 ± 20	Diamond
D60LPI/1380-50	1380	50	97.3	1249 ± 57	Diamond and quartz
D60LPI/1400-50	1400	50	95.9	1294 ± 26	Diamond
D60LPI/1400-70	1400	70	93.7	1047 ± 19	Diamond and quartz

They were all made bimodal diamond, 60% diamond volume fraction, with LPI as the sintering aid/binder. In all cases the temperature did not exceed 1400ºC. The reasons for the higher values have already been given above: The temperature was low enough to avoid to some extend reduction of the SiO_2 component, while the bimodal PCD allows for better packing of the diamond particles.

Figure 42 shows the hardness indentation for the (a) D60LPII/1400-50, (b). polished D60LPI/1370-50 specimen and (c). d35LPI/1300-70. No radial cracks are seen emanating from the indentation, indicating a high fracture toughness for these materials. Of particular interest is Fig 42b, where it can be seen that the diamond grains have weak interfaces with the matrix, thus deflecting cracks along the diamond-matrix interface.

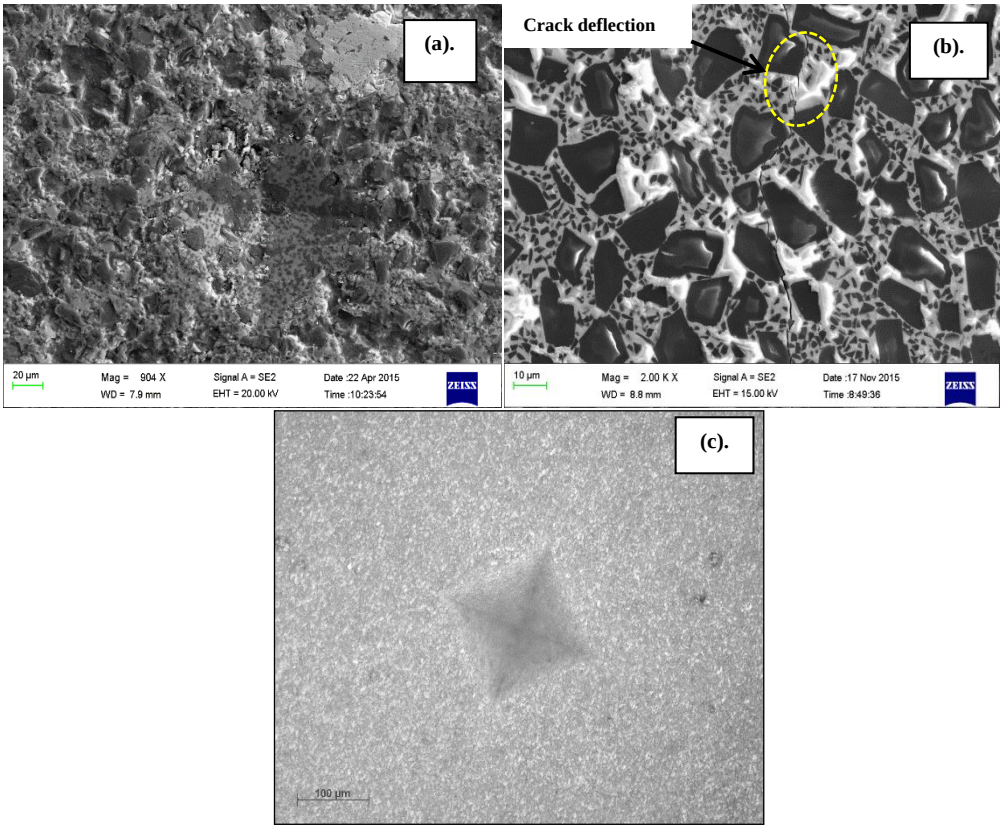

Figure 42: The Vickers hardness indentations (HV_{10}) of the (a). D60LPII/1400-50 (b). polished D60LPI/1370-50 specimen and (c). d35LPI/1300-70

The hardness of composite materials can, to a first approximation, be calculated using the rule of mixtures. From that it would be expected for the composites derived in this work to possess a hardness of the order of 30GPa or 3000 HV_{10}. This was not the case. Apart from the fact that the densities were not high enough, there is one more very important reason for this defect and it is the presence of graphite in the materials made. As explained several times above, the interfaces between diamond and matrix are seen to be weak, allowing cracks to run along the periphery of diamond grains rather than through them. This indicated weak interfaces. The evidence of diamond pull out has also been widely reported in this dissertation. Thus, it has to be accepted that the diamond particles in the materials we made are not well bonded with the matrix. In view of the fact that the LP sintering aid seemed to wet the diamond particles quite well, one would have expected this bond to have been strong. Therefore, it must be concluded that the main reason for these weak interfaces was diamond surface graphitisation. This results in the diamond phase acting more like a void rather than a strengthening component of the materials made. Should this work be ever repeated, it would be necessary to use diamond particles coated with a thin protective layer, such as SiC, which might bond better with an SiO_2 – containing matrix and which would protect the diamond particle surface from graphitization. Also, in such an arrangement, the graphite tooling would need to be better isolated from the sample's powders during sintering.

Chapter 6

CONCLUSION

6.1. Conclusion

In this work, diamond composite materials were made by using mixed components out of the Y_2O_3-Al_2O_3-SiO_2 system as liquid phase sintering aids. By controlling the sintering temperature it was made sure that the only densifying mechanism operating during sintering was particle rearrangement. It was found that the mix LPI: 40wt%Y_2O_3, 25wt%Al_2O_3, 35wt%SiO_2, being very close to the eutectic of the system, gave the best results in terms of densification achieved (97% of theoretical). Using a bimodal diamond mix was also found to significantly assist with densification, by ensuring better particle packing during the rearrangement step in the sintering cycle. It was found that at temperatures exceeding 1400^{o}C reduction of SiO_2 by the graphite in the tooling led to deterioration of the density attained. Generally, it was found that a weak diamond-matrix interface gave rise to hardnesses below what was to be expected from the compositions made. Although graphite was not always detectable in the XRD traces, this weak interface may be ascribed to graphitization of the diamond particle surface.

Still, in view of the possible great advantages in developing strong and hard low pressure sintered diamond composites, this work needs to be seen as a first step in the development of such important ceramics, where the lessons learned here will be used to help overcome the graphitization problems, those being the main culprits for the observed weakening of these materials.

6.2. Recommendations

- In order to optimize the sintering process, it is recommended that the milling technique for the amorphous silica be extended. An effective dispersant for optimal particle distribution should be used.
- Reduce cooling rates to allow for adequate crystallisation of intergranular phases to occur.
- Use SiC-coated diamond powders in the future to protect the surfaces from graphitization.
- Use ceramic high temperature tooling, in order to avoid the problem of the reduction of the SiO_2 by the graphite in said tooling.
- Use of the scaife polishing wheel to successfully polish the diamond composites and perform fracture toughness tests.

Limitations of the study:

It was difficult to establish correlated trends using monomodal diamond composites, due to the liquid phase bursts that occurred during sintering. This was caused by the reduction of the SiO_2 by the graphite tooling. The monomodal diamond composites were used to investigate and identify the optimal sintering region (temperature/pressure conditions) for the bimodal diamond composites.

REFERENCES

Akaishi, M., Kanda, H., Sato, Y., Setaka, N., Ohsawa, T., & Fukunaga, O. (1982). Sintering behaviour of the diamond-cobalt system at high temperature and pressure. *Journal of Materials Science*, *17*(1), 193–198. https://doi.org/10.1007/BF00809051

Anselmi-Tamburini, U., Gennari, S., Garay, J. E., & Munir, Z. A. (2005). Fundamental investigations on the spark plasma sintering/synthesis process. *Materials Science and Engineering: A*, *394*(1–2), 139–148. https://doi.org/10.1016/j.msea.2004.11.019

Axén, N., Hogmark, S., & Jacobson, S. (2000). Friction and Wear Measurement Techniques. https://doi.org/10.1201/9780849377877.ch13

Bauman, I., Ćurić, D., & Boban, M. (2008). Mixing of solids in different mixing devices. *Sadhana*, *33*(6), 721–731. https://doi.org/10.1007/s12046-008-0030-5

Berman, R., & Simon, S. F. (1955). On the Graphite - Diamond Equilibrium. *Berichte Der Bunsengesellschaft Für Physikalische Chemie*, *59*(5), 333–338. https://doi.org/10.1002/BBPC.19550590503

Boecker, W. D. ., & Storm, R. S. (1990). *EP0419271 A2*. Retrieved from https://www.google.com/patents/EP0419271A2?cl=en

Boland, J. (2014). Materials science: Diamond get harder. *Nature*, *510*, 220–221.

Can, A. (2006, February 6). *Densification, microstructure and properties of liquidphase sintered silicon carbide materials*. *WiredSpace*. University of the witwatersrand. Retrieved from http://wiredspace.wits.ac.za/handle/10539/172

Chen, X. ., Khor, K. ., Chan, S. ., & Yu, L. . (2004). Overcoming the effect of contaminant in solid oxide fuel cell (SOFC) electrolyte: spark plasma sintering (SPS) of 0.5wt.% silica-doped yttria-stabilized zirconia (YSZ). *Materials Science and Engineering: A*, *374*(1–2), 64–71. https://doi.org/10.1016/j.msea.2003.12.028

Chen, Y., & Zhang, L. C. (2009). On the Polishing Techniques of Diamond and Diamond Composites. *Key Engineering Materials*, *404*, 85–96. https://doi.org/10.4028/www.scientific.net/KEM.404.85

Choi, G.-S., Kim, J.-Y., & Lee, D.-H. (1992). Resistance/Spark sintering under pressure of intermetallic TiAl powders. *Journal of the Korean Institute of Metals and Materials*, *30*(7), 840–847.

Chu, K., Jia, C., Liang, X., & Chen, H. (2010). Effect of sintering temperature on the microstructure and thermal conductivity of Al/diamond composites prepared by spark plasma sintering. *International Journal of Minerals, Metallurgy, and Materials*, *17*(2), 234–240. https://doi.org/10.1007/s12613-010-0220-0

Claussen, N., Steeb, J., & Pabst, R. F. (1977). Effect on induced microcracking on the fracture toughness of ceramics. *American Ceramic Society Bulletin*, *56*(6), 559–562.

Danchukova, L. V., Ekström, T., Gordeev, S. K., & Zhukov, S. G. (1998). *EP1019337*. Retrieved from https://www.google.com/patents/EP1019337A1?cl=en

Davies, G., & Evans, T. (1972). Graphitization of Diamond at Zero Pressure and at a High Pressure. *Proceedings of the Royal Society of London. Series A, Mathematical and Physical Sciences*, *328*, 413–427. https://doi.org/10.2307/78141

De Jong, B. H. W. S., Beerkens, R. G. C., & van Nijnatten, P. A. (2000). Glass. In *Ullmann's Encyclopedia of Industrial Chemistry*. Weinheim, Germany: Wiley-VCH Verlag GmbH & Co. KGaA. https://doi.org/10.1002/14356007.a12_365

Dennis, M. D. (1992). Cutting composite formed of cemented carbide substrate and diamond layer. Retrieved from https://www.google.com/patents/EP0579662B1?cl=en

Diehl, R., & Brandt, G. (1975). Crystal structure refinement of YAlO3, a promising laser material. *Materials Research Bulletin*, *10*(2), 85–90. https://doi.org/10.1016/0025-5408(75)90125-7

Droty, M. D., Dauskardt, R. H., Kant, A., & Ritchie, R. 0. (1995). Fracture of synthetic diamond. *Journal of Applied Physics*, *78*(5), 3083–3088. Retrieved from http://www2.lbl.gov/ritchie/Library/PDF/Drory_diamond_APL.pdf

Ekimov, E. A., Gavriliuk, A. G., Palosz, B., Gierlotka, S., Dluzewski, P., Tatianin, E., Presz, A. (2000). High-pressure, high-temperature synthesis of SiC–diamond nanocrystalline ceramics. *Applied Physics Letters*, *77*(7), 954. https://doi.org/10.1063/1.1288602

Evans, A. G., & Faber, K. T. (1981). Toughening of Ceramics by Circumferential Microcracking. *Journal of the American Ceramic Society*, *64*(7), 394–398. https://doi.org/10.1111/j.1151-2916.1981.tb09877.x

Feng, Z., Tzeng, Y., & Field, J. E. (1992). Friction of diamond on diamond in ultra-high vacuum and low-pressure environments. *Journal of Physics D: Applied Physics*, *25*(10), 1418–1424. https://doi.org/10.1088/0022-3727/25/10/006

Field, J. E. (1979). *The Properties of diamond*. (C. A. Brookes, Ed.). Academic Press. Retrieved from http://catalogue.nla.gov.au/Record/1115171

Field, J. E. (1983). *Diamond: Properties and definitions*. Cambridge: Cavedish Laboratory .

Field, J. E. (1992). Strength, fracture and erosion properties of diamond. In J. E. Field (Ed.), *The properties of natural and synthetic diamond* (pp. 473–514).

Gao, L., Hong, J., Miyamoto, H., & Torre, S. D. D. . (2000). Bending strength and microstructure of Al2O3 ceramics densified by spark plasma sintering. *Journal of the European Ceramic Society*, *20*(12), 2149–2152. https://doi.org/10.1016/S0955-2219(00)00086-8

German, R. M. (2010). Fundamentals of sintering: Thermodynamics of sintering. In Z.-Z. Fang (Ed.), *Sintering of advanced materials* (pp. 1–31). Cambridge: Elsevier.

German, R. M., Suri, P., & Park, S. J. (2009). Review: liquid phase sintering. *Journal of Materials Science*, *44*(1), 1–39. https://doi.org/10.1007/s10853-008-3008-0

Gong, J., Wu, J., & Guan, Z. (1999). Examination of the indentation size effect in low-load vickers hardness testing of ceramics. *Journal of the European Ceramic Society*, *19*(15), 2625–2631. https://doi.org/10.1016/S0955-2219(99)00043-6

Gordeev, S. K., Zhukov, S. G., Danchukova, L. V., & Ekstrom, T. C. (2001). Low-Pressure Fabrication of Diamond–SiC–Si Composites. *Inorganic Materials*, *37*(6), 579–583. https://doi.org/10.1023/A:1017560132134

Grzonka, J., Kruszewski, M. J., Rosiński, M., Ciupiński, Ł., Michalski, A., & Kurzydłowski, K. J. (2015). Interfacial microstructure of copper/diamond composites fabricated via a powder metallurgical route. *Materials Characterization*, *99*, 188–194. https://doi.org/10.1016/j.matchar.2014.11.032

Hall, D. R. (1985). *US4604106*. Retrieved from https://www.google.com/patents/US4604106

Hampshire, S. (2007). Silicon nitride ceramics – review of structure, processing and properties. *Journal of Achievements in Materials and Manufacturing Engineering*, *24*(1), 43–50. Retrieved from http://jamme.acmsse.h2.pl/papers_vol24_1/24104.pdf

Herrmann, M., Matthey, B., Höhn, S., Kinski, I., Rafaja, D., & Michaelis, A. (2012). Diamond-ceramics composites—New materials for a wide range of challenging applications. *Journal of the European Ceramic Society*, *32*(9), 1915–1923. https://doi.org/10.1016/j.jeurceramsoc.2011.11.005

Hickey, D. P., Jones, K. S., & Elliman, R. G. (2009). Amorphization and graphitization of single-crystal diamond — A transmission electron microscopy study. *Diamond and Related Materials*, *18*(11), 1353–1359. https://doi.org/10.1016/J.DIAMOND.2009.08.012

Hirata, Y., Hara, A., & Aksay, I. A. (2009). Thermodynamics of densification of powder compact.

Ceramics International, *35*(7), 2667–2674. https://doi.org/10.1016/j.ceramint.2009.03.006

Hitchiner, M. P., Wilks, E. M., & Wilks, J. (1984). The polishing of diamond and diamond composite materials. *Wear*, *94*(1), 103–120. https://doi.org/10.1016/0043-1648(84)90169-8

Horton, M. D., & Horton, L. B. (1985). Grades of polycrstalline diamond. In *Proc. SME's Conference on Super abrasives '85* (pp. 1–9). Chicago.

Huang, S., Swarnakar, A. K., Vanmeensel, K., & Vleugels, J. (2013). Diamond dispersed Si3N4 composites obtained by pulsed electric current sintering. *Journal of the European Ceramic Society*, *33*(6), 1237–1247. https://doi.org/10.1016/j.jeurceramsoc.2012.11.025

Hyatt, M. J., & Day, D. E. (1987). Glass Properties in the Yttria-Alumina-Silica System. *Journal of the American Ceramic Society*, *70*(10), C-283-C-287. https://doi.org/10.1111/j.1151-2916.1987.tb04901.x

Ihle, J., Herrmann, M., & Adler, J. (2005). Phase formation in porous liquid phase sintered silicon carbide: Part III: Interaction between Al2O3–Y2O3 and SiC. *Journal of the European Ceramic Society*, *25*(7), 1005–1013. https://doi.org/10.1016/j.jeurceramsoc.2004.04.017

Kang, Q., He, X., Ren, S., Zhang, L., Wu, M., Guo, C., … Qu, X. (2013). Preparation of copper–diamond composites with chromium carbide coatings on diamond particles for heat sink applications. *Applied Thermal Engineering*, *60*(1–2), 423–429. https://doi.org/10.1016/j.applthermaleng.2013.05.038

Kang, S.-J. L. (2004). Basis of liquid phase sintering. In S.-J. L. Kang (Ed.), *Sintering: Densification, grain growth and mirostructure* (pp. 199–201). Oxford: Elsevier Butterworth - Heinemann.

Katzman, H., & Libby, W. F. (1971). Sintered Diamond Compacts with a Cobalt Binder. *Science*, *172*(3988), 1132–1134. https://doi.org/10.1126/science.172.3988.1132

Kidalov, S. V., & Shakhov, F. M. (2009). Thermal Conductivity of Diamond Composites. *Materials*, *2*(4), 2467–2495. https://doi.org/10.3390/ma2042467

Kim, D.-H., & Kim, C. H. (1990). Toughening Behavior of Silicon Carbide with Additions of Yttria and Alumina. *Journal of the American Ceramic Society*, *73*(5), 1431–1434. https://doi.org/10.1111/j.1151-2916.1990.tb05219.x

Kim, H. C., Jeong, I. K., Shon, I. J., Ko, I. Y., & Doh, J. M. (2007). Fabrication of WC–8wt.%Co hard materials by two rapid sintering processes. *International Journal of Refractory Metals and Hard Materials*, *25*(4), 336–340. https://doi.org/10.1016/j.ijrmhm.2006.09.001

Kingery, W. D. (1959). Densification during Sintering in the Presence of a Liquid Phase. I. Theory. *Journal of Applied Physics*, *30*(3), 301–306. https://doi.org/10.1063/1.1735155

Kingery, W. D., Bowen, H. K., & Uhlmann, D. R. (1976). *Introduction to ceramics*. Wiley. Retrieved from https://books.google.co.za/books/about/Introduction_to_ceramics.html?id=Pd90vVkyTPcC&redir_esc=y

Klemm, H. (2010). Silicon Nitride for High-Temperature Applications. *Journal of the American Ceramic Society*, *93*(6), 1501–1522. https://doi.org/10.1111/j.1551-2916.2010.03839.x

Klimczyk, P., & Urbanovich, V. (2009). Micro-, submicro- and nano-Si3N4 - SiC composites sintered by the HPHT method. *Archives of Materials Science and Engineering*, *Vol. 39*(nr 2), 92–96. Retrieved from https://yadda.icm.edu.pl/baztech/element/bwmeta1.element.baztech-article-BSL8-0030-0013

Ko, Y. S., Tsurumi, T., Fukunaga, O., & Yano, T. (2001). High pressure sintering of diamond-SiC composite. *Journal of Materials Science*, *36*(2), 469–475. https://doi.org/10.1023/A:1004840915607

Kolitsch, U., Seifert, H. J., Ludwig, T., & Aldinger, F. (1999). Phase equilibria and crystal chemistry in the Y2O3–Al2O3–SiO2 system. *Journal of Materials Research*, *14*(2), 447–455. https://doi.org/10.1557/JMR.1999.0064

Kyocera International Inc. (1994). Thermal Expansion. Retrieved October 1, 2017, from https://global.kyocera.com/fcworld/charact/heat/thermaexpan.html

Lammer, A. (1988). Mechanical properties of polycrystalline diamonds. *Materials Science and Technology*, *4*(11), 949–955. https://doi.org/10.1179/mst.1988.4.11.949

Lee, D.-D., Kang, S.-J. L., Petzow, G., & Yoon, D. N. (1990). Effect of alpha to beta (beta') Phase Transition on the Sintering of Silicon Nitride Ceramics. *Journal of the American Ceramic Society*, *73*(3), 767–769. https://doi.org/10.1111/j.1151-2916.1990.tb06591.x

Lee, S.-M., & Kang, S.-J. L. (1998). Theoretical analysis of liquid-phase sintering: Pore filling theory. *Acta Materialia*, *46*(9), 3191–3202. https://doi.org/10.1016/S1359-6454(97)00489-8

Liang, X., Jia, C., Chu, K., Chen, H., Nie, J., & Gao, W. (2012). Thermal conductivity and microstructure of Al/diamond composites with Ti-coated diamond particles consolidated by spark plasma sintering. *Journal of Composite Materials*, *46*(9), 1127–1136. https://doi.org/10.1177/0021998311413689

Mamedov, V. (2002). Spark plasma sintering as advanced PM sintering method. *Powder Metallurgy*, *45*(4), 322–328. https://doi.org/10.1179/003258902225007041

Mao, H., Selleby, M., & Fabrichnaya, O. (2008). Thermodynamic reassessment of the Y 2O3–

Al2O3–SiO2 system and its subsystems. *Computer Coupling of the Phase Diagrams and Thermochemistry*, *32*(2), 399–412. https://doi.org/10.1016/j.calphad.2008.03.003

Michalski, A., & Rosiński, M. (2008). Sintering Diamond/Cemented Carbides by the Pulse Plasma Sintering Method. *Journal of the American Ceramic Society*, *91*(11), 3560–3565. https://doi.org/10.1111/j.1551-2916.2008.02738.x

Miess, D., & Rai, G. (1996). Fracture toughness and thermal resistance of polycrystalline diamond compacts. *Materials Science and Engineering: A*, *209*(1–2), 270–276. https://doi.org/10.1016/0921-5093(95)10105-5

Mitomo, M., & Mizuno, K. (1986). Sintering Behavior of Si3N4 with Y2O3 and Al2O3 Addition. *Journal of the Ceramic Association, Japan*, *94*(1085), 106–111. https://doi.org/10.2109/jcersj1950.94.106

Mizuuchi, K., Inoue, K., Agari, Y., Sugioka, M., Tanaka, M., Takeuchi, T., … Ito, M. (2015). Bimodal and monomodal diamond particle effect on the thermal properties of diamond-particle-dispersed silver matrix composite fabricated by SPS. *Journal of Metallurgical Engineering*, *4*, 1–12. https://doi.org/10.14355/me.2015.04.001

Mlungwane, K. (2009). The development of a diamond-silicon carbide composite. Retrieved from http://wiredspace.wits.ac.za/handle/10539/6937

Mlungwane, K., Herrmann, M., & Sigalas, I. (2008). The low-pressure infiltration of diamond by silicon to form diamond–silicon carbide composites. *Journal of the European Ceramic Society*, *28*(1), 321–326. https://doi.org/10.1016/j.jeurceramsoc.2007.06.010

Mlungwane, K., Sigalas, I., Herrmann, M., & Rodríguez, M. (2009). The wetting behaviour and reaction kinetics in diamond–silicon carbide systems. *Ceramics International*, *35*(6), 2435–2441. https://doi.org/10.1016/j.ceramint.2009.02.019

Moriguchi, H., Tsuduki, K., Ikegaya, A., Miyamoto, Y., & Morisada, Y. (2007). Sintering behavior and properties of diamond/cemented carbides. *International Journal of Refractory Metals and Hard Materials*, *25*(3), 237–243. https://doi.org/10.1016/j.ijrmhm.2006.05.006

Moriguchi, H., Tsuzuki, K., & Ikegaya, A. (2001). Diamond dispersed cemented carbide produced without using ultra high pressure equipment. *15th International Plansee Seminar*, *15*(2). Retrieved from http://www.iaea.org/inis/collection/NCLCollectionStore/_Public/32/068/32068466.pdf

Munir, Z. A., Anselmi-Tamburini, U., & Ohyanagi, M. (2006). The effect of electric field and pressure on the synthesis and consolidation of materials: A review of the spark plasma sintering

method. *Journal of Materials Science*, *41*(3), 763–777. https://doi.org/10.1007/s10853-006-6555-2

Muzart, J. L. R., Batista, V. J., Franco, C. V., & Klein, A. N. (1997). Plasma sintering of AISI 316 L stainless. *Advances in Powder Metallurgy and Particulate Materials*, *1*, 3. Retrieved from https://scholar.google.co.za/scholar?cluster=3914818345999613191&hl=en&oi=scholarr&sa=X&ved=0ahUKEwiFq6mC59vWAhWI7YMKHRbaAqQQgAMIIygAMAA

Nazare, M. H., & Neves, A. J. (1999). Erosion of diamond surfaces. In J. E. Field (Ed.), *Properties, growth and applications of diamond* (pp. 111–114). UK: Institute of Electrical Engineers.

Negita, K. (1986). Effective Sintering Aids for Silicon Carbide Ceramics: Reactivities of Silicon Carbide with Various Additives. *Journal of the American Ceramic Society*, *69*(12), C-308-C-310. https://doi.org/10.1111/j.1151-2916.1986.tb07398.x

Omori, M., & Takei, H. (1982). Pressureless Sintering of SiC. *Journal of the American Ceramic Society*, *65*(6), c92–c92. https://doi.org/10.1111/j.1151-2916.1982.tb10460.x

Peng, H. (2004). Spark Plasma Sintering of Si3N4-Based Ceramics -Sintering mechanism-Tailoring microstructure-Evaluating properties. *Unpublished*. Retrieved from http://citeseerx.ist.psu.edu/viewdoc/download?doi=10.1.1.729.4599&rep=rep1&type=pdf

Pope, B. J., Taylor, J. K., Dixon, R. H., Gardinier, C. F., Pope, L. M., Blackburn, D. C., … Jensen, K. M. (2000). *US6494918 B1*. Retrieved from https://www.google.com/patents/US6494918

Prinsloo, G., Spektorov, Y., & Linde, O. (2011). The global diamond industry - lifting the veil of mystery. *Bain Report*.

Qian, J., Voronin, G., Zerda, T. W., He, D., & Zhao, Y. (2002). High-pressure, high-temperature sintering of diamond–SiC composites by ball-milled diamond–Si mixtures. *Journal of Materials Research*, *17*(8), 2153–2160. https://doi.org/10.1557/JMR.2002.0317

Rahaman, M. N. (2003). *Ceramic processing and sintering*. M. Dekker. Retrieved from https://books.google.co.za/books/about/Ceramic_Processing_and_Sintering.html?id=5yERCU5miKkC&redir_esc=y

Raichenko, A. I., Kolchinskii, M. Z., & Levina, D. A. (1976). Electric-discharge sintering of oxidized metal powders. Retrieved September 6, 2017, from https://www.researchgate.net/publication/226392555_Electric-discharge_sintering_of_oxidized_metal_powders

Ribeiro, S., & Strecker, K. (2004). Si3N4 ceramics sintered with Y2O3/SiO2 and R2O3(ss)/SiO2: a comparative study of the processing and properties. *Materials Research*, *7*(3), 377–383.

https://doi.org/10.1590/S1516-14392004000300003

Rice, R. W. (1984). Elastic anisotropy and the grain size dependence of ceramic fracture energies. *Journal of Materials Science*, *19*(4), 1267–1271. https://doi.org/10.1007/BF01120037

Rice, R. W., Freiman, S. W., & Becher, P. F. (1981). Grain-Size Dependence of Fracture Energy in Ceramics: I, Experiment. *Journal of the American Ceramic Society*, *64*(6), 345–350. https://doi.org/10.1111/j.1151-2916.1981.tb10300.x

Risbud, S. H., Groza, J. R., & Kim, M. J. (1994). Clean grain boundaries in aluminium nitride ceramics densified without additives by a plasma-activated sintering process. *Philosophical Magazine Part B*, *69*(3), 525–533. https://doi.org/10.1080/01418639408240126

Rodger, A. S., Wells, G. D., Moffett, R. J., & Bailey, G. J. (2001). The variability of Joule heating, and its effects on the ionosphere and thermosphere. *European Geophysical Society*, *19*, 773–781. Retrieved from https://www.ann-geophys.net/19/773/2001/angeo-19-773-2001.pdf

Sangsuwan, P., Tewari, S. N., Gatica, J. E., Singh, M., Dickerson, R., Tewari, S. N., & Gatica, J. E. (1999). Reactive Infiltration of Silicon Melt Through Microporous Amorphous Carbon Preforms. *Metallurgical and Materials Transactions B*, *16*(30), 933–944. Retrieved from http://engagedscholarship.csuohio.edu/encbe_facpub

She, J. H., & Ueno, K. (1999). Effect of additive content on liquid-phase sintering on silicon carbide ceramics. *Materials Research Bulletin*, *34*(10–11), 1629–1636. https://doi.org/10.1016/S0025-5408(99)00172-5

Shen, Z., Peng, H., & Nygren, M. (2003). Formidable Increase in the Superplasticity of Ceramics in the Presence of an Electric Field. *Advanced Materials*, *15*(12), 1006–1009. https://doi.org/10.1002/adma.200304863

Slamovich, E. B., & Lange, F. F. (1990). Densification Behavior of Single-Crystal and Polycrystalline Spherical Particles of Zirconia. *Journal of the American Ceramic Society*, *73*(11), 3368–3375. https://doi.org/10.1111/j.1151-2916.1990.tb06463.x

Sōmiya, S., Aldinger, F., Claussen, N., Spriggs, R. M., Uchino, K., Koumoto, K., … Rahaman, M. N. (2003). Chapter 4 – 4.1 Sintering of Ceramics. In *Handbook of Advanced Ceramics* (pp. 187–264). https://doi.org/10.1016/B978-012654640-8/50006-7

Stromberg, H. D., & Stephens, D. R. (1970). Sintering of Diamond at 1800-1900°C and 60-65kBar. *The American Ceramic Society* , *49*(12), 1030–1032.

Suarez, M., Fernandez, A., Menendez, J. L., Torrecillas, R., U., H., Hennicke, J., … Kessel, T. (2013). Challenges and Opportunities for Spark Plasma Sintering: A Key Technology for a New

Generation of Materials. In *Sintering Applications*. InTech. https://doi.org/10.5772/53706

SwiffGlass. (2015). Quartz vs. Fused Silica: What's the Difference? | Swift Glass. Retrieved January 26, 2018, from https://www.swiftglass.com/quartz-vs-fused-silica-whats-the-difference/

Taguchi, S. ., Motta, F. ., Balestra, R. ., & Ribeiro, S. (2004). Wetting behaviour of SiC ceramics. *Materials Letters*, *58*(22–23), 2810–2814. https://doi.org/10.1016/j.matlet.2004.05.004

Taguchi, S. P., Ribeiro, S., & Balestra, R. M. (2008). Infiltration of Al2O3/Y2O3 mix into SiC ceramics preforms. *Ceramics International* , *34*(3), 625–629.

Tao, J., Zhu, X., Tian, W., Yang, P., & Yang, H. (2014). Properties and microstructure of Cu/diamond composites prepared by spark plasma sintering method. *Transactions of Nonferrous Metals Society of China*, *24*(10), 3210–3214. https://doi.org/10.1016/S1003-6326(14)63462-2

Tokita, M. (1999). *Mechanism of spark plasma sintering*. Japan .

van Dijen, F. K., & Mayer, E. (1996). Liquid phase sintering of silicon carbide. *Journal of the European Ceramic Society* , *16*, 413–420.

Williams, D. J., & Johnson, W. (1982). Neck Formation and Growth in High-Voltage Discharge Forming of Metal Powders. *Powder Metallurgy*, *25*(2), 85–89. https://doi.org/10.1179/pom.1982.25.2.85

Winn, E. J., & Clegg, W. J. (2004). Role of the Powder Bed in the Densification of Silicon Carbide Sintered with Yttria and Alumina Additives. *Journal of the American Ceramic Society*, *82*(12), 3466–3470. https://doi.org/10.1111/j.1151-2916.1999.tb02266.x

Wise, J. L., Raymond, D. W., Cooley, C. H., & Bertagnolli, K. (2002). Effects of design and processing parameters on performance of PDC drag cutters for hardrock drilling. *Technical Report, Sandia National Laboraties*.

Wu, L., Lui, G., Li, J., He, B., Yang, Z., & Chen, Y. (1990). Dependence of glass forming ability on starting compositions in the Y2O3-Al2O3-SiO2 system. *Ceramics*, *55*(3), 228. Retrieved from http://journaldatabase.info/articles/dependence_glass-forming_ability_on.html

Xie, G., Ohashi, O., Song, M., Mitsuishi, K., & Furuya, K. (2005). Reduction mechanism of surface oxide films and characterization of formations on pulse electric-current sintered Al–Mg alloy powders. *Applied Surface Science*, *241*(1–2), 102–106. https://doi.org/10.1016/j.apsusc.2004.09.025

Yahiaoui, M., Gerbaud, L., Paris, J.-Y., Denape, J., & Dourfaye, A. (2013). A study on PDC drill bits quality. *Wear*, *298–299*, 32–41. https://doi.org/10.1016/J.WEAR.2012.12.026

Yamamoto, T. A., Kondou, T., Kodera, Y., Ishii, T., Ohyanagi, M., & Munir, Z. A. (2005). Mechanical Properties of β-SiC Fabricated by Spark Plasma Sintering. *Journal of Materials Engineering and Performance*, *14*(4), 460–466. https://doi.org/10.1361/105994905X56250

Yang, J.-F., Ohji, T., & Niihara, K. (2004). Influence of Yttria-Alumina Content on Sintering Behavior and Microstructure of Silicon Nitride Ceramics. *Journal of the American Ceramic Society*, *83*(8), 2094–2096. https://doi.org/10.1111/j.1151-2916.2000.tb01520.x

Zhao, Y., Qian, J., Daemen, L. L., Pantea, C., Zhang, J., Voronin, G. A., & Zerda, T. W. (2004). Enhancement of fracture toughness in nanostructured diamond–SiC composites. *Applied Physics Letters*, *84*(8), 1356–1358. https://doi.org/10.1063/1.1650556

Zhou, X., Wang, Y., Li, T., Li, X., Cheng, X., Dong, L., … Xu, X. (2015). Fabrication of diamond–SiC–TiC composite by a spark plasma sintering-reactive synthesis method. *Journal of the European Ceramic Society*, *35*(1), 69–76. https://doi.org/10.1016/j.jeurceramsoc.2014.08.006

Zhu, C., Lang, J., & Ma, N. (2012). Preparation of Si–diamond–SiC composites by in-situ reactive sintering and their thermal properties. *Ceramics International*, *38*(8), 6131–6136. https://doi.org/10.1016/J.CERAMINT.2012.04.062